Compounding effects of sea level rise and fluvial flooding

Hamed R. Moftakhari[a], Gianfausto Salvadori[b], Amir AghaKouchak[a,c,1], Brett F. Sanders[a,d], and Richard A. Matthew[d,e]

[a]Department of Civil and Environmental Engineering, University of California, Irvine, CA 92697; [b]Dipartimento di Matematica e Fisica, Università del Salento, Lecce, 73100 Italy; [c]Department of Earth System Science, University of California, Irvine, CA 92697; [d]Department of Urban Planning and Public Policy, University of California, Irvine, CA 92697; and [e]Blum Center for Poverty Alleviation, University of California, Irvine, CA 92697

Edited by Anny Cazenave, Centre National d'Etudes Spatiales, Toulouse, France, and approved July 24, 2017 (received for review December 19, 2016)

Sea level rise (SLR), a well-documented and urgent aspect of anthropogenic global warming, threatens population and assets located in low-lying coastal regions all around the world. Common flood hazard assessment practices typically account for one driver at a time (e.g., either fluvial flooding only or ocean flooding only), whereas coastal cities vulnerable to SLR are at risk for flooding from multiple drivers (e.g., extreme coastal high tide, storm surge, and river flow). Here, we propose a bivariate flood hazard assessment approach that accounts for compound flooding from river flow and coastal water level, and we show that a univariate approach may not appropriately characterize the flood hazard if there are compounding effects. Using copulas and bivariate dependence analysis, we also quantify the increases in failure probabilities for 2030 and 2050 caused by SLR under representative concentration pathways 4.5 and 8.5. Additionally, the increase in failure probability is shown to be strongly affected by compounding effects. The proposed failure probability method offers an innovative tool for assessing compounding flood hazards in a warming climate.

sea level rise | coastal flooding | compound extremes | copula | failure probability

Flooding hazard, characterized by the intensity/frequency of flood events (1), is an important consideration in local level planning and adaptation (2). Coastal cities are especially demanding sites for flood hazard assessment because of exposure to multiple flood drivers such as coastal water level (WL), river discharge, and precipitation (3, 4). Furthermore, dependence among the flood drivers [e.g., coastal surge/tide, sea level rise (SLR), and river flow] can lead to compound events (5) in which the simultaneous or sequential occurrence of extreme or non-extreme events may lead to an extreme event or impact (6). For example, in estuarine systems, the interplay between coastal WL and freshwater inflow determines the surface WL (and hence the flood probability) at subtidal (7) and tidal (8–11) frequencies.

In the United States, flood hazard assessment practices are typically based on univariate methods. For example, procedures for rivers often treat oceanic contributions (e.g., tides and storm surges) using static base flood levels (e.g., ref. 12), and do not consider the dynamic effects of coastal WL (e.g., ref. 13). Similarly, flood hazard procedures for coastal WLs (e.g., ref. 14) do not account for terrestrial factors such as river discharge or direct precipitation into urban areas. Previous studies indicate that univariate extreme event analysis may not correctly estimate the probability of a given hydrologic event (15, 16). This points to the potential importance of multivariate analysis of extreme events in coastal/estuarine systems and consideration of compounding effects between flood drivers (6). Bivariate extreme event analysis has been explored in a coastal context with different variables and in different areas (5, 17–33) (see *SI Appendix*, Table S2 for more details). Bivariate flood hazard studies have been performed for coasts of the United Kingdom (34–36) and Australia (37, 38); however, they do not consider the impacts of SLR on the estimated flood hazard.

SLR is a well-documented and urgent aspect of anthropogenic global warming (39–46) that threatens coastal communities all around the world. Without flood adaptation, annual losses of 0.3 to 9.3% of global gross domestic product are expected by 2100 (47), while only ∼70% of the coastal landscapes projected to experience future flooding have some capacity to respond dynamically to SLR (48). High-quality sea surface WL data, recorded at tide gauges around the world over the last 100+ y, document a significant globally averaged acceleration in mean SLR of about 0.009 $mm{\cdot}y^{-2}$ since 1880 and 0.022 ± 0.015 $mm{\cdot}y^{-2}$ between 1952 and 2011, and a globally averaged mean SLR of ∼2.8 $mm{\cdot}y^{-1}$ between 1993 and 2009 (39, 49–53). Analysis of satellite altimetry records suggests an SLR rate of 3.3 ± 0.4 $mm{\cdot}y^{-1}$ between 1993 and 2014 (54). The rate of SLR over recent decades is one order of magnitude larger than SLR over the past millennia (55), and projections of SLR over the 21st century, based on current trajectories of anthropogenic activities and greenhouse gases emissions (56), cannot rule out an increase greater than 1 m (55, 57–59).

SLR brings the height of high tides closer to flood stage, and increases the frequency of both nuisance floods (60–64) and destructive flood events (65, 66), such that today's century-level floods are expected to become decadal by 2050 (67–70). SLR further complicates coastal flood hazard analysis by introducing nonstationarity (71). Physically, SLR adds to the height of future storm tides, reduces pressure gradients that are important for transporting fluvial water to the ocean, and enables greater upstream tide/wave propagation (72, 73).

In this study, we propose a framework that takes the impacts of SLR into account for flood hazard analysis in coastal systems under multiple flood drivers and integrates the concepts of

Significance

Population and assets in coastal regions are threatened by both oceanic and fluvial flooding hazards. Common flood hazard assessment practices typically focus on one flood driver at a time and ignore potential compounding impacts. Here we outline a unique bivariate flood hazard assessment framework that accounts for the interactions between a primary oceanic flooding hazard, coastal water level, and fluvial flooding hazards. Using the notion of "failure probability," we also assess coastal flood hazard under different future sea level rise scenarios. The results show that, in a warming climate, future sea level rise not only increases the failure probability, but also exacerbates the compounding effects of flood drivers.

Author contributions: H.R.M., A.A., B.F.S., and R.A.M. designed research; H.R.M. performed research; G.S. contributed new analytic tools; H.R.M. and G.S. analyzed data; and H.R.M., G.S., A.A., B.F.S., and R.A.M. wrote the paper.

The authors declare no conflict of interest.

This article is a PNAS Direct Submission.

[1]To whom correspondence should be addressed. Email: amir.a@uci.edu.

This article contains supporting information online at www.pnas.org/lookup/suppl/doi:10.1073/pnas.1620325114/-/DCSupplemental.

bivariate hazard analysis (74) and nonstationary hazard assessment. We first propose a bivariate flooding assessment approach that accounts for the compounding effects of fluvial flooding and coastal sea level (with future SLR). We then integrate the notion of failure probability to achieve a practical tool for assessing future hazards. Using this framework, we show that ignoring SLR and its compounding impacts may lead to a significant underestimation of future coastal flooding hazard.

Although the framework outlined here is general and can be applied to different regions, for illustration, we focus on the United States, in which over half of the population live in coastal regions (75). Also, 8 out of the 20 most vulnerable cities in terms of average annual losses due to flooding in the globe are located in the United States (2). Using copulas and bivariate dependence analysis (*Methods*), we quantify increases in flood probabilities caused by SLR based on 2030 and 2050 projections, under representative concentration pathways (RCPs) 4.5 and 8.5. Finally, we evaluate the change in failure probability of compound flood events due to SLR. Note that an inverse analysis for identifying potentially dangerous multivariate occurrences having a fixed level of "acceptable risk," as clarified in ref. 76, can be carried out by inverting the formulas outlined in *Methods*. However, this is outside the scope of the present work; for further details please see also refs. 30, 31, 74, and 77.

Here we use three sets of data, available at eight estuarine systems along the coasts of United States (*SI Appendix*, Fig. S1): (*i*) hourly WL, (*ii*) daily freshwater inflow to the lower estuary as a representative of fluvial flow, and (*iii*) future local SLR projections to describe the impacts of SLR on increased likelihood of flooding by 2030 and 2050. Using these data, we implement univariate and bivariate analysis of coastal flooding for the current and future climate with rising sea levels. In each case, the observation gauges are carefully chosen to make sure that the longest and highest-quality data in that system are analyzed. For extreme WL analysis along tidal rivers, when significant dependence between deriving factors is detected, it is critical to appropriately characterize correlation structure and carefully take the nonlinear interaction between freshwater inflow and upcoming surge tides into account. Otherwise, either large astronomic tidal variabilities may mask the correlation between meteorologically driven components or potential adjustments of WL measured at tide gauge by river discharge may not be appropriately treated.

Coastal WLs resulting from tides and nontidal processes (e.g., storm surge) are taken from hourly coastal WL data at eight tide gauges shown in *SI Appendix*, Fig. S1 and provided by National Oceanic and Atmospheric Association (https://tidesandcurrents.noaa.gov/). The Galveston and San Francisco records with 70 y and 157 y of data have the shortest and longest available WL series, respectively (see *SI Appendix*, Table S1 for more information).

The estimated daily freshwater discharges for all of the estuaries are obtained from United States Geological Survey website (waterdata.usgs.gov/nwis/rt), except for San Francisco Bay (SF Bay), for which the Net Delta Outflow Index (NDOI), an output of the California Department of Water Resources Dayflow program (www.water.ca.gov/dayflow/), is used as a proxy for tidally averaged daily river inflow to SF Bay from the Sacramento River delta. NDOI accounts for about 90% of the inflow to SF Bay; and accounts for river inflows, precipitation, agricultural consumptive demand, and California Water Project exports (78, 79). The Columbia River and Buffalo Bayou River, with 660,500 km^2 (80) and 270 km^2 watersheds, (waterdata.usgs.gov/tx/nwis) are the largest and the smallest watersheds, respectively, in this study. Size and drainage characteristics of the watershed (e.g., time of concentration) and different forcing mechanisms cause the fluvial flow to occur on different time scales ranging from a few hours (i.e., due to intense local precipitation) to a few days (i.e., rain on snow events) and even weeks (i.e., Spring snowmelt freshets). The case studies investigated here, with relatively long records available, cover a wide range of estuarine systems from moderately (e.g., Hudson River) to strongly (e.g., Potomac River) convergent and from moderately (e.g., Delaware River) to strongly (e.g., Columbia River) dissipative (81); this points to the potential applicability of our proposed approach to many estuarine/coastal systems around the world.

The probability distribution of local SLR projections (F_{SLR}) at the eight sites of interest, under RCPs 4.5 and 8.5 of Coupled Model Intercomparison Project Phase 5 (CMIP5) scenarios, are provided by ref. 59 in a discrete form by specifying seven quantiles of the following orders: $q_i = 0.005, 0.05, 0.17, 0.5, 0.83, 0.95,$ and 0.995. A continuous version of F_{SLR} is constructed via a suitable linear interpolation (see *SI Appendix* for further details).

Results and Discussion

First, we discuss the differences between univariate and bivariate flooding probabilities for three selected estuarine systems along the coasts of United States, where the variables of interest (fluvial flow and coastal WL) are statistically dependent, namely, Philadelphia, PA; San Francisco, CA; and Washington, DC. The results for the rest of the studied estuarine systems, with no significant dependence between variables, are presented in *SI Appendix*. Here, a direct approach to the hazard assessment is adopted, as clarified in ref. 76. The target is to compute the return periods and/or the failure probabilities associated with observed (and future projected) occurrences.

Fig. 1*A* shows the annual maximum fluvial flow versus the associated maximum coastal WL measured within 1 day of the flood peak (black dots). For the sake of illustration, a reference bivariate occurrence $z^* = (x^*, y^*)$ is chosen, and is indicated by a red circle. Here x^* and y^* correspond, respectively, to 20-y return levels of the variables X (fluvial flow) and Y (coastal WL), so that z^* has marginal univariate return periods (RPs) equal to 20 y (*Methods*). These univariate hazard scenarios (HSs) for z^* are shown by a thick green line on the x axis (for X) and a thick blue line on the y axis (for Y). In the bivariate framework, we use copulas to model the compounding effects of fluvial flow and coastal WL (*Methods*). Here, the HS of interest is the "OR" one, meaning that it is sufficient that either the fluvial flow or the coastal WL or both be large to make a bivariate occurrence hazardous (i.e., the union of the regions *i*, *ii*, and *iii* in Fig. 1*A*, where either $X > x^*$, $Y > y^*$, or both). To highlight the differences between the case of assuming the variables X and Y as dependent or independent within this bivariate framework, in Fig. 1, the red curve indicates the isoline of the actual joint distribution F_{XY} crossing z^*, whereas the black curve indicates the isoline of F_{XY} under the unreasonable assumption of independence between the variables X and Y. Indeed, the more the variables are dependent, the more the two curves are different (e.g., compare Fig. 1 *C* and *D*).

The univariate analysis (i.e., green and blue dashed lines in Fig. 1), however useful for flood events driven only by river discharge (i.e., far upstream in tidal rivers) or only by coastal WL (i.e., at coastal regions not influenced by fluvial flow), may not appropriately characterize the flood hazard at/near estuaries. In estuaries, flood hazard can be influenced by interactions between fluvial flooding and coastal WL (30, 31, 33, 82), and hence a particular hazard level may be more frequent than expected.

For the case of z^* (indicated by the red circle) with a marginal univariate RP of 20 y, the associated estimates of the bivariate OR RPs are shown in Fig. 1, for Philadelphia, PA (Fig. 1*B*), San Francisco, CA (Fig. 1*C*), and Washington, DC (Fig. 1*D*). In all cases, it is evident that the bivariate OR RP is shorter than the 20-y univariate RP (see also *Methods*): ∼13 y for Philadelphia, ∼11 y for San Francisco, and ∼16 y for Washington, DC. This indicates that ignoring the compounding impacts of fluvial flow

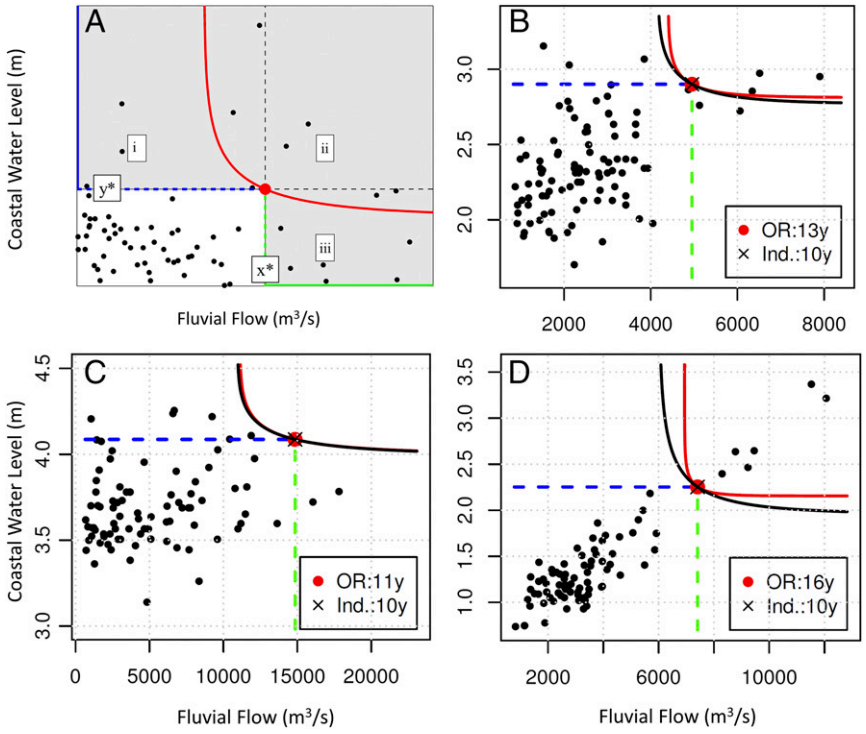

Fig. 1. (*A*) Illustration of the univariate and bivariate HSs. The black circles represent observed bivariate occurrences, the red circle is the reference occurrence z^*, and the red line is the isoline of F_{XY} crossing z^*. The hazardous regions *i*, *ii*, and *iii* are indicated as shaded areas. The estimates of the bivariate OR RPs associated with the occurrence z^* are indicated in the legends for (*B*) Philadelphia, PA, (*C*) San Francisco, CA, and (*D*) Washington, DC, with Kendall tau rank correlation coefficients of 0.3, 0.15, and 0.53, respectively. In *B*–*D*, the black line shows the isoline of F_{XY} crossing z^*, under the unreasonable assumption of independence between fluvial flow and Coastal WL.

and coastal WLs may inappropriately characterize the coastal flood hazard, and can lead to underestimation of it: Actually, a shorter RP entails a larger frequency of occurrence. The results for 5-, 10-, 20-, and 50-y RPs for all of the studied coastal systems are shown in *SI Appendix*, *Section 5* and Figs. S20–S27.

The dependence between coastal WL and fluvial flow strongly influences the joint flood probability and, in turn, the OR RP. In Washington, DC (Fig. 1*D*), where the two flood drivers are highly correlated (Kendall tau rank correlation coefficient of 0.53; see also *SI Appendix*, Figs. S10 and S18), an event with marginal univariate RPs of 20 y, and a ∼10-y OR RP based on the incorrect assumption of independence, becomes a ∼16-y event when the dependence structure is resolved. On the other hand, in San Francisco (Fig. 1*C*), where the two flood drivers are weakly correlated (Kental tau ∼0.15), an event with a marginal univariate RP of 20 y, and a ∼10-y OR RP based on the assumption of independence, becomes an ∼11-y event. According to the theory of copulas, the marginal univariate RP becomes a better predictor of the OR RP with increasing correlation between the two drivers. Thus, resolving the correlation structure is critical to quantifying the compound OR RP precisely.

A further key question is, to what extent will the flood hazard change as a result of increasing sea levels? With rising sea levels, the likelihood of high WLs at any given time increases. Consequently, the bivariate OR flood hazard necessarily increases as well, and we can quantify the effects of SLR conditions on coastal flooding using a failure probability approach (*Methods*). The term "failure probability" refers to the probability of observing a potentially hazardous flood event (i.e., lying in a specific HS) at least once in a given design lifetime (e.g., 30 y) (74, 83). Fig. 2 shows the failure probability computed following a univariate approach (black curves), and compounding fluvial flow and coastal WL for current (red curves) and future SLR conditions over a 30-y temporal horizon for 2030 SLR based on RCP 4.5 (purple curves) and 2050 SLR based on RCP 8.5 (green curves). In each case, it is assumed that the WL distribution does not change over the design lifetime.

Considering the three sites where the dependence is significant [namely, Philadelphia (PA), San Francisco (CA), and Washington (DC)], the plots also show the OR failure probabilities under an unreasonable independence assumption (blue lines in Fig. 2). As a result, these probabilities are always larger than the ones computed using the true copula fitted on the data; in turn, including compounding effects but (falsely) assuming independence may overestimate the hazard (at least in the OR case), suggesting that a correct modeling of the dependencies should always be carried out. Thus, Fig. 2 suggests that (*i*) neglecting the compounding impacts of flood drivers causes significant underestimation of failure probabilities; (*ii*) the assumption of independence between variables, when there is significant correlation, results in overestimation of failure probabilities; and (*iii*) SLR significantly increases the failure probability in the near future/midfuture in all of the cases studied here. For example, we consider New York, NY, which is projected to experience US$174 million per year of loss due to flooding if no further flood management measures are implemented (84). Based on the current conditions, the failure probability at the 20-y return level over a 10-y design life time (e.g., 2017–2026) is expected to be 0.40 based on univariate analysis, and 0.65 based on the bivariate OR analysis. Now considering 2030 sea levels based on RCP 4.5, the failure probability at the same return level based on the bivariate OR analysis increases to 0.95 (0.82 to 1.00 with 95% confidence), a significantly larger value. The situation becomes worse under more-threatening SLRs. At the same return level, 2050 SLR under RCP 8.5, representing the worst-case scenario among the CMIP5 models used for AR5

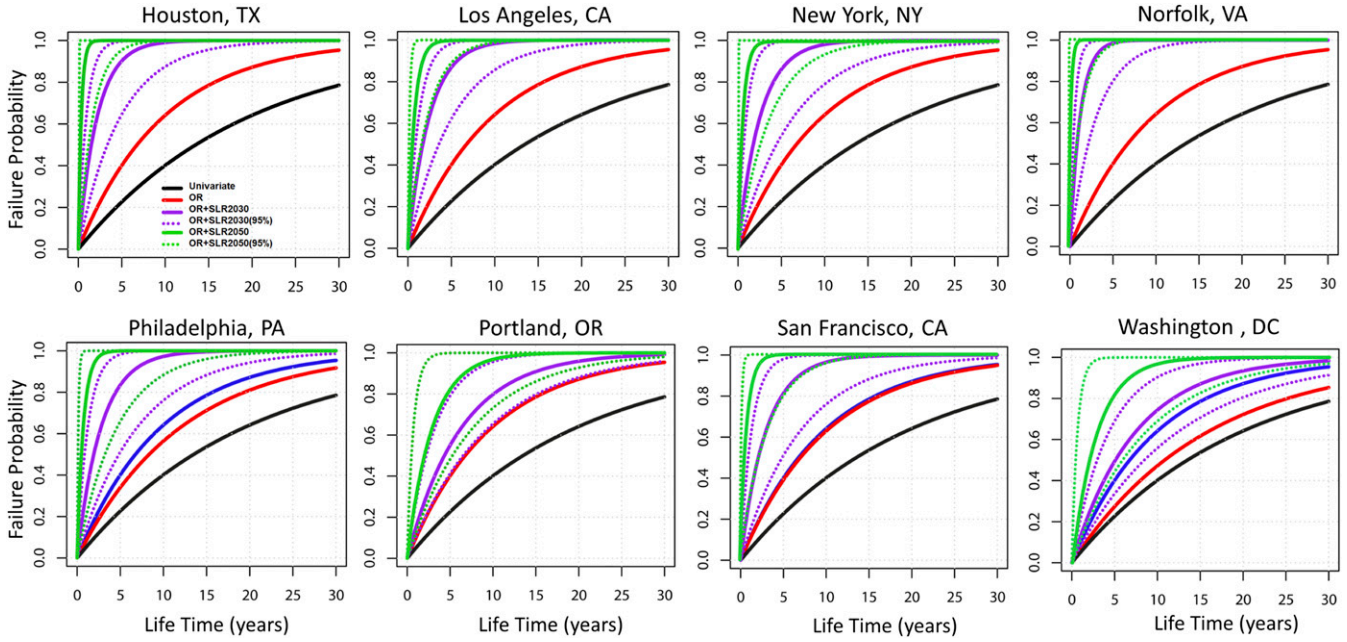

Fig. 2. Estimated failure probability due to a 20-y event for a temporal horizon of 30 y. The solid black and red curves show the estimated failure probability computed based on, respectively, the univariate and bivariate OR HSs, according to present climate. Failure probability (and 95% confidence bands) for projected SLR is shown with solid (and dashed) curves for 2030 under RCP 4.5 (purple) and for 2050 under RCP 8.5 (green). In cases with significant correlation between fluvial flow and coastal WL (namely, Philadelphia, San Francisco, and Washington, DC), failure probability under the unreasonable assumption of independence is shown as a blue curve.

(85), failure probability increases even more in the following decades. The results suggest that, under this scenario, the failure probability approaches one in six of the study areas (namely, Houston, TX; Los Angeles, CA; New York, NY; Norfolk, VA; Philadelphia, PA; and San Francisco, CA). Similar failure probability figures for different HSs are shown in *SI Appendix*, *Section 6* and Figs. S28–S59.

This increase in failure probability due to SLR is a natural consequence of compounding effects of flood drivers. Given the expected rise in incidence and/or magnitude of high coastal WLs in the coming decades, this bivariate OR approach may be important for assessing socioeconomic impacts on coastal communities. The United States, for example, has two of the three top at-risk coastal cities in terms of assets exposed to flooding, and 17 port cities with populations larger than 1 million (44, 45, 85), and so suffers and will suffer from increased frequency of coastal flooding. However, in addition to the rise in mean coastal WL due to SLR, we expect that other impacts may also affect the frequency of flooding in estuaries, like changes in future fluvial flow regimes, wave–tide interaction, and geomorphic evolution affecting tide/surge propagation along the channel (72, 73, 76, 84, 86–89). In this study, we focus on the interactions between different SLR scenarios and current fluvial flood information, mainly because we have more confidence in the sign of change in future sea levels in a warming climate. The other components of coastal flood hazard (e.g., change in local fluvial flow regimes) are more uncertain and require further in-depth research. Hence, a key issue is developing datasets for coastal communities with contemporaneous measurements of different flood drivers. Nevertheless, the proposed framework can incorporate any combination of two (or even more) flood hazard drivers. It is also able to systematically deal with nonstationarity, and thus it can quantify the change in failure probability in response to the trending nature of drivers/hazards.

Methods

In this work, we consider annual maxima, and use the corresponding block maxima mathematical framework. Robust definition of compound events (3) and the efficient sampling for joint probability analysis (90) are challenging tasks. A desired approach should appropriately represent the information entailed in the data while simplifying the sources data (i.e., refs. 5, 91, and 92). The two variables of interest here are (*i*) the largest annual freshwater inflow to the lower estuary and (*ii*) the corresponding largest observed hourly WL within ±1 d. This procedure provides the pairs of interest for any given year (annual bivariate vectors) that can be assumed to be independent for physical reasons.

First, we need to identify suitable HSs that refer to the regions where the values of the variable(s) of interest may be considered as hazardous according to appropriate criteria. An HS is simultaneously characterized by (*i*) a geometrical component (i.e., a hazardous region, either on the real line in the univariate case or in the real plane in the bivariate case) and (*ii*) a probabilistic component (i.e., the probability that an occurrence belongs to the hazardous region). This makes it possible to use the HS for both RP and failure probability analyses (74, 77).

In the univariate case, given a critical threshold x^*, the corresponding univariate HS is defined as the set of occurrences such that $\{X > x^*\}$. In the bivariate case, given a critical pair $z^* = (x^*, y^*)$, the corresponding bivariate HS is taken to be the inclusive OR one, defined as the set of occurrences such that either $\{X > x^*\}$, $\{Y > y^*\}$, or both (74). The choice of a bivariate OR approach is a natural one in the present context, since it is sufficient that either the fluvial discharge, the coastal WL, or both be large to produce a potentially hazardous occurrence. This represents a valuable approximation of the dynamics of coastal flooding, in which the combined events due to nonextreme discharges and WLs might also potentially generate hazardous occurrences.

The geometry of the HSs introduced above are illustrated in Fig. 1*A*, for given critical thresholds x^* and y^*. The green half-line on the horizontal axis indicates the univariate HS $\{X > x^*\}$ corresponding to the variable X, and the blue half-line on the vertical axis indicates the univariate HS $\{Y > y^*\}$ corresponding to the variable Y. The shaded region is the bivariate OR HS corresponding to the pair (X, Y), where either $X > x^*$, $Y > y^*$, or both.

The fundamental difference between a univariate and a bivariate approach lies in the related failure mechanism. In the former case, failure is ruled solely by a single variable, whereas, in the latter, the compounding effects of two variables may result in hazardous occurrences, even if none of the variables take on extreme values. An occurrence may be labeled as

hazardous or not, depending on the chosen failure mechanism. For instance, the occurrences in regions *ii* and *iii* of Fig. 1*A* would be considered as hazardous if the ruling variable were the fluvial flow X, but the ones in region *iii* would not be hazardous according to their WL (since $Y \le y^*$). Similarly, the occurrences in regions *i* and *ii* would be hazardous if the ruling variable were the WL Y, but the ones in region *i* would not be such in terms of the river flows (since $X \le x^*$). Instead, all of the occurrences in the regions *i*, *ii*, and *iii* would be hazardous according to the (bivariate) OR criterion. Thus, the OR approach may account for the physically based fact that the combined events of X and Y (even if not extreme) may yield hazardous events.

Univariate and Bivariate Models. Below, the construction of an appropriate probability model is explained, separately, for the univariate and the bivariate approaches.

Univariate model. In this case, only one flood driver (either fluvial flow or coastal WL) is considered for hazard assessment. The generalized extreme value (GEV) distribution turns out to adequately fit the available samples of both flood drivers according to the bootstrap p values of the goodness-of-fit tests, which, in all cases, are larger than 5% (*SI Appendix*, Figs. S2–S9).

Bivariate model. A variety of parametric and nonparametric methods have been developed for bivariate frequency analysis (93). We use copulas to construct a bivariate model. Copulas offer several advantages for multivariate modeling, such as the following: (*i*) It is possible to account separately for the marginals and the joint behavior of the variables of interest, (*ii*) the mathematical formulation is feasible, and (*iii*) marginal distributions can be freely chosen. Also, copulas allow computing the RPs and the failure probabilities of interest (15, 74, 77). See refs. 94–96 for a theoretical introduction, and see refs. 97–99 for practical descriptions.

According to Sklar's Theorem (100), the joint distribution F_{XY} of the pair (X,Y), with marginal distributions F_X and F_Y, for all $(x,y) \in R^2$, can simply be written as

$$F_{XY}(x,y) = C_{XY}(F_X(x), F_Y(y)), \quad [1]$$

where the function $C_{XY} : [0,1] \times [0,1] \to [0,1]$ is the bivariate copula of (X,Y) providing the analytical formula of the dependence structure ruling the random joint dynamics of X and Y. Practically, a bivariate model can be constructed by fitting suitable univariate laws on the marginals (in the present context, distributions), and fitting an appropriate copula on the observed pairs (97, 98). To select an appropriate bivariate model, here a thorough statistical analysis was carried out, involving 24 copula models covering a wide variety of dependence structures (see *SI Appendix, Section 4*).

RP Analysis. In the present annual-based framework, the RP T associated with a given HS (either univariate or bivariate) can be defined as

$$T = 1/P\{HS\}, \quad [2]$$

where, $P\{HS\}$ is the probability that an event occurs in the HS of interest (74, 77).

In the univariate case, where the HS is identified via a critical threshold x^* (or y^*), Eq. **2** reduces to the traditional formula

$$T_X = 1/(1 - F_X(x^*)), \quad [3]$$

where F_X is the distribution of X, and $1 - F_X(x^*)$ represents the probability that an occurrence lies on the horizontal green half-line in Fig. 1*A* (or, equivalently, the probability of the region *ii*∪*iii*). The same approach can be taken to define the RP T_Y for Y and the region *i*∪*ii*.

In the bivariate OR case, where the HS is identified via a critical pair $z^* = (x^*, y^*)$ as in Fig. 1*A*, exploiting the Sklar's Theorem, Eq. **2** becomes

$$T_{OR} = 1/(1 - F_{XY}(x^*, y^*)) = 1/(1 - C_{XY}(F_X(x^*), F_Y(y^*))), \quad [4]$$

where, F_{XY} is the joint distribution of the pair (X,Y), and $1 - F_{XY}(x^*, y^*)$ is equal to the probability of $X > x^*$ OR $Y > y^*$, i.e., the probability that a bivariate occurrence lies in the shaded region *i*∪*ii*∪*iii* in Fig. 1*A*. For a thorough mathematical treatment, see refs. 74 and 77.

Since, for all copulas, $C_{XY}(F_X(x^*), F_Y(y^*)) \le \min\{F_X(x^*), F_Y(y^*)\}$, it turns out that both $T_{OR} < T_X$ and $T_{OR} < T_Y$. Thus, potentially hazardous bivariate OR regions are more frequent than the corresponding univariate ones. Therefore, neglecting the compounding effects of hazard drivers may result in an underestimation of the hazard when the combined action of X and Y plays a significant role.

Failure Probability Analysis. For a given design lifetime T (typically in years), let $(S_1, \ldots, S_T)$ be a sequence of relevant annual bivariate HSs (in the present case, the OR ones). In general, the corresponding failure probability p_T can be defined as

$$p_T = 1 - P\{(X_1, Y_1) \notin S_1, \ldots, (X_T, Y_T) \notin S_T\}, \quad [5]$$

equivalent to the complement of the probability that no hazardous event occurs in T years. For an OR HS, identified by a critical pair $z^* = (x^*, y^*)$, in the case of independent identically distributed occurrences, the failure probability is a monotonically increasing function of T, and is given by

$$p_T = 1 - [C_{XY}(F_X(x^*), F_Y(y^*))]^T, \quad [6]$$

representing the probability that at least one bivariate OR hazardous occurrence happens during a T-year temporal horizon (see ref. 74 for further details). As explained earlier, since $C_{XY}(F_X(x^*), F_Y(y^*)) \le \min\{F_X(x^*), F_Y(y^*)\}$, and $F_X(x^*)$ and $F_Y(y^*)$ represent the probabilities of "safe" univariate X and Y occurrences, it turns out that $p_{T,OR} \ge p_{T,X}$ and $p_{T,OR} \ge p_{T,Y}$ for all Ts, implying that OR occurrences are generally more hazardous than univariate ones.

To integrate the concept of nonstationarity to the proposed bivariate HS and failure probability estimates framework, we perturbed the annual bivariate vectors using Monte Carlo simulations exploiting the projected distribution of SLR. The details are explained in *SI Appendix*. In *Results and Discussion*, it is shown how the SLR may increase the failure probability of coastal flood defenses in the future.

1. Tessler ZD, et al. (2015) Profiling risk and sustainability in coastal deltas of the world. *Science* 349:638–643.
2. Hallegatte S, Green C, Nicholls RJ, Corfee-Morlot J (2013) Future flood losses in major coastal cities. *Nat Clim Change* 3:802–806.
3. Leonard M, et al. (2014) A compound event framework for understanding extreme impacts. *Wiley Interdiscip Rev Clim Change* 5:113–128.
4. Coles SG, Tawn JA (1994) Statistical methods for multivariate extremes: An application to structural design. *Appl Stat* 43:1–48.
5. Wahl T, Jain S, Bender J, Meyers SD, Luther ME (2015) Increasing risk of compound flooding from storm surge and rainfall for major US cities. *Nat Clim Change* 5:1093–1097.
6. Intergovernmental Panel on Climate Change (2012) *Managing the Risks of Extreme Events and Disasters to Advance Climate Change Adaption: Special Report of the Intergovernmental Panel on Climate Change*, ed Field CB (Cambridge Univ Press, New York).
7. Buschman FA, Hoitink AJF, van der Vegt M, Hoekstra P (2009) Subtidal water level variation controlled by river flow and tides. *Water Resour Res* 45:W10420.
8. Kukulka T, Jay DA (2003) Impacts of Columbia River discharge on salmonid habitat: 1. A nonstationary fluvial tide model. *J Geophys Res* 108:3293.
9. Kukulka T, Jay DA (2003) Impacts of Columbia River discharge on salmonid habitat: 2. Changes in shallow-water habitat. *J Geophys Res* 108:3294.
10. Cai H, Savenije HHG, Jiang C (2014) Analytical approach for predicting fresh water discharge in an estuary based on tidal water level observations. *Hydrol Earth Syst Sci* 18:4153–4168.
11. Cai H, Savenije HHG, Jiang C, Zhao L, Yang Q (2015) Analytical approach for determining the mean water level profile in an estuary with substantial fresh water discharge. *Hydrol Earth Syst Sci Discuss* 12:8381–8417.
12. Federal Emergency Management Agency (2015) *Guidance for Flood Risk Analysis and Mapping; Combined Coastal and Riverine Floodplain* (Fed Emergency Manage Agency, Washington, DC).
13. United States Geological Society (1981) *Guidlines for Determining Flood Flow Frequency* (US Dep Interior, Washington, DC).
14. Zervas C (2013) *Extreme Water Levels of the United States* 1893–2010 (Natl Oceanic Atmos Assoc, Silver Spring, MD).
15. Salvadori G, De Michele C (2004) Frequency analysis via copulas: Theoretical aspects and applications to hydrological events. *Water Resour Res* 40:W12511.
16. De Michele C, Salvadori G, Canossi M, Petaccia A, Rosso R (2005) Bivariate statistical approach to check adequacy of dam spillway. *J Hydrol Eng* 10:50–57.
17. Kotz S, Johnson NL, Balakrishnan N, Johnson NL (2000) *Continuous Multivariate Distributions* (Wiley, New York), 2nd Ed.
18. Svensson C, Jones DA (2002) Dependence between extreme sea surge, river flow and precipitation in eastern Britain. *Int J Climatol* 22:1149–1168.
19. Svensson C, Jones DA (2004) Dependence between sea surge, river flow and precipitation in south and west Britain. *Hydrol Earth Syst Sci* 8:973–992.
20. van den Brink HW, Können GP, Opsteegh JD, van Oldenborgh GJ, Burgers G (2005) Estimating return periods of extreme events from ECMWF seasonal forecast ensembles. *Int J Climatol* 25:1345–1354.
21. Benestad RE, Haugen JE (2007) On complex extremes: Flood hazards and combined high spring-time precipitation and temperature in Norway. *Clim Change* 85: 381–406.
22. De Michele C, Salvadori G, Passoni G, Vezzoli R (2007) A multivariate model of sea storms using copulas. *Coast Eng* 54:734–751.
23. Renard B, Lang M (2007) Use of a Gaussian copula for multivariate extreme value analysis: Some case studies in hydrology. *Adv Water Resour* 30:897–912.

24. Archetti R, Bolognesi A, Casadio A, Maglionico M (2011) Development of flood probability charts for urban drainage network in coastal areas through a simplified joint assessment approach. *Hydrol Earth Syst Sci* 15:3115–3122.
25. Gräler B, et al. (2013) Multivariate return periods in hydrology: A critical and practical review focusing on synthetic design hydrograph estimation. *Hydrol Earth Syst Sci* 17:1281–1296.
26. Kew SF, Selten FM, Lenderink G, Hazeleger W (2013) The simultaneous occurrence of surge and discharge extremes for the Rhine delta. *Nat Hazards Earth Syst Sci* 13:2017–2029.
27. Lian JJ, Xu K, Ma C (2013) Joint impact of rainfall and tidal level on flood risk in a coastal city with a complex river network: A case study of Fuzhou city, China. *Hydrol Earth Syst Sci* 17:679–689.
28. Zheng F, Westra S, Sisson SA (2013) Quantifying the dependence between extreme rainfall and storm surge in the coastal zone. *J Hydrol (Amst)* 505:172–187.
29. Chen W-B, Liu W-C (2014) Modeling flood inundation induced by river flow and storm surges over a river basin. *Water* 6:3182–3199.
30. Salvadori G, Tomasicchio GR, D'Alessandro F (2014) Practical guidelines for multivariate analysis and design in coastal and off-shore engineering. *Coast Eng* 88:1–14.
31. Salvadori G, Durante F, Tomasicchio GR, D'Alessandro F (2015) Practical guidelines for the multivariate assessment of the structural risk in coastal and off-shore engineering. *Coast Eng* 95:77–83.
32. Masina M, Lamberti A, Archetti R (2015) Coastal flooding: A copula based approach for estimating the joint probability of water levels and waves. *Coast Eng* 97:37–52.
33. Bevacqua E, Maraun D, Hobæk Haff I, Widmann M, Vrac M (2017) Multivariate statistical modelling of compound events via pair-copula constructions: Analysis of floods in Ravenna (Italy). *Hydrol Earth Syst Sci* 21:2701–2723.
34. Hawkes PJ (2006) *Use of Joint Probability Methods in Flood Management: A Guide to Best Practice* (Dep Environ Food Rural Affairs, London).
35. Hawkes PJ, Svensson C (2005) *Joint Probability: Dependence Mapping and Best Practice* (Dep Environ Food Rural Affairs, London).
36. Svensson C, Jones DA (2006) *Joint Probability: Dependence between Extreme Sea Surge, River Flow and Precipitation: A Study in South and West Britain* (Dep Environ Food Rural Affairs, London).
37. Westra S (2012) Australian Rainfall and Runoff Revision Project 18: Interaction of Coastal Processes and Severe Weather Events: Phase 2 - Pilot Study into Joint Probability Modelling of Extreme Rainfall and Storm Surge in the Coastal Zone. Available at arr.ga.gov.au/__data/assets/pdf_file/0018/40527/ARR_Project18_Stage_Report_Final.pdf. Accessed August 14, 2017.
38. Zheng F, Westra S, Leonard M (2014) Australian Rainfall and Runoff: Revision Project 18: Coincidence of Fluvial Flooding Events and Coastal Water Levels in Estuarine Areas (Stage 3 Report).
39. Intergovernmental Panel on Climate Change (2013) *Climate Change: The Physical Science Basis. Contribution of Working Group I to the Fifth Assessment Report of the Intergovernmental Panel on Climate Change* (Cambridge Univ Press, New York).
40. Hansen JE (2007) Scientific reticence and sea level rise. *Environ Res Lett* 2:024002.
41. Syvitski JPM, et al. (2009) Sinking deltas due to human activities. *Nat Geosci* 2: 681–686.
42. Hamlington BD, et al. (2014) Uncovering an anthropogenic sea-level rise signal in the Pacific Ocean. *Nat Clim Change* 4:782–785.
43. Dangendorf S, et al. (2015) Detecting anthropogenic footprints in sea level rise. *Nat Commun* 6:7849.
44. Karl TR, Trenberth KE (2003) Modern global climate change. *Science* 302:1719–1723.
45. Wallace JM, Held IM, Thompson DWJ, Trenberth KE, Walsh JE (2014) Global warming and winter weather. *Science* 343:729–730.
46. Bordbar MH, Martin T, Latif M, Park W (2015) Effects of long-term variability on projections of twenty-first century dynamic sea level. *Nat Clim Change* 5:343–347.
47. Hinkel J, et al. (2014) Coastal flood damage and adaptation costs under 21st century sea-level rise. *Proc Natl Acad Sci USA* 111:3292–3297.
48. Lentz EE, et al. (2016) Evaluation of dynamic coastal response to sea-level rise modifies inundation likelihood. *Nat Clim Change* 6:696–700.
49. Church JA, White NJ (2011) Sea-level rise from the late 19th to the early 21st century. *Surv Geophys* 32:585–602.
50. Domingues CM, et al. (2008) Improved estimates of upper-ocean warming and multi-decadal sea-level rise. *Nature* 453:1090–1093.
51. Calafat FM, Chambers DP (2013) Quantifying recent acceleration in sea level unrelated to internal climate variability. *Geophys Res Lett* 40:3661–3666.
52. Watson CS, et al. (2015) Unabated global mean sea-level rise over the satellite altimeter era. *Nat Clim Change* 5:565–568.
53. Church JA, White NJ (2006) A 20th century acceleration in global sea-level rise. *Geophys Res Lett* 33:L01602.
54. Cazenave A, et al. (2014) The rate of sea-level rise. *Nat Clim Change* 4:358–361.
55. Milne GA, Gehrels WR, Hughes CW, Tamisiea ME (2009) Identifying the causes of sea-level change. *Nat Geosci* 2:471–478.
56. Lyu K, Zhang X, Church JA, Slangen ABA, Hu J (2014) Time of emergence for regional sea-level change. *Nat Clim Change* 4:1006–1010.
57. Rahmstorf S (2007) A semi-empirical approach to projecting future sea-level rise. *Science* 315:368–370.
58. Nicholls RJ, Cazenave A (2010) Sea-level rise and its impact on coastal zones. *Science* 328:1517–1520.
59. Kopp RE, et al. (2014) Probabilistic 21st and 22nd century sea-level projections at a global network of tide-gauge sites. *Earths Future* 2:383–406.
60. Sweet W, Zervas C, Gill S, Park J (2013) Hurricane Sandy inundation probabilities today and tomorrow. *Bull Am Meteorol Soc* 94:S17–S20.
61. Sweet WV, Park J (2014) From the extreme to the mean: Acceleration and tipping points of coastal inundation from sea level rise. *Earths Future* 2:579–600.
62. Moftakhari HR, et al. (2015) Increased nuisance flooding along the coasts of the United States due to sea level rise: Past and future. *Geophys Res Lett* 42:9846–9852.
63. Vandenberg-Rodes A, et al. (2016) Projecting nuisance flooding in a warming climate using generalized linear models and Gaussian processes. *J Geophys Res Oceans* 121:8008–8020.
64. Moftakhari HR, AghaKouchak A, Sanders BF, Matthew RA (2017) Cumulative hazard: The case of nuisance flooding. *Earths Future* 5:214–223.
65. Kemp AC, Horton BP (2013) Contribution of relative sea-level rise to historical hurricane flooding in New York city: Historical hurricane flooding in New York City. *J Quat Sci* 28:537–541.
66. Vousdoukas MI, Mentaschi L, Voukouvalas E, Verlaan M, Feyen L (2017) Extreme sea levels on the rise along Europe's coasts. *Earths Future* 5:304–323.
67. Tebaldi C, Strauss BH, Zervas CE (2012) Modelling sea level rise impacts on storm surges along US coasts. *Environ Res Lett* 7:014032.
68. Buchanan MK, Oppenheimer M, Kopp RE (2017) Amplification of flood frequencies with local sea level rise and emerging flood regimes. *Environ Res Lett* 12:064009.
69. Vitousek S, et al. (2017) Doubling of coastal flooding frequency within decades due to sea-level rise. *Sci Rep* 7:1399.
70. Wahl T, et al. (2017) Understanding extreme sea levels for broad-scale coastal impact and adaptation analysis. *Nat Commun* 8:16075.
71. Buchanan MK, Kopp RE, Oppenheimer M, Tebaldi C (2016) Allowances for evolving coastal flood risk under uncertain local sea-level rise. *Clim Change* 137:347–362.
72. Guo L, et al. (2015) River-tide dynamics: Exploration of nonstationary and nonlinear tidal behavior in the Yangtze River estuary: River tidal dynamics. *J Geophys Res Oceans* 120:3499–3521.
73. Hoitink AJF, Jay DA (2016) Tidal river dynamics: Implications for deltas. *Rev Geophys* 54:240–272.
74. Salvadori G, Durante F, De Michele C, Bernardi M, Petrella L (2016) A multivariate copula-based framework for dealing with hazard scenarios and failure probabilities. *Water Resour Res* 52:3701–3721.
75. Scavia D, et al. (2002) Climate change impacts on U.S. coastal and marine ecosystems. *Estuaries* 25:149–164.
76. Idier D, Rohmer J, Bulteau T, Delvallée E (2013) Development of an inverse method for coastal risk management. *Nat Hazards Earth Syst Sci* 13:999–1013.
77. Salvadori G, De Michele C, Durante F (2011) On the return period and design in a multivariate framework. *Hydrol Earth Syst Sci* 15:3293–3305.
78. Moftakhari HR, Jay DA, Talke SA, Kukulka T, Bromirski PD (2013) A novel approach to flow estimation in tidal rivers. *Water Resour Res* 49:4817–4832.
79. Moftakhari HR, Jay DA, Talke SA, Schoellhamer DH (2015) Estimation of historic flows and sediment loads to San Francisco Bay, 1849–2011. *J Hydrol (Amst)* 529:1247–1261.
80. Moftakhari HR, Jay DA, Talke SA (2016) Estimating river discharge using multiple-tide gauges distributed along a channel. *J Geophys Res Oceans* 121:2078–2097.
81. Lanzoni S, Seminara G (1998) On tide propagation in convergent estuaries. *J Geophys Res Oceans* 103:30793–30812.
82. Salvadori G, De Michele C (2010) Multivariate multiparameter extreme value models and return periods: A copula approach. *Water Resour Res* 46:W10501.
83. Serinaldi F (2015) Dismissing return periods! *Stochastic Environ Res Risk Assess* 29: 1179–1189.
84. Ganju NK, Schoellhamer DH (2010) Decadal-timescale estuarine geomorphic change under future scenarios of climate and sediment supply. *Estuaries Coasts* 33:15–29.
85. Hinkel J, et al. (2015) Sea-level rise scenarios and coastal risk management. *Nat Clim Change* 5:188–190.
86. Dissanayake DMPK, Ranasinghe R, Roelvink JA (2012) The morphological response of large tidal inlet/basin systems to relative sea level rise. *Clim Change* 113:253–276.
87. van Maanen B, Coco G, Bryan KR, Friedrichs CT (2013) Modeling the morphodynamic response of tidal embayments to sea-level rise. *Ocean Dyn* 63:1249–1262.
88. Monbaliu J, et al. (2014) Risk assessment of estuaries under climate change: Lessons from Western Europe. *Coast Eng* 87:32–49.
89. Arns A, et al. (2017) Sea-level rise induced amplification of coastal protection design heights. *Sci Rep* 7:40171.
90. Hawkes PJ (2008) Joint probability analysis for estimation of extremes. *J Hydraul Res* 46(Suppl 2):246–256.
91. Bender J, Wahl T, Müller A, Jensen J (2016) A multivariate design framework for river confluences. *Hydrol Sci J* 61:471–482.
92. Zheng F, Westra S, Leonard M, Sisson SA (2014) Modeling dependence between extreme rainfall and storm surge to estimate coastal flooding risk. *Water Resour Res* 50:2050–2071.
93. Hao Z, Singh VP (2016) Review of dependence modeling in hydrology and water resources. *Prog Phys Geogr* 40:549–578.
94. Nelsen RB (2010) *An Introduction to Copulas* (Springer, New York), 2nd Ed.
95. Joe H (2015) *Dependence Modeling with Copulas* (CRC, Boca Raton, FL).
96. Durante F, Sempi C (2016) *Principles of Copula Theory* (CRC, Boca Raton, FL).
97. Salvadori G, De Michele C, Kottegoda N, Rosso R (2007) *Extremes in Nature: An Approach Using Copulas* (Springer, Dordrecht, The Netherlands).
98. Genest C, Favre A-C (2007) Everything you always wanted to know about copula modeling but were afraid to ask. *J Hydrol Eng* 12:347–368.
99. Salvadori G, De Michele C (2007) On the use of copulas in hydrology: Theory and practice. *J Hydrol Eng* 12:369–380.
100. Sklar A (1959) Fonctions de répartition à n dimensions et leurs marges. *Publ Inst Stat Univ Paris* 8:229–231.

Compounding Effects of Sea Level Rise and Fluvial Flooding

SUPPLEMENTARY MATERIALS

H.R. Moftakhari
Department of Civil and Environmental Engineering
University of California, Irvine (USA)

G. Salvadori
Dipartimento di Matematica e Fisica
Università del Salento, Lecce (Italy)

A. AghaKouchak
Department of Civil and Environmental Engineering
University of California, Irvine (USA)

B.F. Sanders
Department of Civil and Environmental Engineering
University of California, Irvine (USA)

R.A. Matthew
Blum Center for Poverty Alleviation
University of California, Irvine (USA)

June 20, 2017

1 Study Area and Data Resources

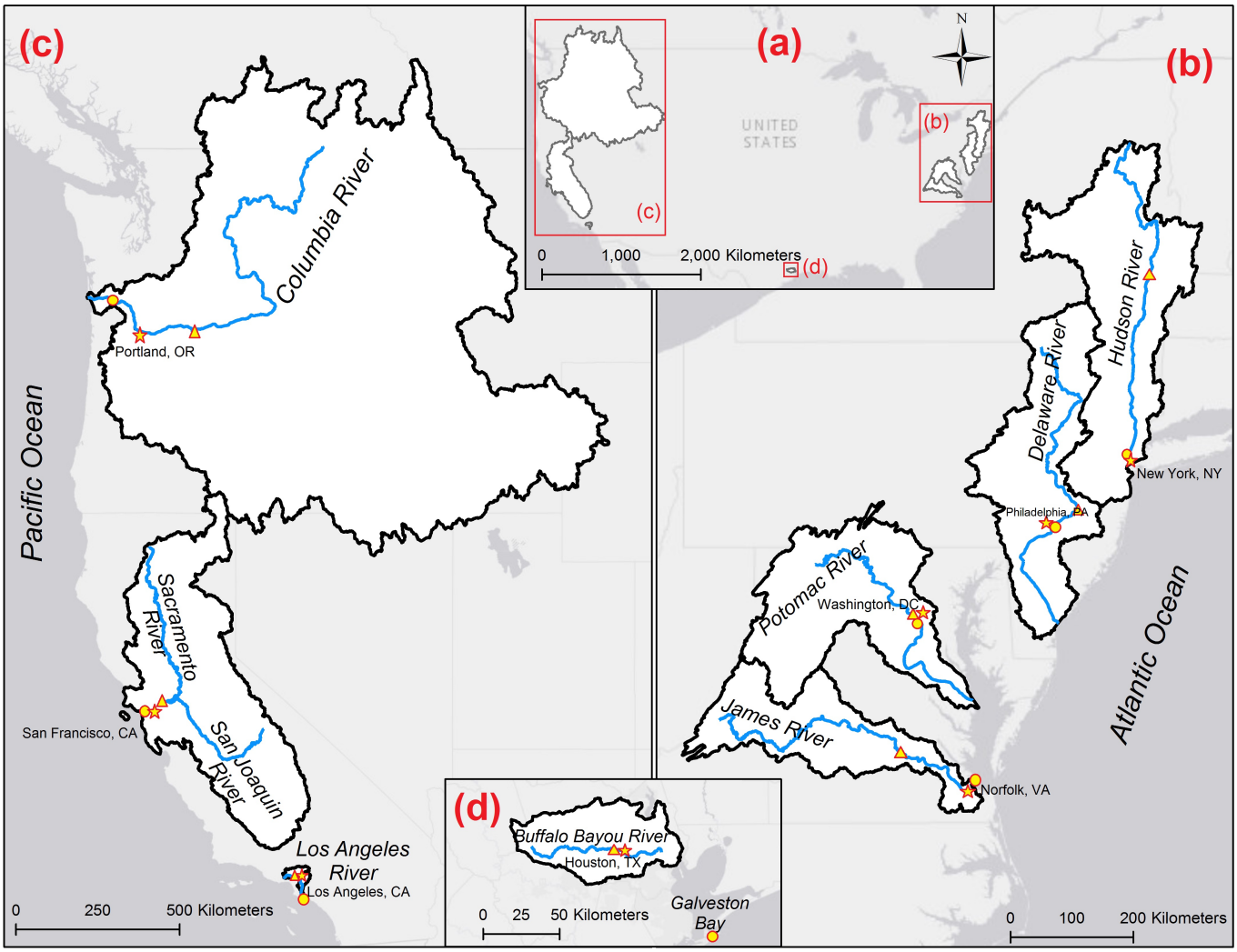

Figure SM.1: Locations of the selected coastal-estuarine systems; the white closed area show the watershed that drains freshwater into ocean at/near a tide gauge. The star, triangle, and circle marks show, respectively, the nearby major town, river flow measurement gauge, and tide gauge.

Table SM.1: Data info

Location	River Flow				Water Level		
	River Name	Measured by	Station ID	Length of Record (years)	Tide gauge	NOAA ID	Length of Record (years)
Houston, TX	Buffalo Bayou	USGS	08073500	70	Galveston	8771450	70
Los Angeles, CA	Los Angeles	USGS	11092450	84	Los Angeles	9410660	91
New York, NY	Hudson	USGS	01335754	128	Battery	8518750	89
Norfolk, VA	James	USGS	02037500	81	Sewells point	8638610	88
Philadelphia, PA	Delaware	USGS	01463500	103	Philadelphia	8545530	103
Portland, OR	Columbia	USGS	14105700	137	Astoria	9439040	90
San Francisco, CA	Delta Outflow	CDWR	Net Delta Outflow Index	85	San Francisco	9414290	157
Washington, DC	Potomac	USGS	01646500	85	Washington	8594900	84

Table SM.2: Previous studies on bivariate flood hazard analysis on a Country base

Study	Region	Variables	Method
Hawkes et al. [2002]	UK	Waves/Water level	Bivariate Normal and Empirical Copulas
Svensson and Jones [2002]	UK	Storm Surge/River Flow	Bivariate Extreme Value
Svensson and Jones [2004]	UK	Storm Surge/River Flow/Precipitation	Bivariate Extreme Value
Lamb et al. [2010]	UK	River Flow/Sea Level	Conditional Exceedence
Chini and Stansby [2012]	UK	Waves	Gumbel Copulas
Zheng et al. [2013]	Australia	Storm Surge/Precipitation	Bivariate Extreme Value
Zheng et al. [2014]	Australia	Storm Surge/Precipitation	Bivariate Extreme Value
Zheng et al. [2015b]	Australia	Storm Surge/Precipitation	Design Variable
Zheng et al. [2015a]	Australia	Storm Surge/Precipitation	Design Variable
van den Hurk et al. [2015]	Netherlands	Storm Surge/Precipitation	Physical Model Ensembles
Kew et al. [2013]	Netherlands	Storm Surge/River Flow	Physical Model Ensembles
Klerk et al. [2015]	Netherlands	Storm Surge/River Flow	Joint Tail Dependence
Li et al. [2014a]	Netherlands	Wave variables	Copulas and logistic models
Li et al. [2014b]	Netherlands	Wave variables	Copulas
De Michele et al. [2007]	Italy	Storm Surge Parameters	Vine Copulas
Salvadori et al. [2014]	Italy	Storm Surge Parameters	Khoudraji-Liebscher Copulas
Salvadori et al. [2015]	Italy	Storm Surge Parameters	Khoudraji-Liebscher Copulas and Struct function
Gouldby et al. [2014]	Spain	Offshore sea condition data	multivariate extremes model
Rueda et al. [2016]	Spain	Wave height, wave period, storm surge	Gaussian Copula
Wahl et al. [2012]	Germany	Storm Surge Height and Intensity	Archimedean Copulas
Bender et al. [2016]	Germany	River Flows	Archimedean Copulas
Lian et al. [2013]	China	Precipitation/Tidal Level	Elliptical and Archimedean Copulas
Corbella and Stretch [2012]	South Africa	Storm Parameters	Archimedean Copulas
Corbella and Stretch [2013]	South Africa	Storm Surge Parameters	Archimedean Copulas
Serafin and Ruggiero [2014]	USA	Wave, tide, non-tidal residuals	Conditional dependence
Wahl et al. [2015]	USA	Storm Surge/Precipitation	Extreme Value and Archimedean Copulas
Wahl et al. [2016]	USA	Wave/Water Level	Elliptical Copulas

2 Univariate Analysis

Each sub-section contains the following plots concerning the gauge site indicated by the sub-section name: namely, Houston, Los Angeles, New York, Norfolk, Philadelphia, Portland, San Francisco, and Washington. The variables considered are:

- $\mathbf{X}$: River flow (discharge), in m^3/s [left column];
- $\mathbf{Y}$: Water level, in m [right column].

The number of Bootstrap iterations is $B = 1000$. The legend of the figures is as follows.

1st row. Estimates of the AIC (Akaike Information Criterion) statistics, for all the distributions considered: viz., from left to right, Birnbaum-Saunders (BS), Exponential (Exp), Gamma (Gam), Generalized Extreme Value (GEV), Generalized Pareto (GP), Inverse Gaussian (InvG), Loglogistic (LogL), Lognormal (LogN), and Weibull (Weib). The *black* bar indicates the probability law selected via the AIC, i.e. the one yielding the smallest AIC statistics.

2nd row. Bootstrap estimates of the approximate p-Value of the Kolmogorov-Smirnov Goodness-of-Fit test, for all the univariate distributions considered. The *black* bar indicates the probability law selected via the AIC, and the horizontal *dashed* line the critical 5% level. A distribution is considered as admissible, at a 5% level, only if the corresponding p-Value is larger than 5%

3rd row. Empirical distribution function of the available data (*markers*) and corresponding fit (*solid* line) using the distribution selected via the AIC. The *dashed* lines indicate a 95% bootstrap confidence band.

4th row. Empirical distribution function of the available data (*markers*) and corresponding fit (*solid* line) using the GEV distribution. The *dashed* lines indicate a 95% bootstrap confidence band. In this work, only the GEV distribution is used, independently of the indications provided by the AIC procedure.

2.1 Houston, TX

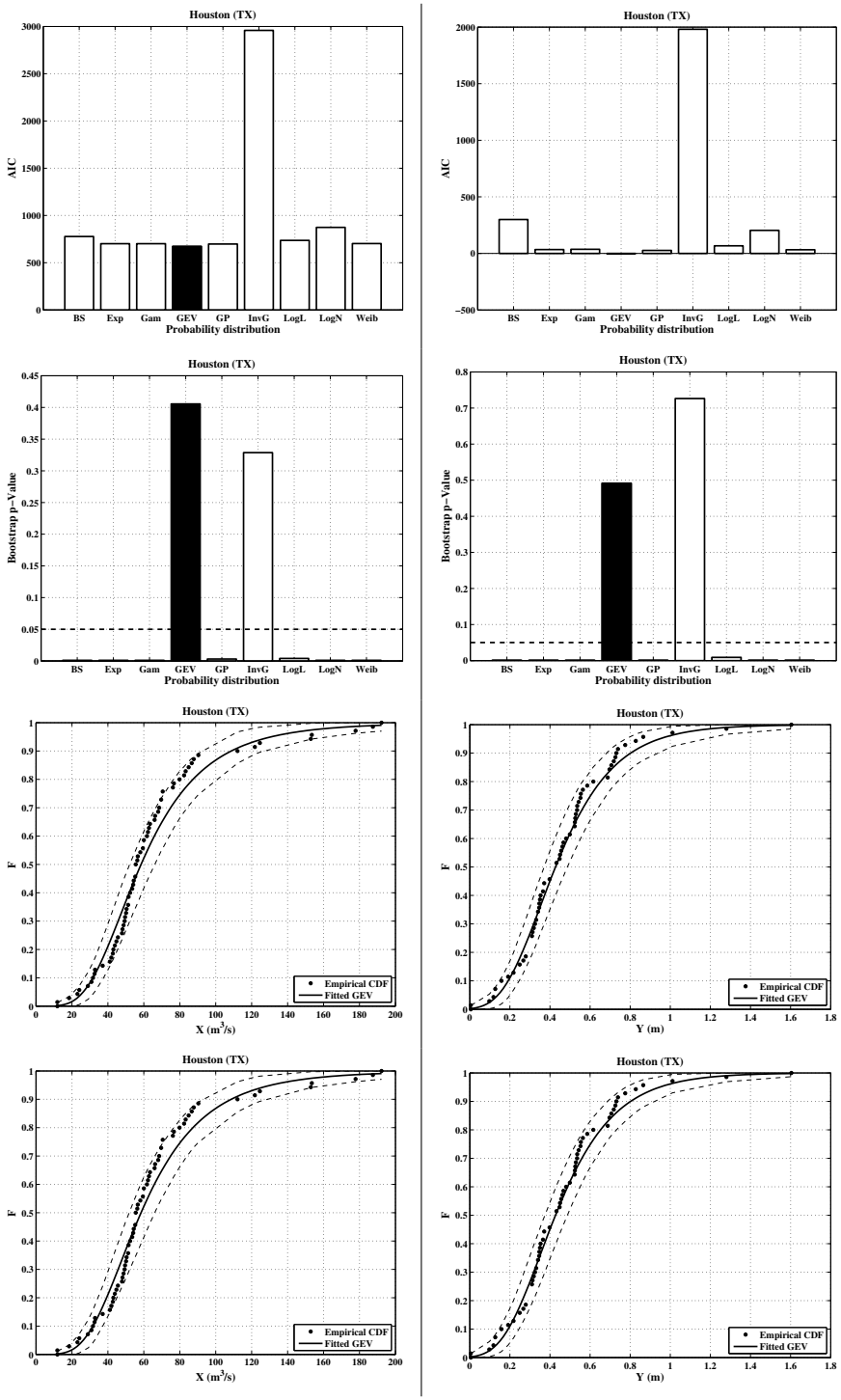

Figure SM.2: see text for explanation.

2.2 Los Angeles, CA

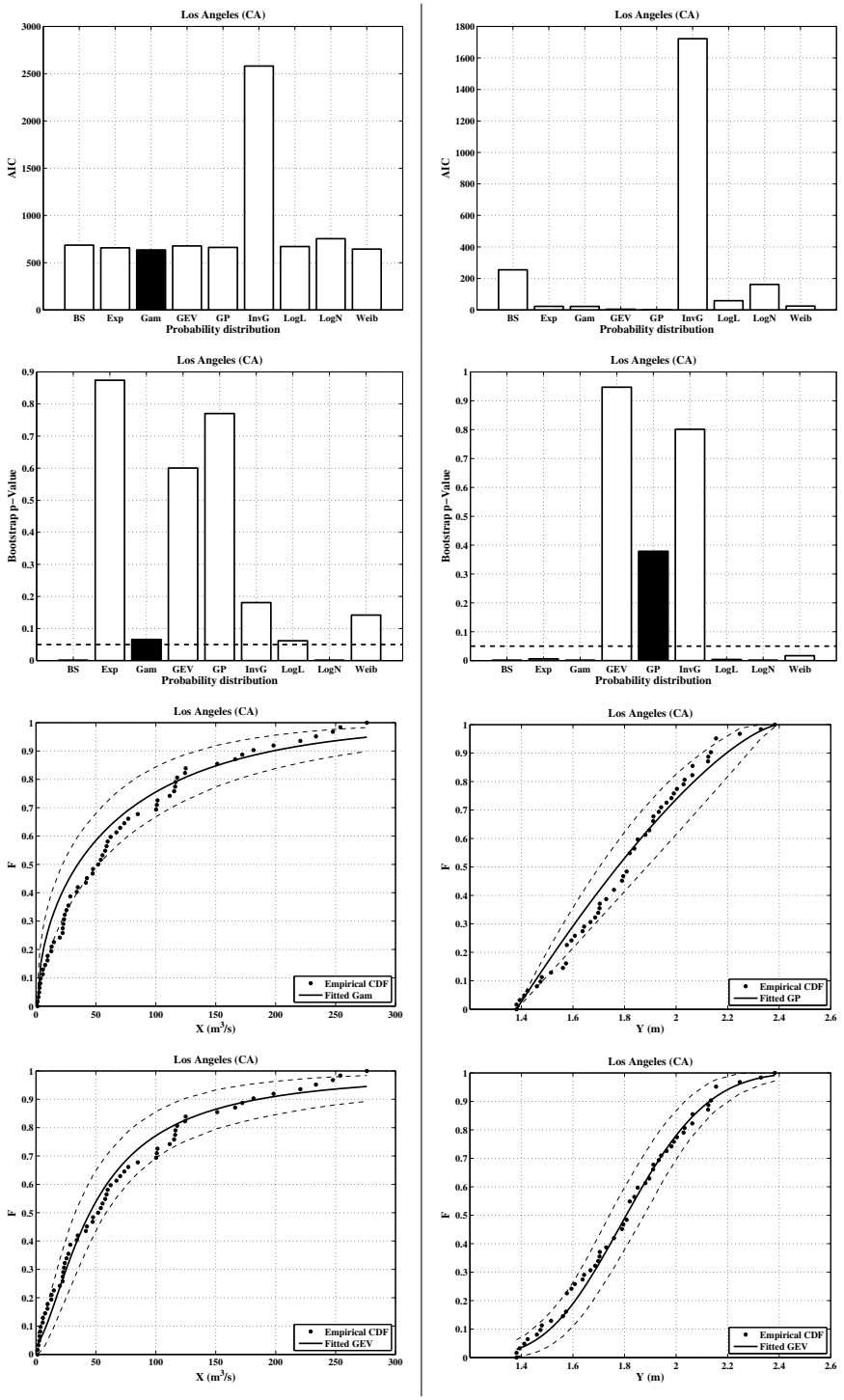

Figure SM.3: see text for explanation.

2.3 New York, NY

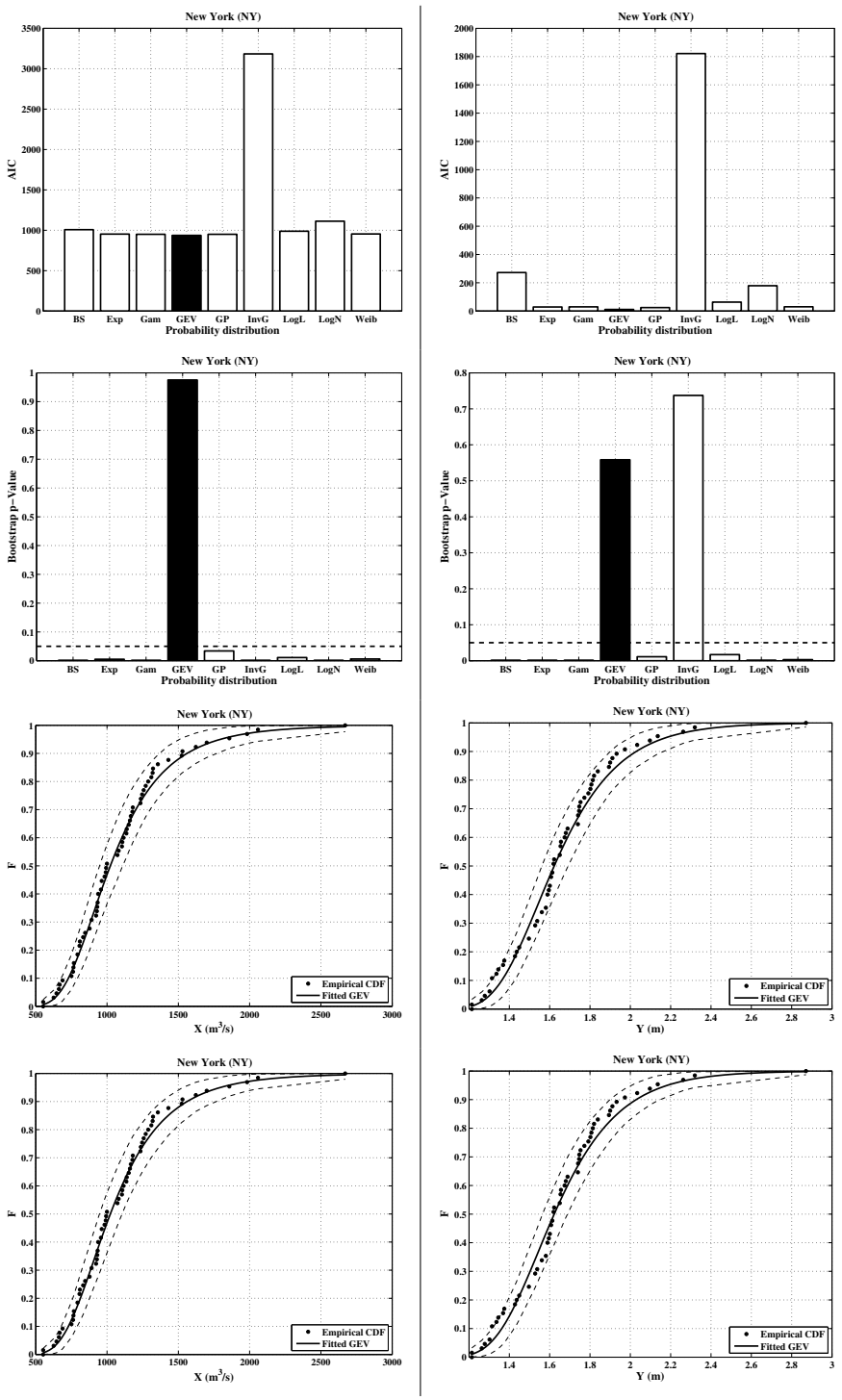

Figure SM.4: see text for explanation.

2.4 Norfolk, VA

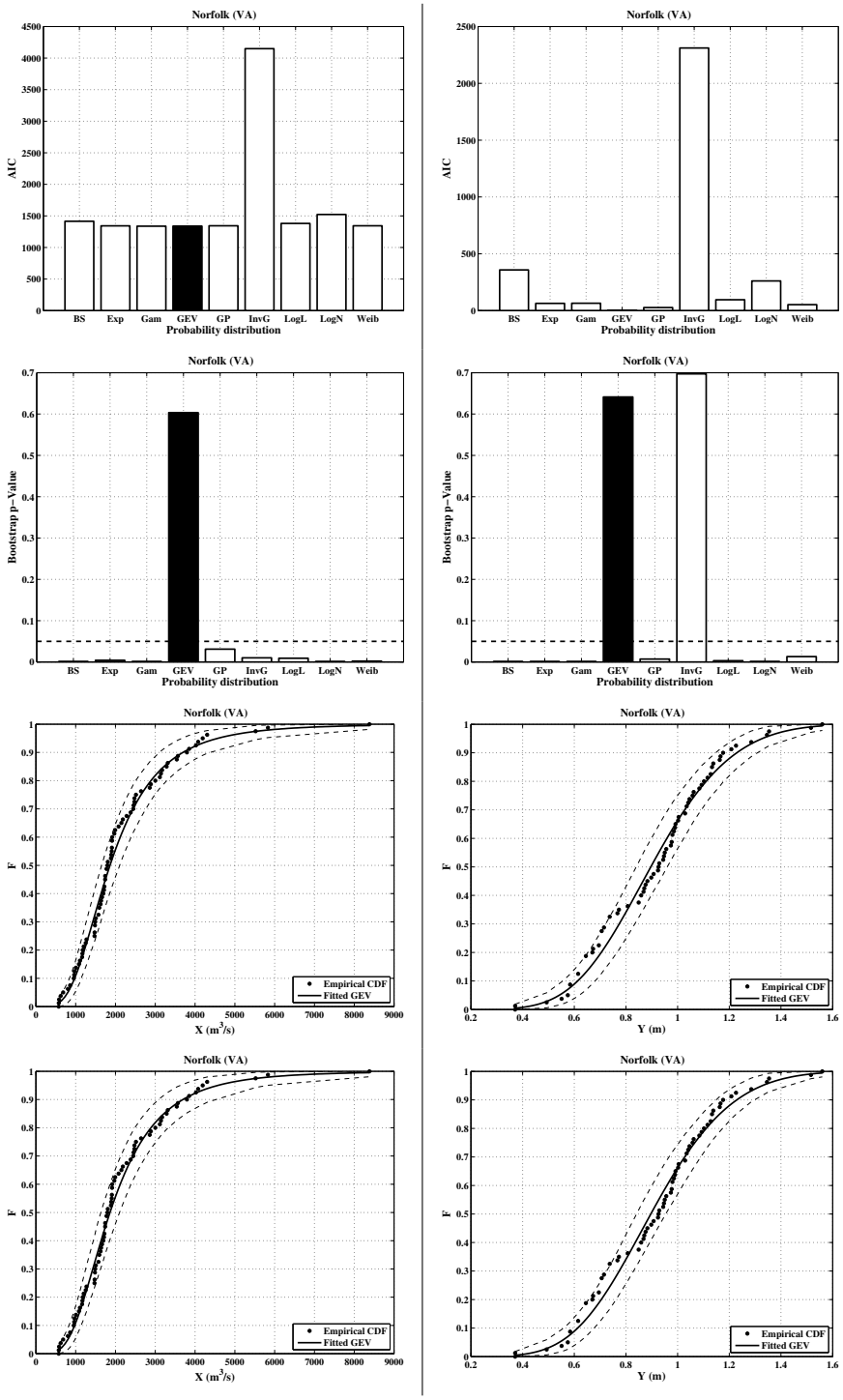

Figure SM.5: see text for explanation.

2.5 Philadelphia, PA

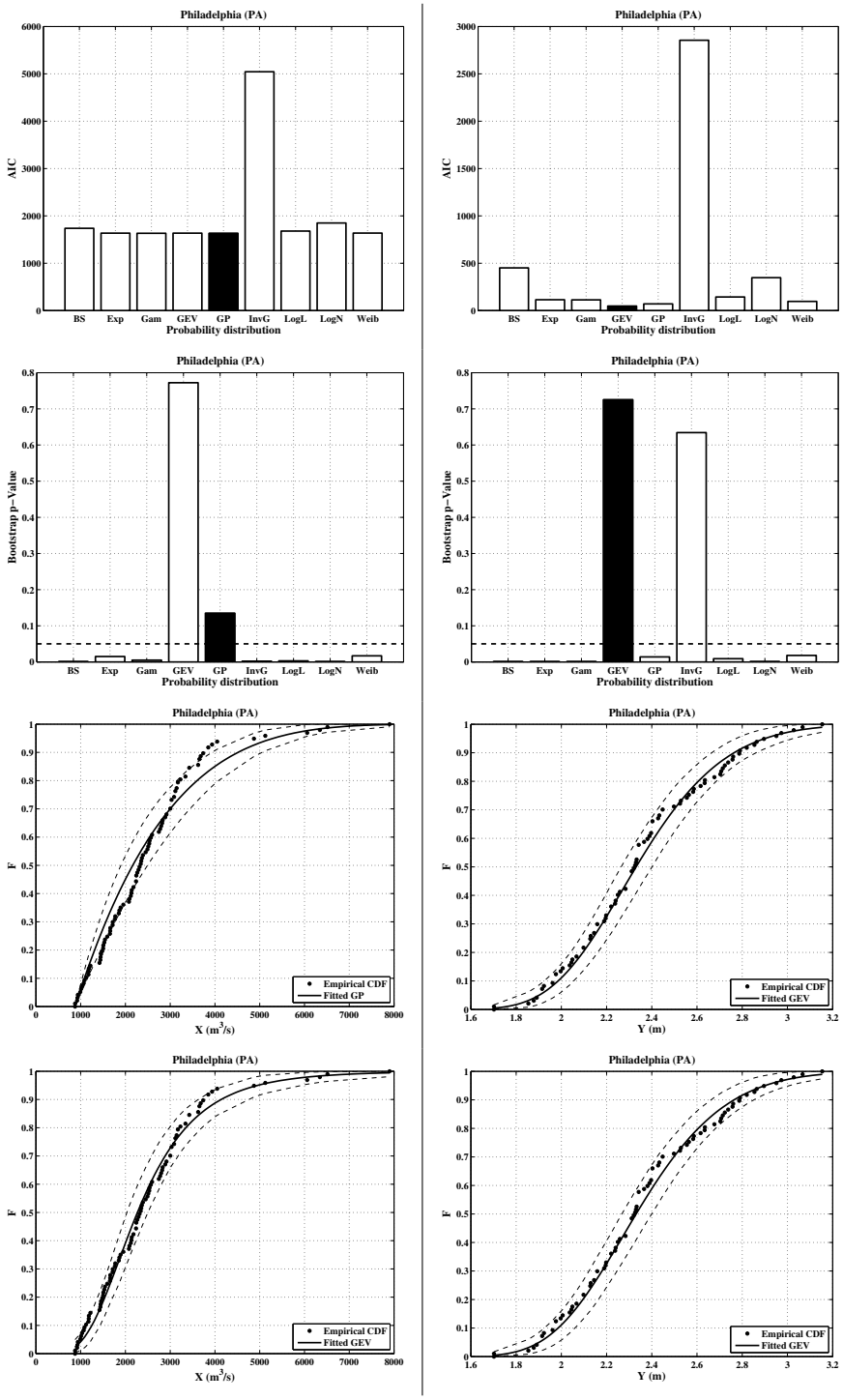

Figure SM.6: see text for explanation.

2.6 Portland, OR

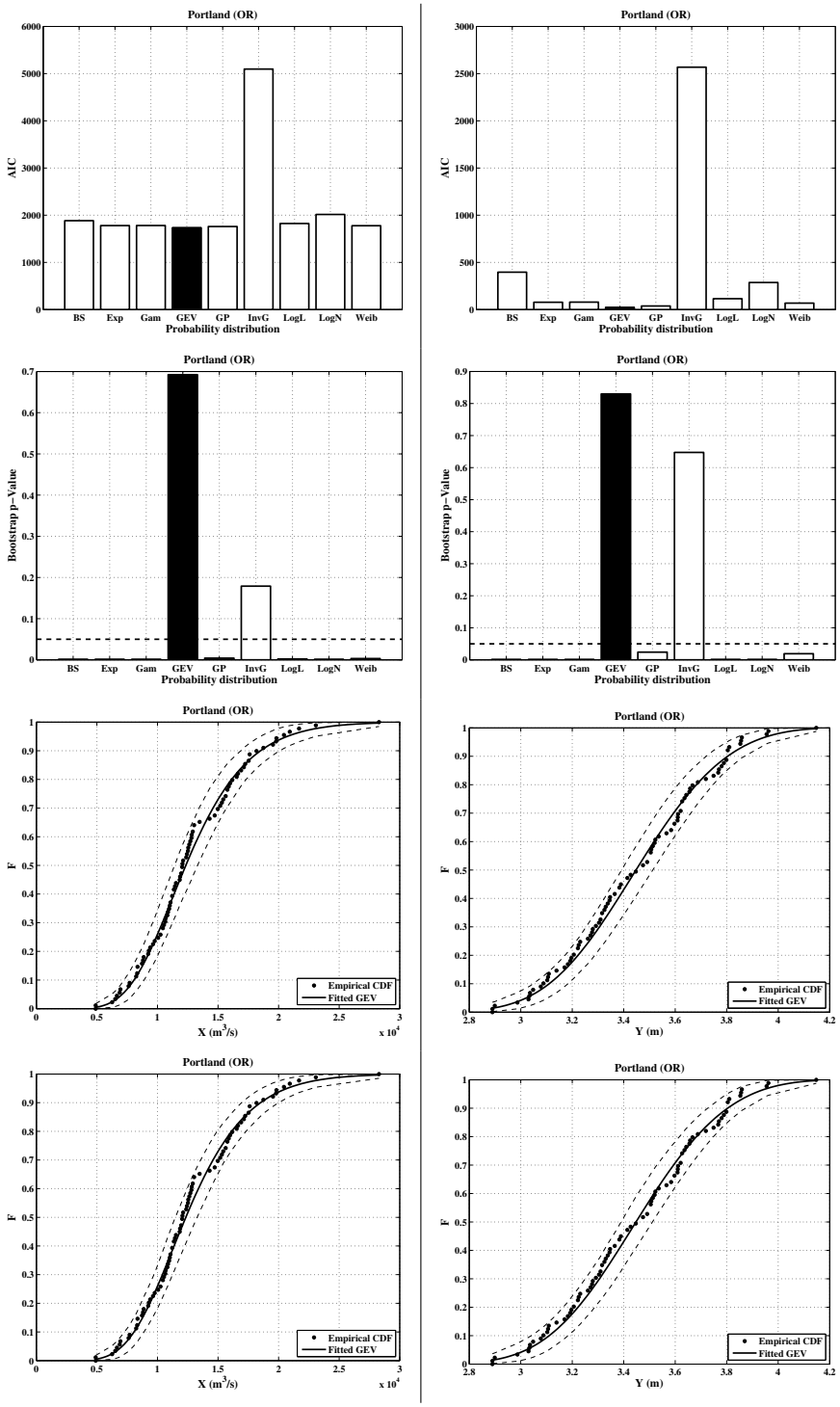

Figure SM.7: see text for explanation.

2.7 San Francisco, CA

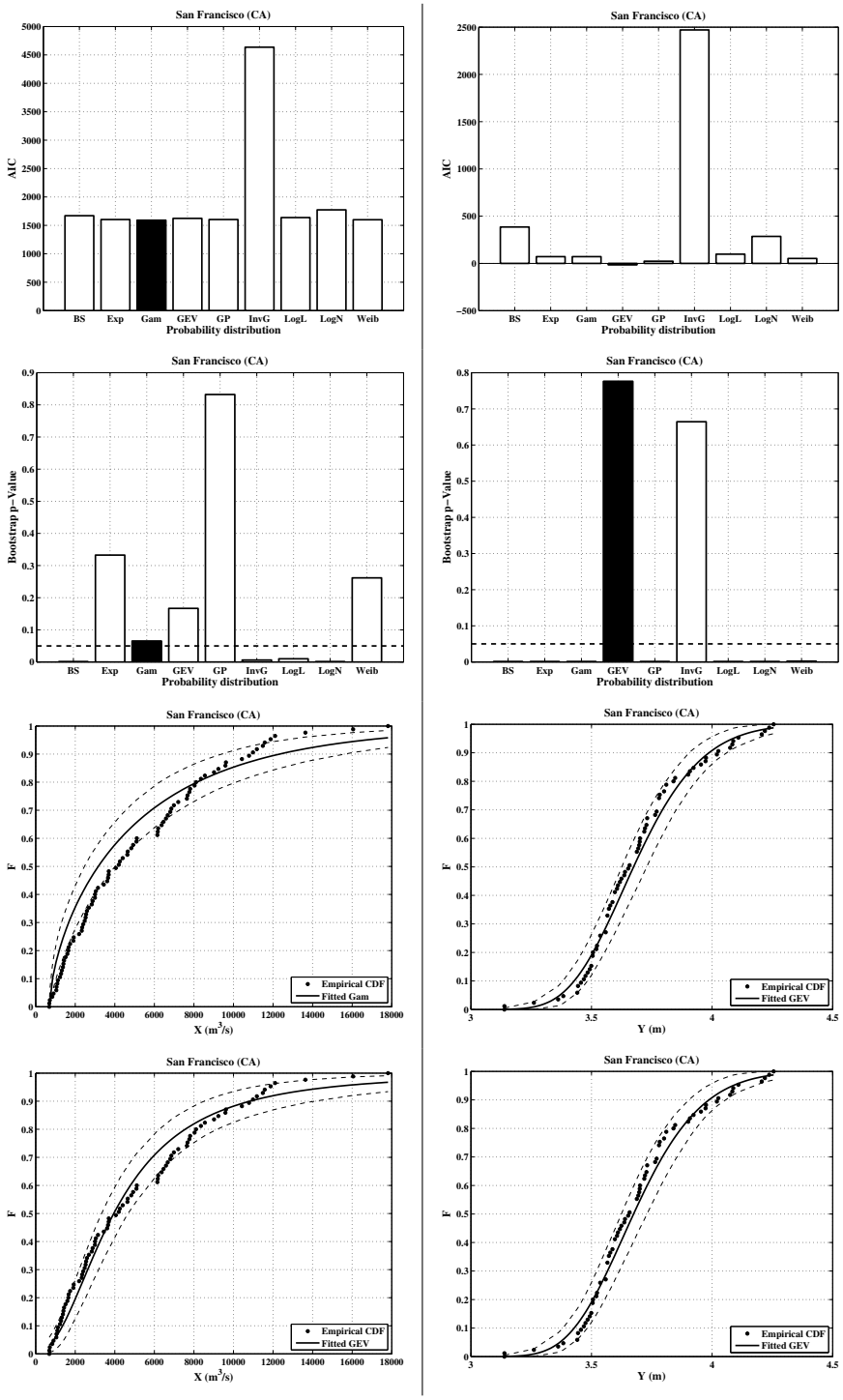

Figure SM.8: see text for explanation.

2.8 Washington, DC

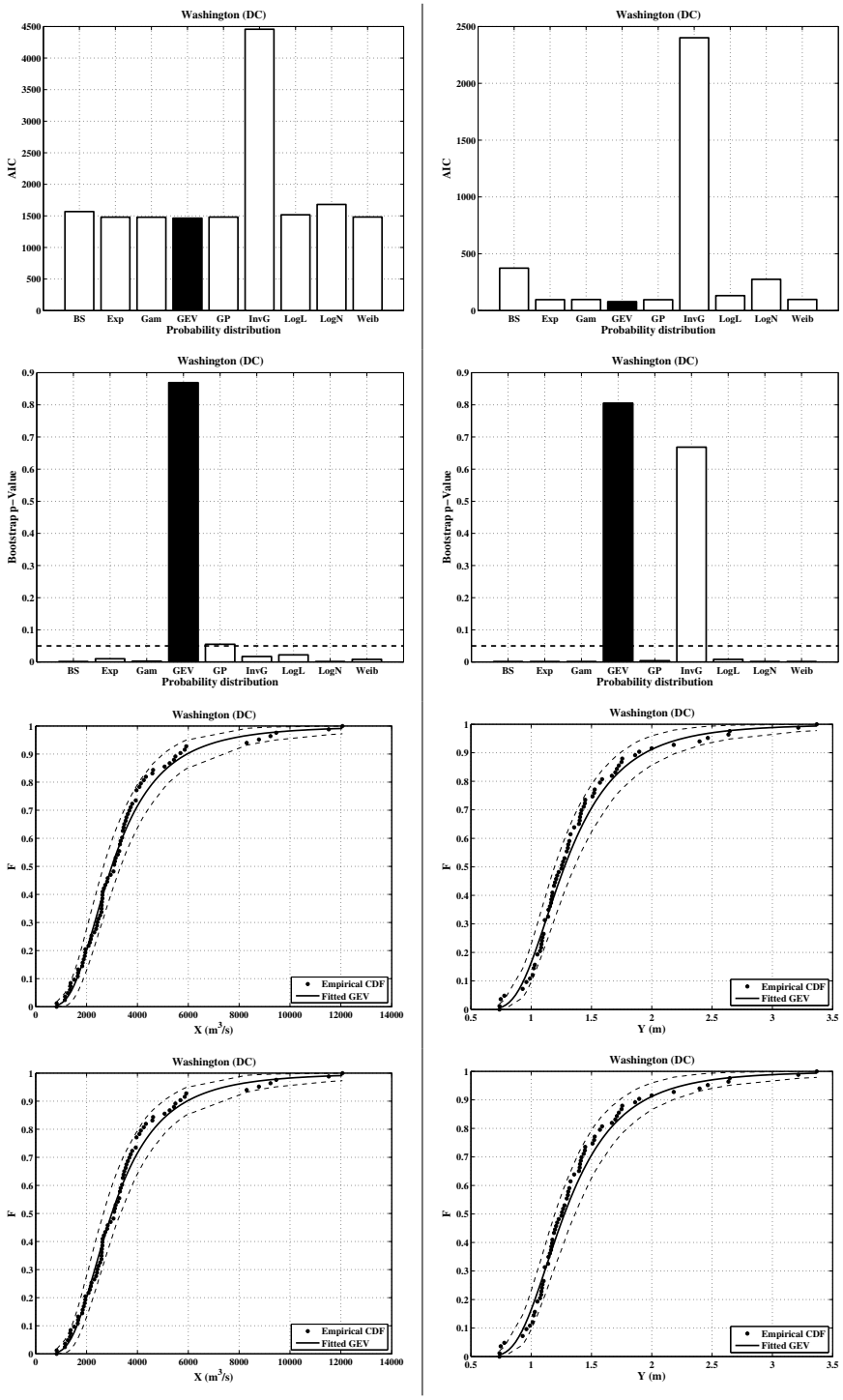

Figure SM.9: see text for explanation.

3 Bivariate Analysis: Kendall τ & Spearman ρ

The estimates of the Kendall τ and the Spearman ρ rank correlation coefficients [Lehman et al., 2005] are computed for the eight sites considered: namely, Houston, Los Angeles, New York, Norfolk, Philadelphia, Portland, San Francisco, and Washington — in the plots, these are abbreviated as Hou, LA, NY, Nfk, Phi, Por, SF, and Wsh. Also shown are the p-Values of the corresponding independence tests: values larger than 5% indicate that (at a 5% level) the null assumption that X and Y are independent cannot be rejected — the 5% level is indicated by a *dashed* line. Apparently, Philadelphia, San Francisco, and Washington data show some statistically significant dependence.

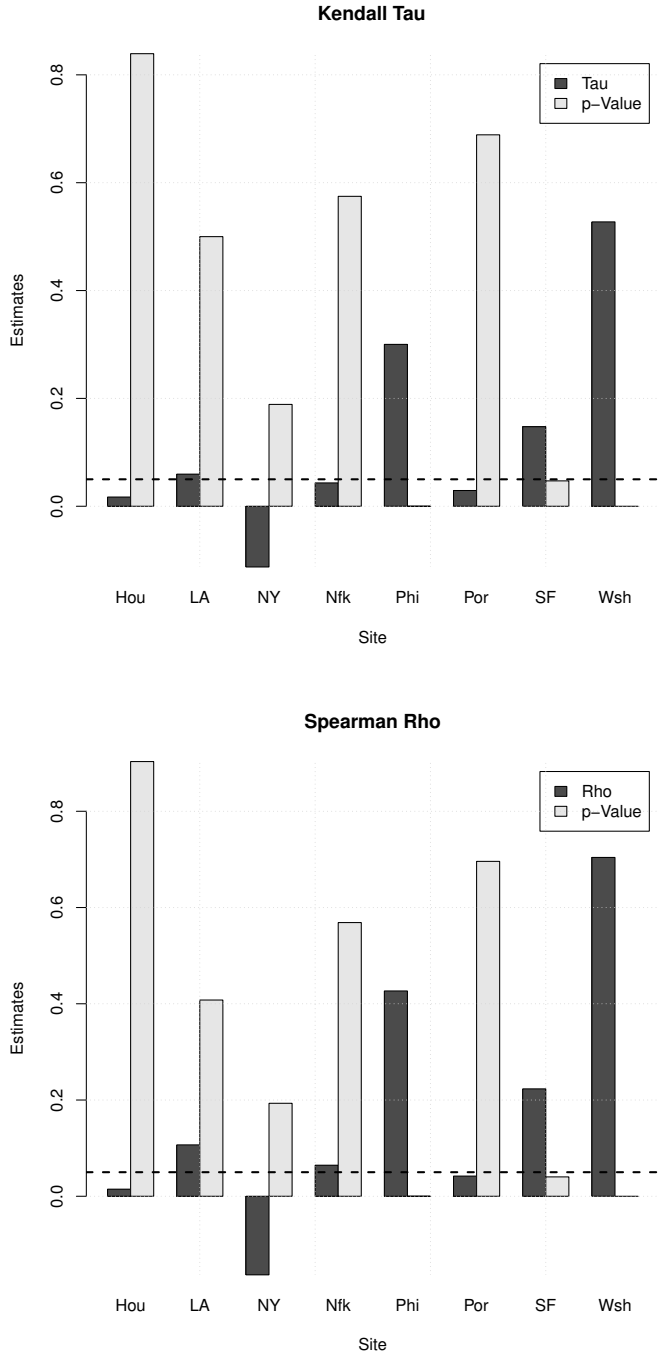

Figure SM.10: see text for explanation.

4 Bivariate Analysis: fits

As a result of the univariate analyses, the Generalized Extreme Value (GEV) distribution turns out to adequately fit the marginal distributions of the two variables of interest here. Indeed, the corresponding approximate bootstrap p-Values are always larger than 5% (see the statistical results shown in Section 2 in this Supplementary Materials, and Figures SM.2–SM.9).

Concerning the bivariate analysis, suitable non-parametric independence tests (i.e., the Kendall and the Spearman ones shown in Section 3) indicate that only for three, out of the eight stations considered, the independence assumption can be rejected: viz., Philadelphia, San Francisco, and Washington. In these cases, several bivariate copulas (12), as well as the corresponding survival copulas (for a total of 24 copulas), are fitted to the available data. The survival copulas are denoted by a "s"-prefix before the names/abbreviations of the dependence structures of interest.

The families of copulas considered here are as follows.

Archimedean: Ali-Mikhail-Haq, Clayton, Frank, Gumbel, Joe — in the plots, these are abbreviated as A, Cl, Fr, Gb, J.

Elliptical: Normal, t-Student — in the plots, these are abbreviated as N, t.

Extreme Value: Galambos, Husler-Reiss, Tawn [the Gumbel and t-Student Extreme Value copulas have already been considered] — in the plots, these are abbreviated as Gs, HR, Tw.

Farlie-Gumbel-Morgenstern: Farlie-Gumbel-Morgenstern — in the plots, it is abbreviated as M.

Plackett: Plackett — in the plots, it is abbreviated as P.

Using the R-package "copula" [Hofert et al., 2016], all these 24 copulas were tested, and those who passed suitable non-parametric Goodness-of-Fit tests (available in the package) were compared via a standard Akaike criterion, in order to select the "best" model among the ones considered. In turn, the following families are chosen: Tawn (Philadelphia), Survival Ali-Mikhail-Haq (San Francisco), and Survival Clayton (Washington). For all the other stations, the assumption of independent discharge and water level cannot be rejected at a standard 5% level, and the copula $\Pi_2(u, v) = uv$ modeling independent variables is used.

According to the results of the Kendall τ and the Spearman ρ independence tests shown in Section 3, different figures are plotted. On the one hand, if X and Y are assumed to be independent, then only the data are plotted, as well as the pseudo-observations (i.e., the normalized ranks), the isolines of the Empirical Copula (viz., a non-parametric estimate of the copula at play), and the isolines of the copula Π_2 (labeled "Prod." in the legends) corresponding to the case of independent variables. On the other hand, if X and Y show possible dependence, then the following plots are presented:

- the estimates of the AIC (Akaike Information Criterion) statistics for copula selection: the family associated with the smaller AIC value should be chosen;
- the estimates of the p-Values of a copula Cramér-von Mises Goodness-of-Fit test — the critical 5% level is indicated by a *dashed* line: copula families associated with p-Values smaller than the critical level should not be considered;
- the data;
- the pseudo-observations, the isolines of the Empirical Copula, and the isolines of the copula selected via the AIC.

4.1 Houston, TX

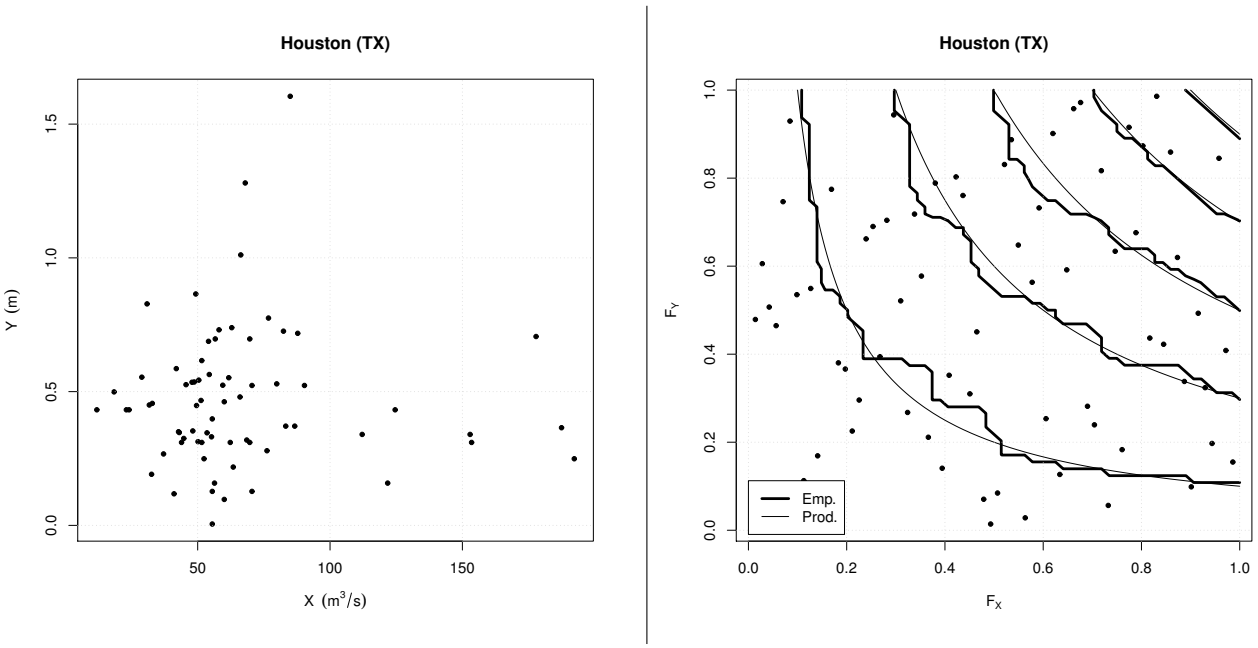

Figure SM.11: see text for explanation.

4.2 Los Angeles, CA

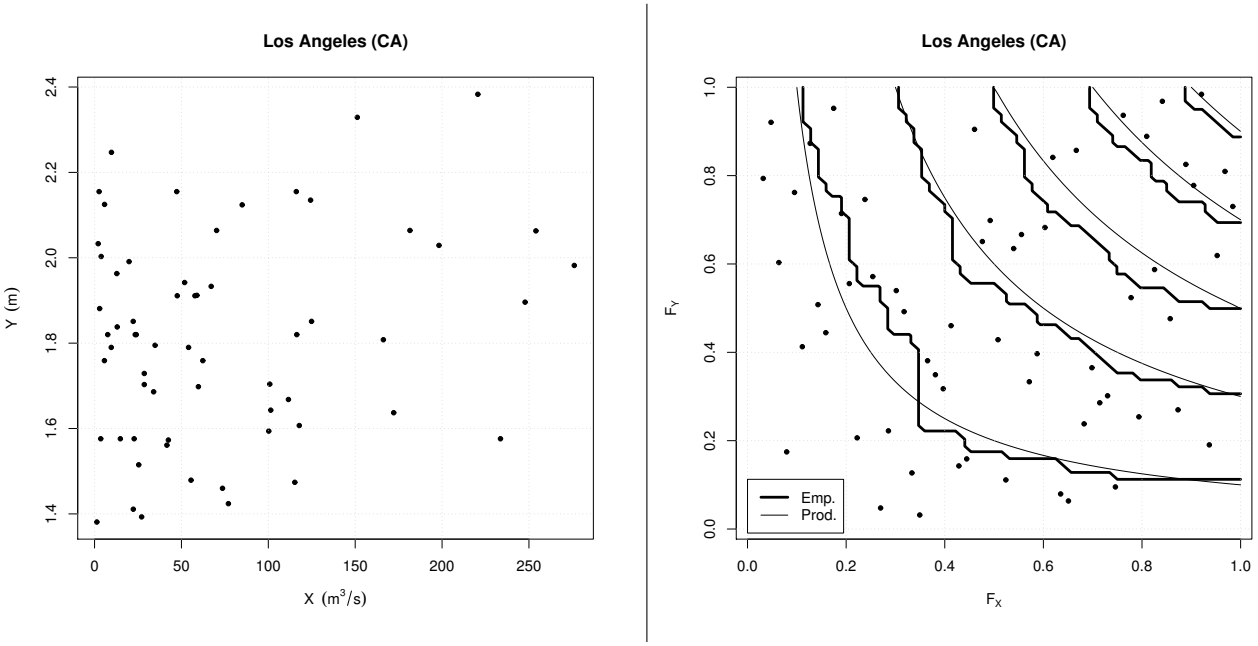

Figure SM.12: see text for explanation.

4.3 New York, NY

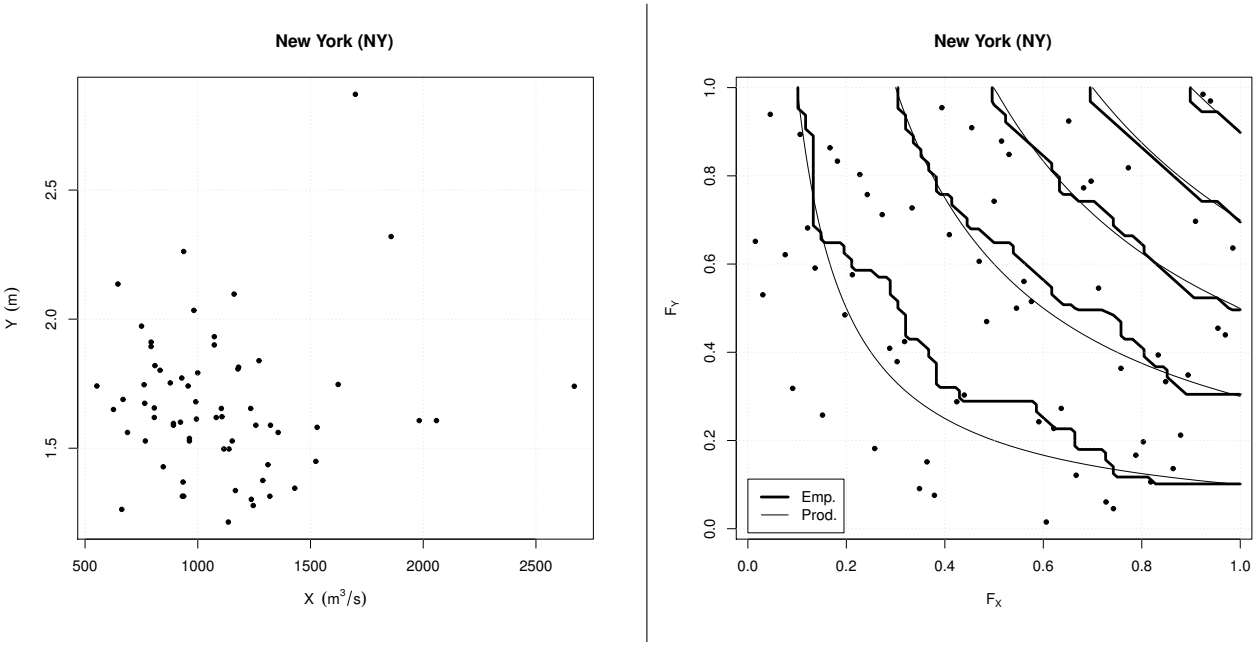

Figure SM.13: see text for explanation.

4.4 Norfolk, VA

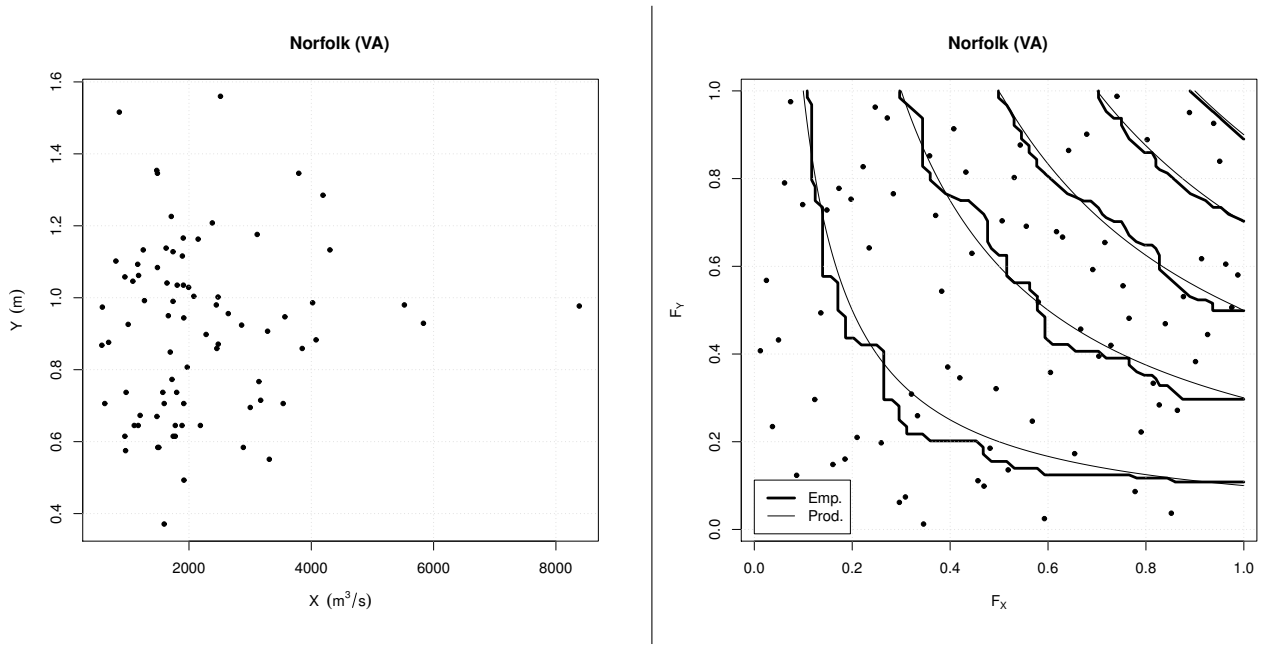

Figure SM.14: see text for explanation.

4.5 Philadelphia, PA

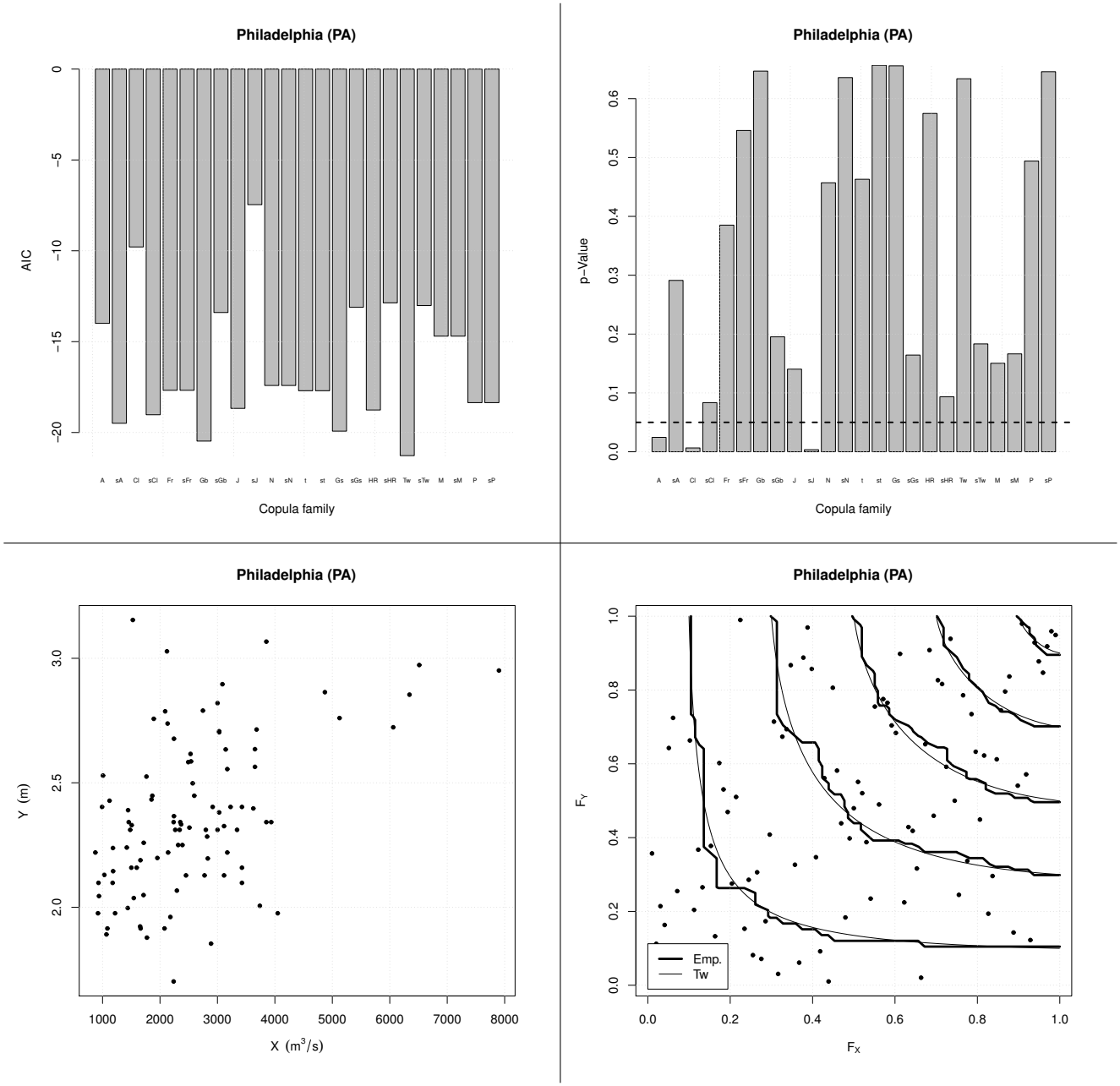

Figure SM.15: see text for explanation.

4.6 Portland, OR

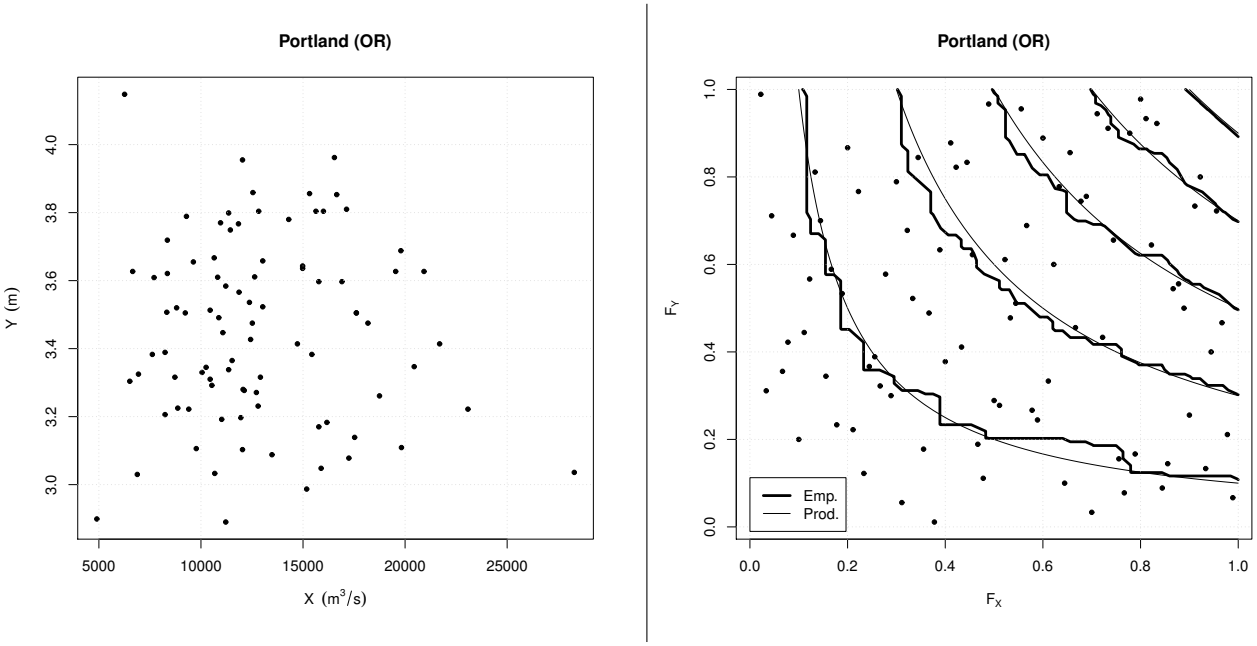

Figure SM.16: see text for explanation.

4.7 SanFrancisco, CA

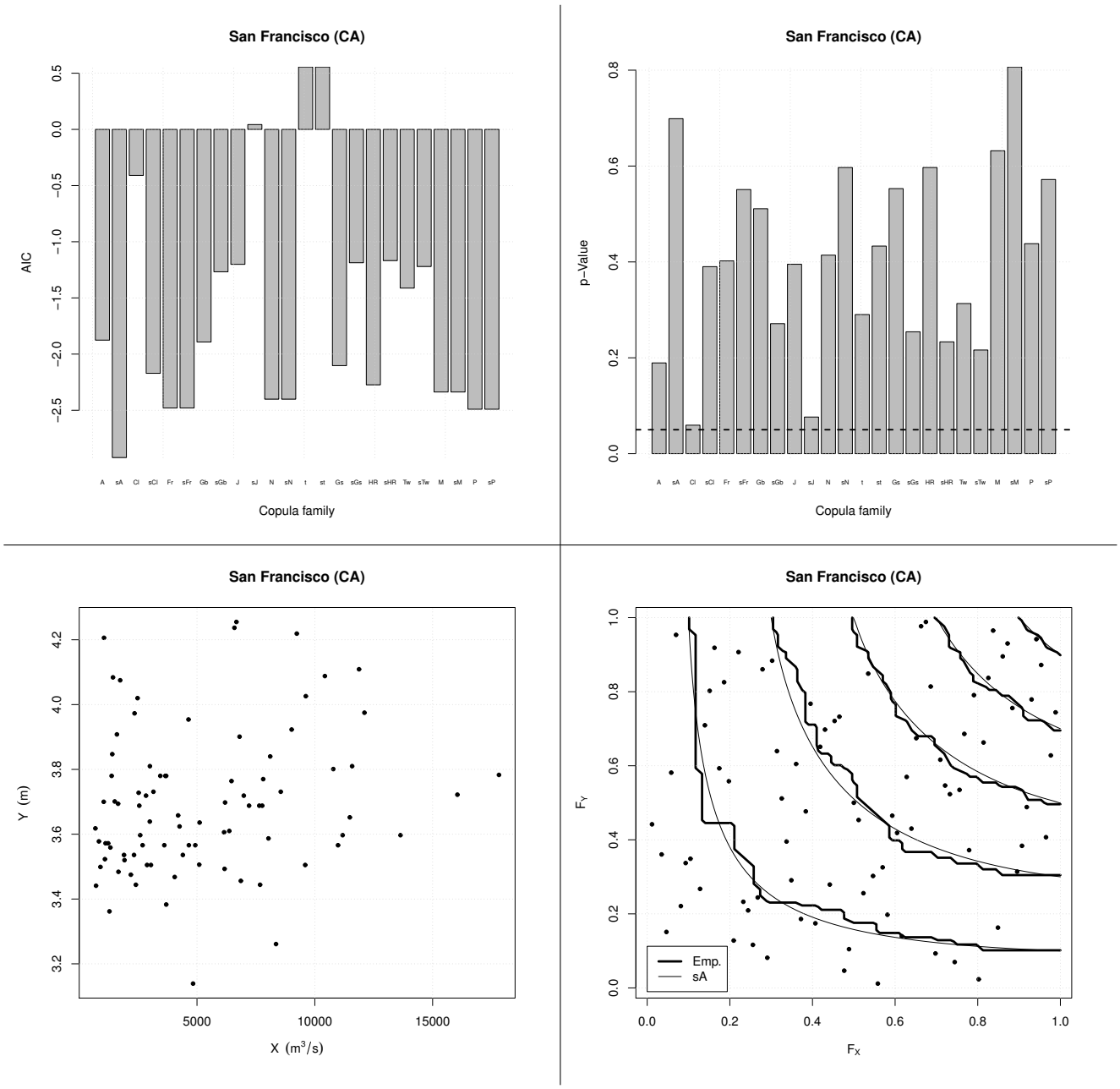

Figure SM.17: see text for explanation.

4.8 Washington, DC

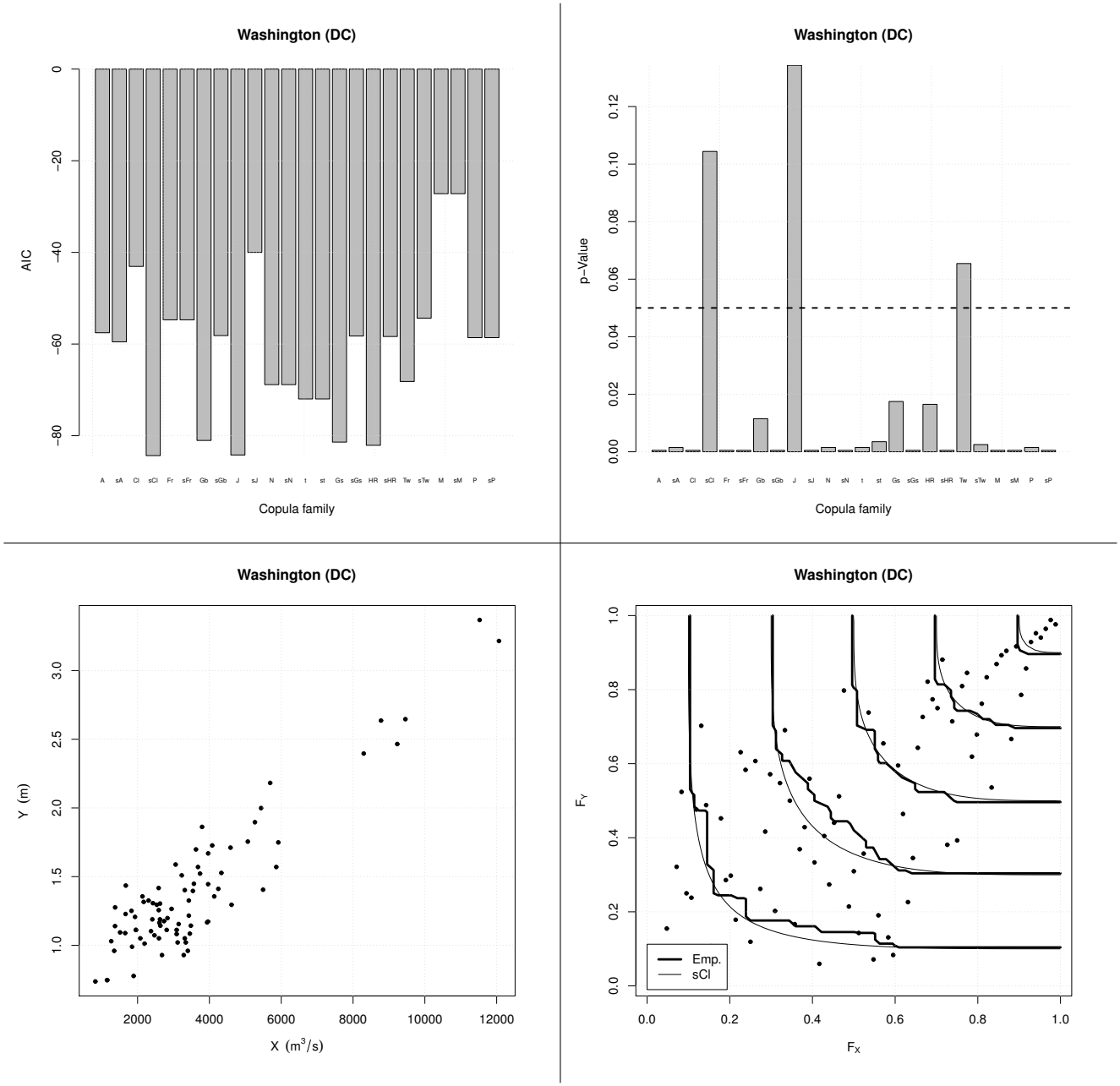

Figure SM.18: see text for explanation.

5 Bivariate Analysis: Return Period

For all the eight sites of interest (viz., Houston, Los Angeles, New York, Norfolk, Philadelphia, Portland, San Francisco, and Washington), four different Hazard Scenarios (HS) are considered (for further details see Salvadori et al. [2016]). Each scenario is identified via a pair of critical values (x^*, y^*) given by, respectively:

HS #1: a 80% percentile threshold is chosen, yielding

- x^*: quantile of order $p_X^* = 0.8$ of the distribution F_X fitted over the X data;
- y^*: quantile of order $p_Y^* = 0.8$ of the distribution F_Y fitted over the Y data.

HS #2: a 90% percentile threshold is chosen, yielding

- x^*: quantile of order $p_X^* = 0.9$ of the distribution F_X fitted over the X data;
- y^*: quantile of order $p_Y^* = 0.9$ of the distribution F_Y fitted over the Y data.

HS #3: a 95% percentile threshold is chosen, yielding

- x^*: quantile of order $p_X^* = 0.95$ of the distribution F_X fitted over the X data;
- y^*: quantile of order $p_Y^* = 0.95$ of the distribution F_Y fitted over the Y data.

HS #4: a 98% percentile threshold is chosen, yielding

- x^*: quantile of order $p_X^* = 0.98$ of the distribution F_X fitted over the X data;
- y^*: quantile of order $p_Y^* = 0.98$ of the distribution F_Y fitted over the Y data.

In Figure SM.19, the pair of critical values (x^*, y^*) is plotted as a red circle, and the corresponding univariate HS's for X and Y are indicated on, respectively, the horizontal and the vertical axes, by a green and a blue thick line.

The pair (x^*, y^*) also identifies an (inclusive) OR Hazard Scenario, plotted as a shaded region in Figure SM.19, given by the union of the three sub-regions A, B, and C: from a physical point of view, it is enough that one of the two variables be larger than the corresponding univariate critical threshold in order to get, say, a "dangerous" situation.

In the present annual framework, the general formula for calculating the RP T associated with a given HS is given by [Salvadori et al., 2011]

$$T = 1/\mathbf{P}(\text{HS}), \tag{1}$$

where $\mathbf{P}(\text{HS})$ is the probability of the HS of interest, viz. the probability that a realization of the phenomenon under investigation takes place in the given HS. In turn, in the univariate case, Eq. (1) reduces to the standard formulas

$$T_{X,x^*} = 1/(1 - F_X(x^*)) = 1/(1 - p_X^*)$$

and

$$T_{Y,y^*} = 1/(1 - F_Y(y^*)) = 1/(1 - p_Y^*),$$

while in the OR case the bivariate Return Period is given by

$$T_{OR,(x^*,y^*)} = 1/(1 - F_{XY}(x^*, y^*)) = 1/(1 - C_{XY}(F_X(x^*), F_Y(y^*))) = 1/(1 - C_{XY}(p_X^*, p_Y^*)),$$

where C_{XY} is the copula modeling the joint random behavior of the pair (X, Y).

It is worth noting that, in the present annual framework, the chosen univariate quantiles correspond to, respectively, univariate Return Periods (RP) of 5, 10, 20, and 50 years for both the variables X (river flow) and Y (water level) of interest here, since $p_X^* = p_Y^*$. Furthermore, should the variables X and Y be independent, then $F_{XY} = F_X \cdot F_Y$. In turn,

$$T_{OR,(x^*,y^*)} = 1/(1 - F_X(x^*) \cdot F_Y(y^*)) = 1/(1 - p_X^* \cdot p_Y^*),$$

yielding both $T_{OR,(x^*,y^*)} \leq T_{X,x^*}$ and $T_{OR,(x^*,y^*)} \leq T_{Y,y^*}$, since a distribution function is always smaller than (or equal to) 1.

In this Section, the quantities plotted in the Figures are as follows.

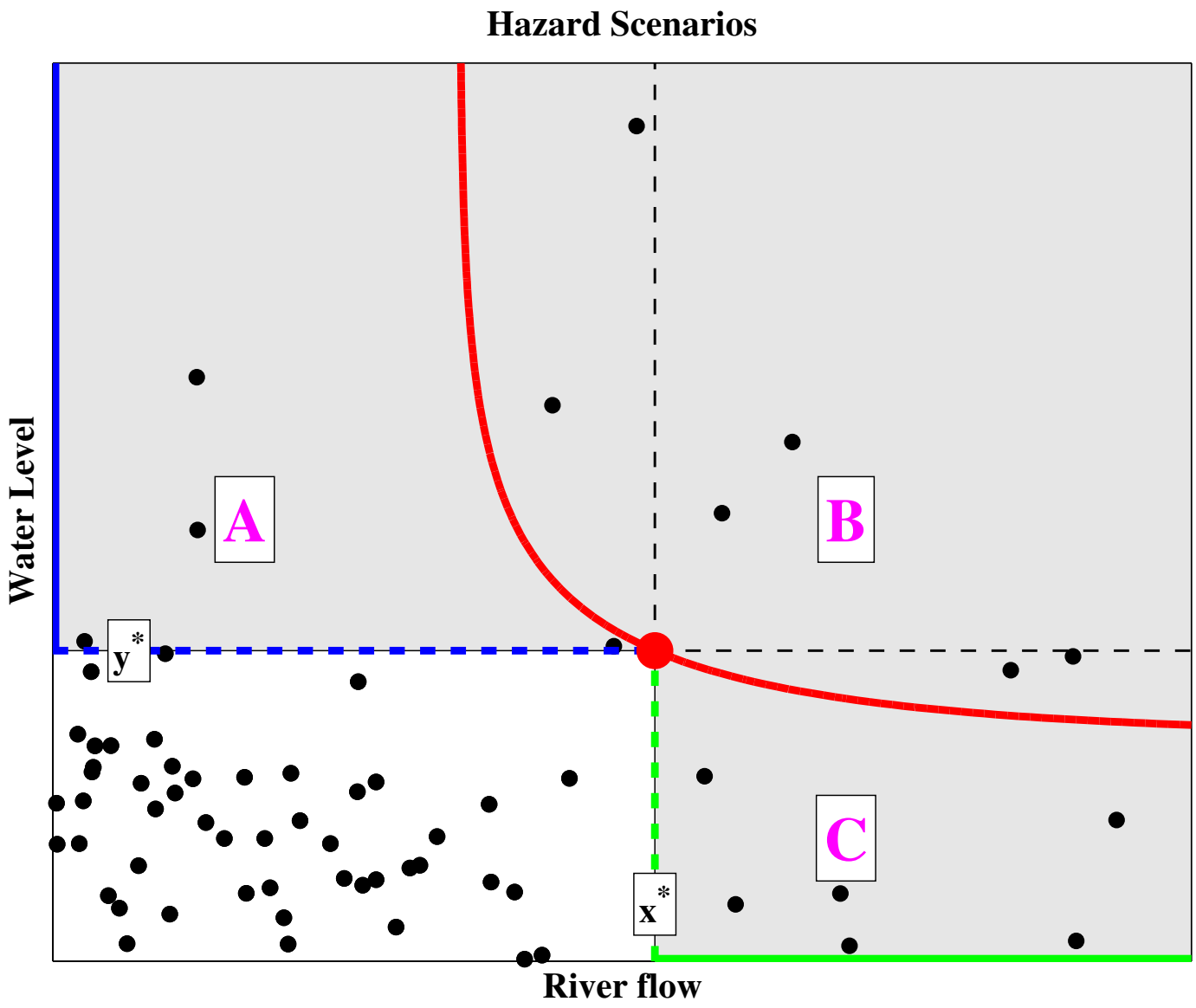

Figure SM.19

Black circles: the available data.

Red circle: the critical pair (x^*, y^*) corresponding to the univariate RP's reported in each figure title.

Red thick line: the isoline of the joint distribution F_{XY} crossing (x^*, y^*).

The legend in each plot indicates the bivariate OR RP associated with (x^*, y^*), to be compared with the univariate one reported in each figure title.

For the sake of comparison, if the variables are not independent, a **Black thick line** shows the isoline of the (wrong) Independence distribution $F_{XY} = F_X \cdot F_Y$ crossing (x^*, y^*). The corresponding bivariate OR RP is reported in the legend, marked by a **Black cross**.

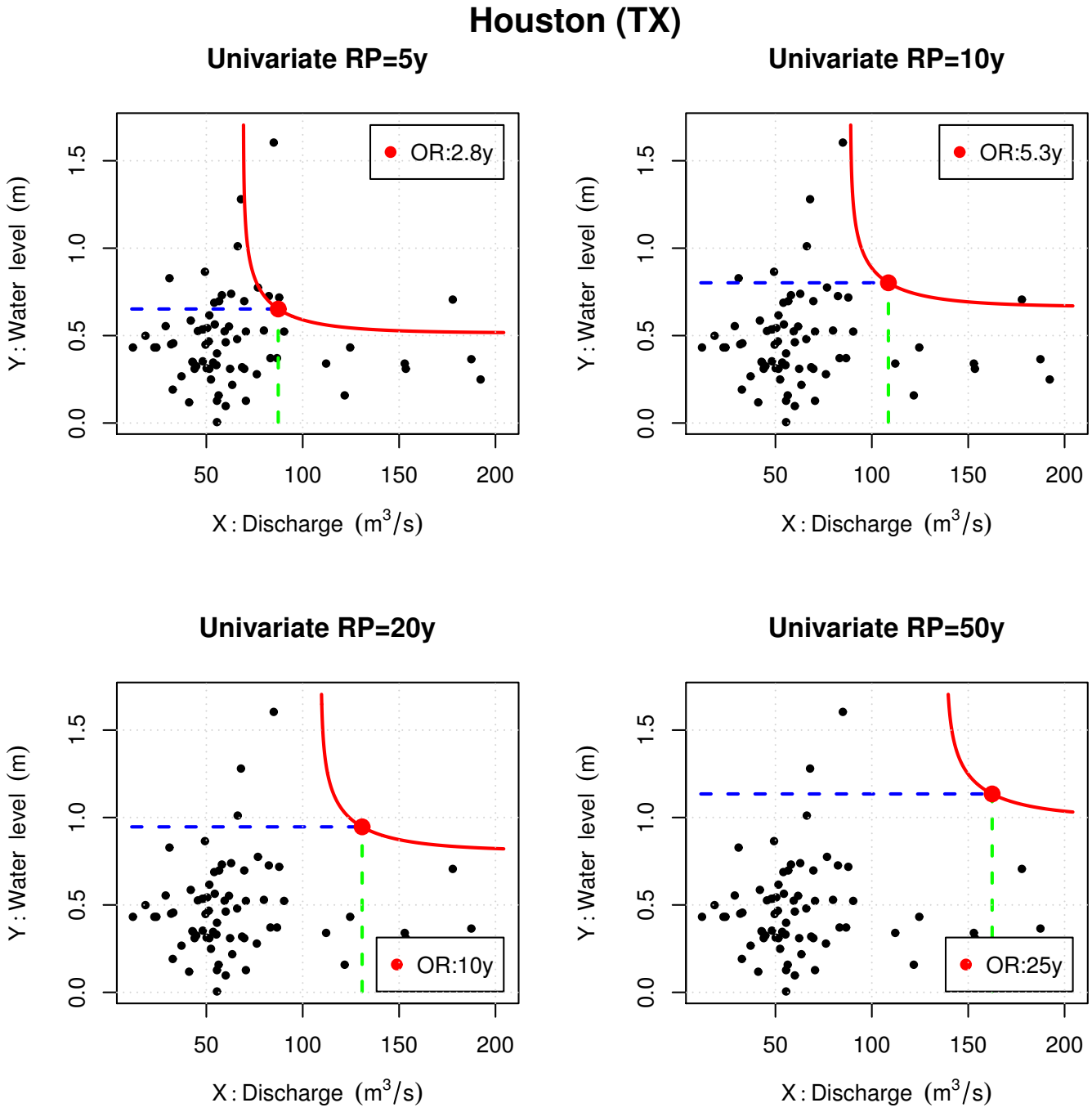

Figure SM.20: see text for explanation.

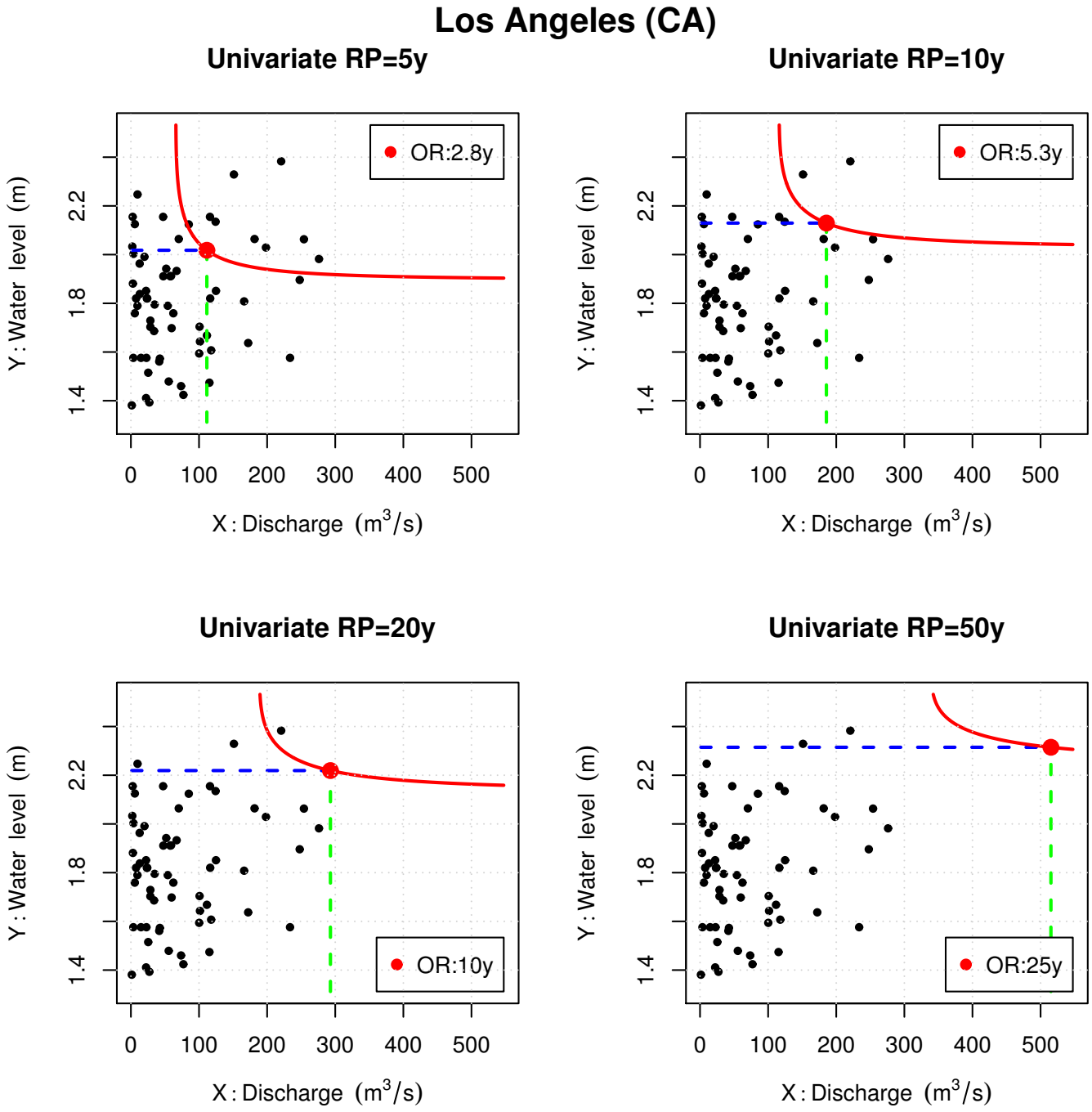

Figure SM.21: see text for explanation.

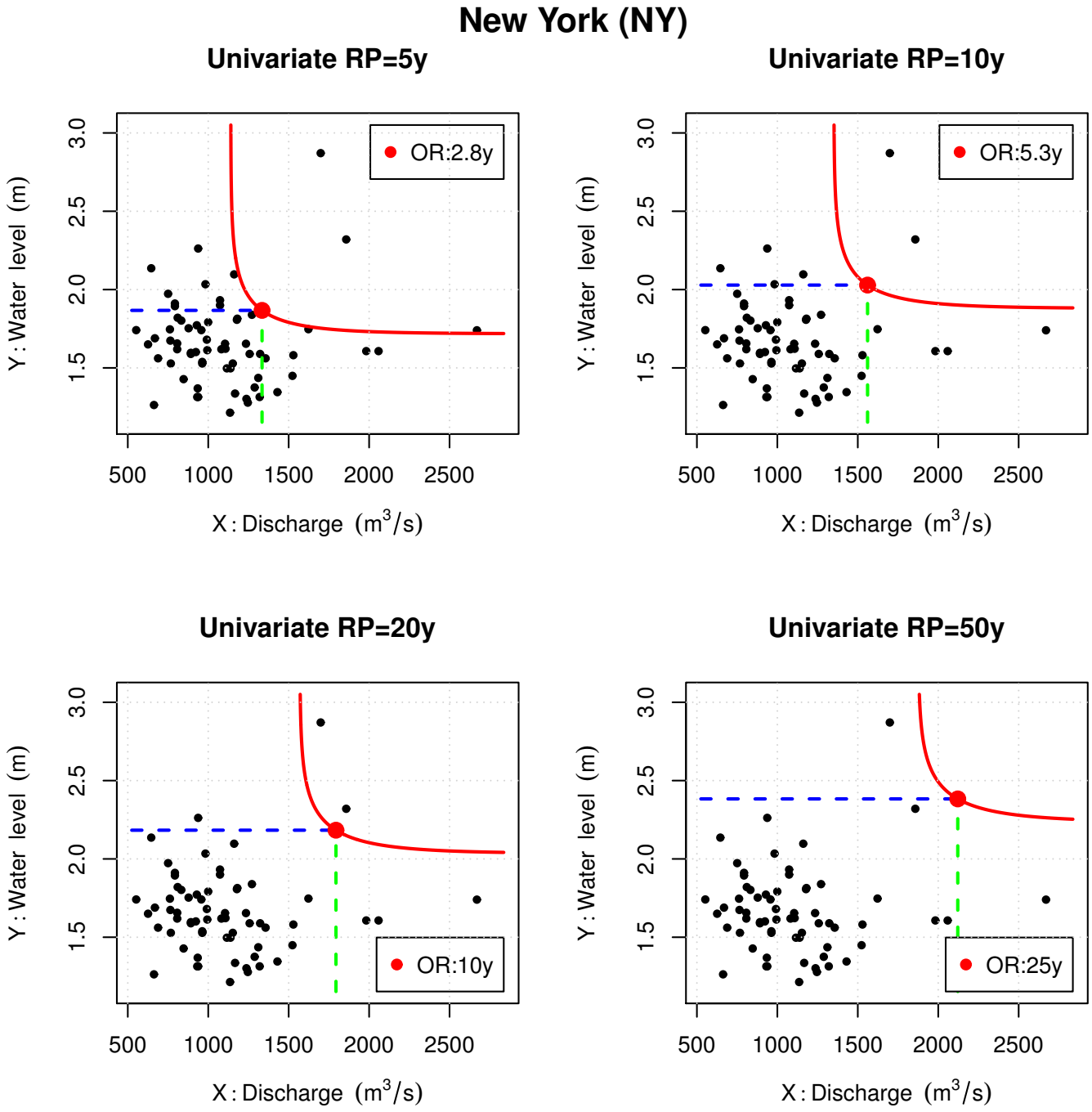

Figure SM.22: see text for explanation.

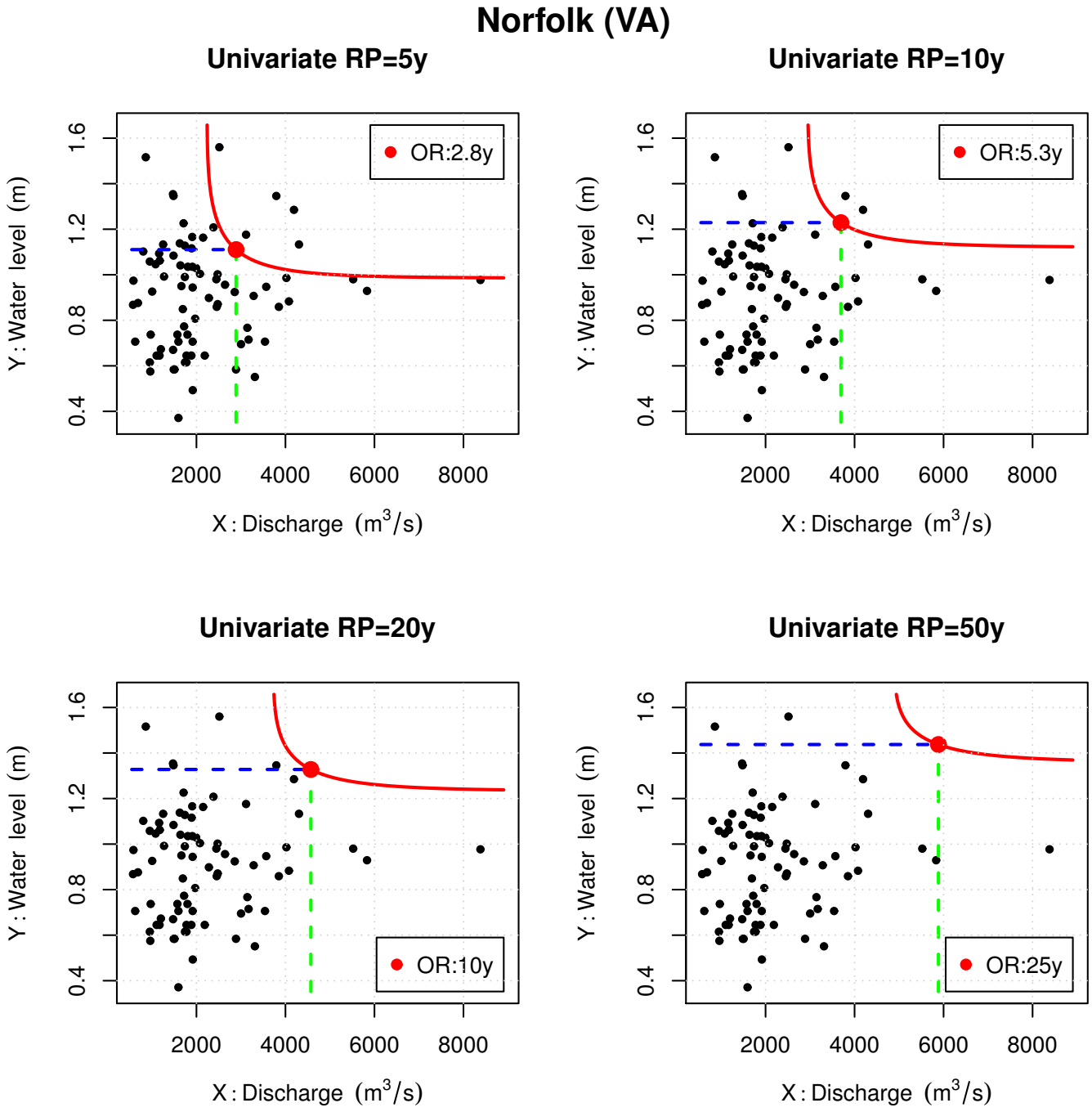

Figure SM.23: see text for explanation.

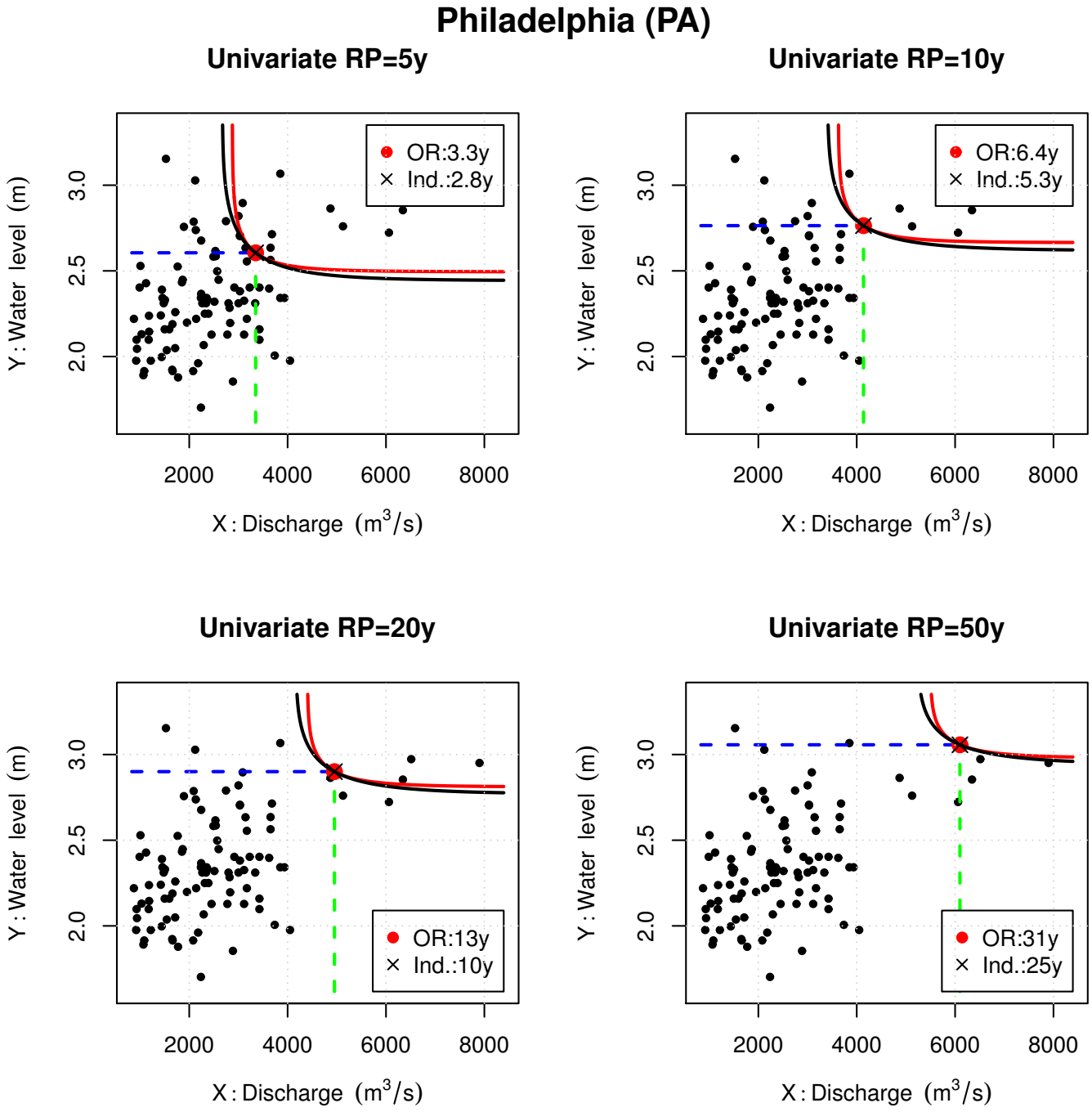

Figure SM.24: see text for explanation.

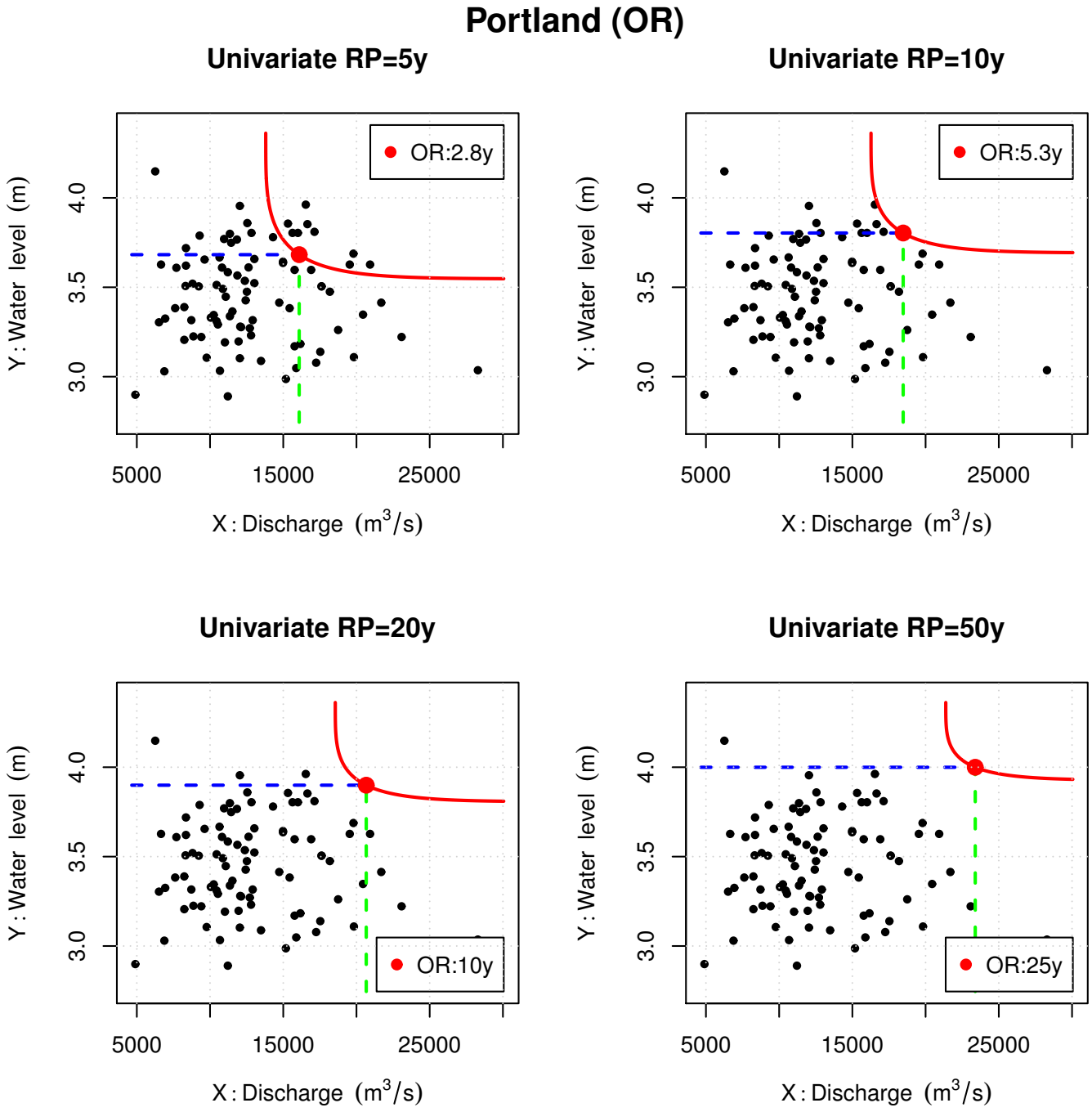

Figure SM.25: see text for explanation.

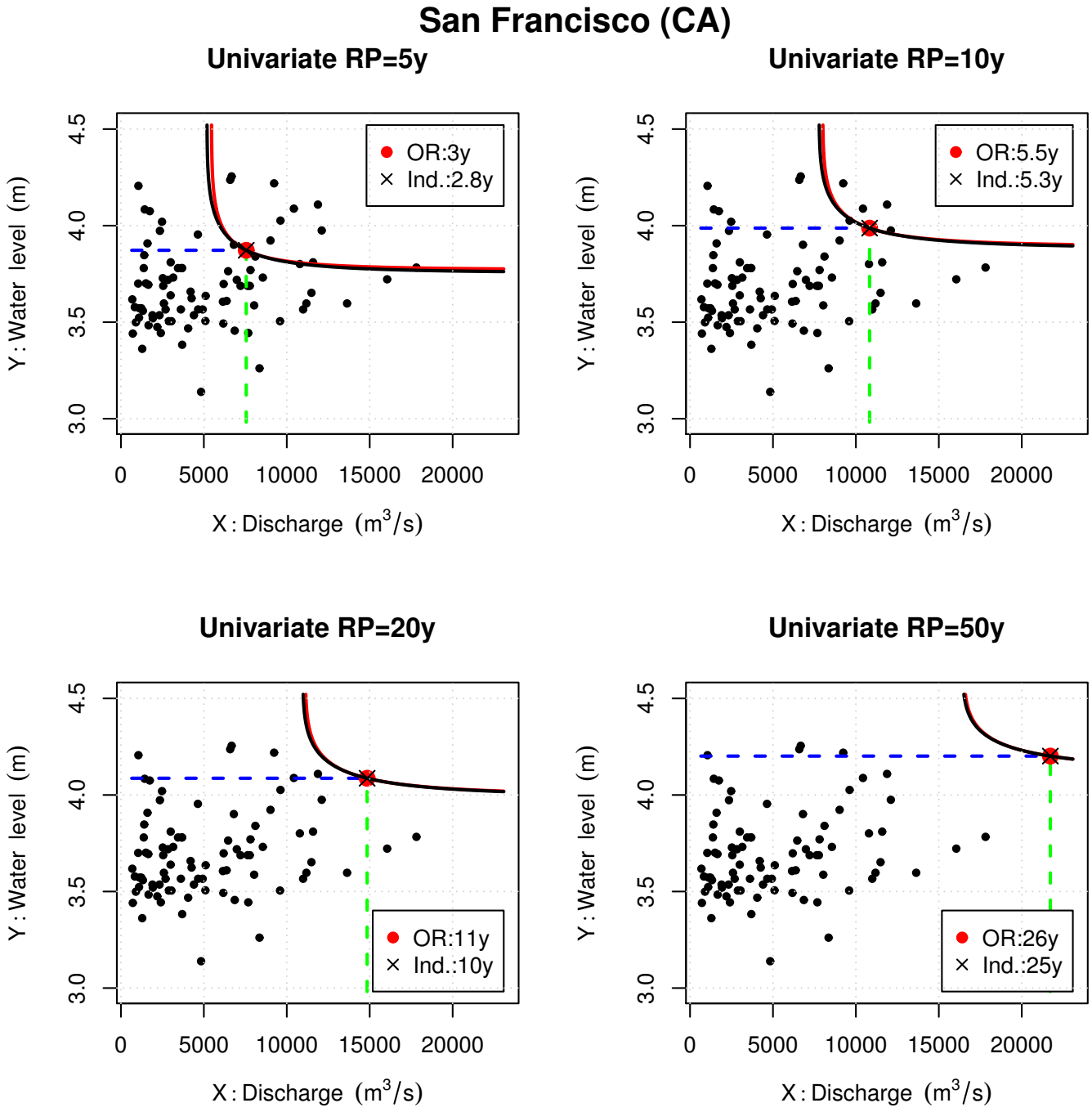

Figure SM.26: see text for explanation.

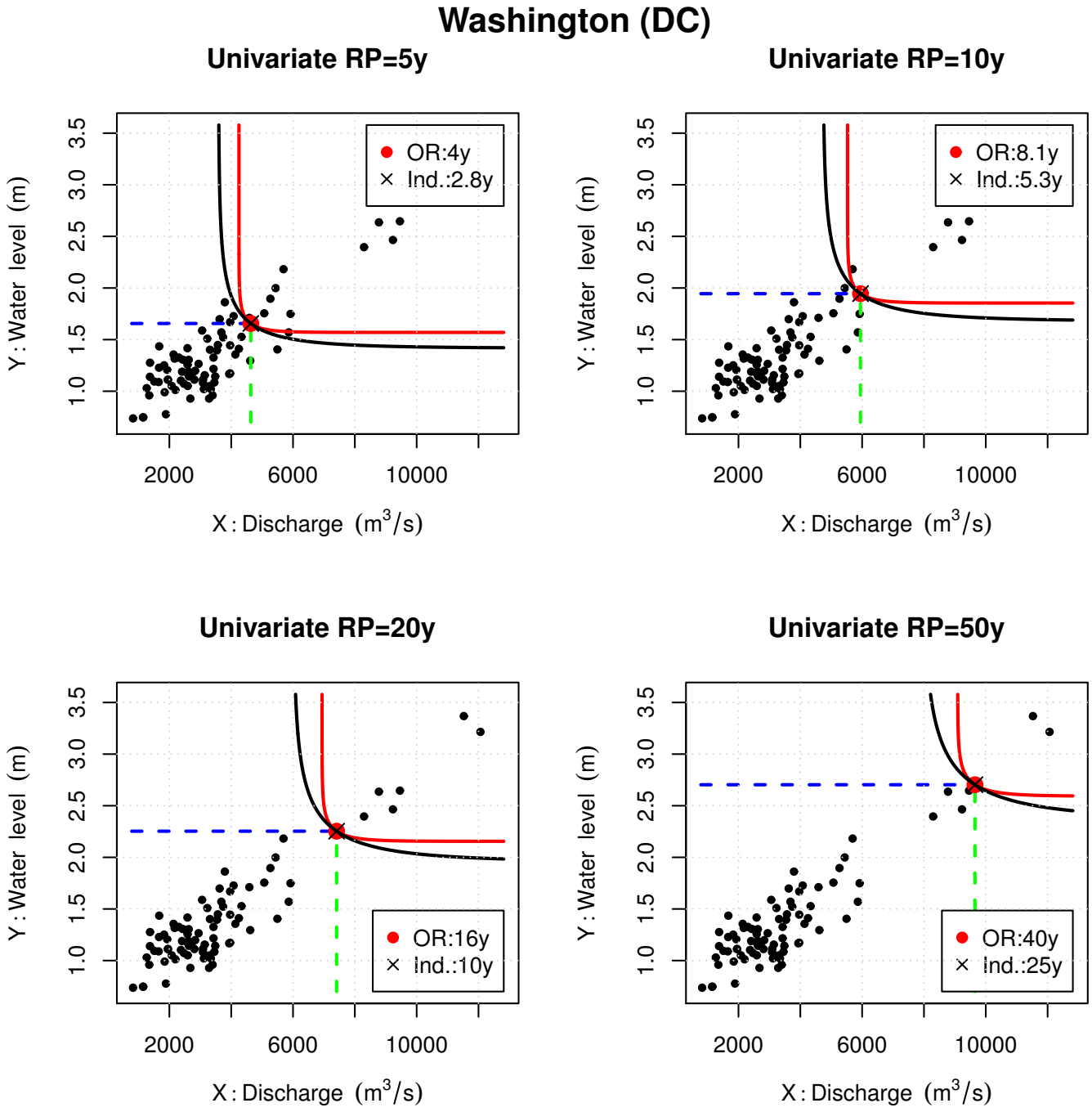

Figure SM.27: see text for explanation.

6 Bivariate Analysis: Failure Probabilities

For all the eight sites of interest (viz., Houston, Los Angeles, New York, Norfolk, Philadelphia, Portland, San Francisco, and Washington), the same four Hazard Scenarios (HS) used in Section 5 (concerning Return Periods) are considered.

In this study, we estimate the probability of coastal flooding under projected local rise in sea level (SLR) by 2030 and 2050 and Representative Concentration Pathways (RCP) 4.5 and 8.5, in order to quantify the effect of SLR on increased Failure Probability of coastal flood defenses in the mid-term future. A standard Monte Carlo analysis is used to estimate 95% bootstrap confidence bands of the Failure Probability (FP) over a 30-year temporal horizon, under different sea level rise scenarios. Here, 1000 independent bootstrap iterations are used, each involving huge simulated samples of size 10^6 to evaluate the uncertainties: for further details see Salvadori et al. [2016].

Four different SLR future projection are considered: viz., (RCP=4.5, Year=2030), (RCP=8.5, Year=2030), (RCP=4.5, Year=2050), and (RCP=8.5, Year=2050) — these are indicated in the main figure titles. Remember that the FP is simply the probability that (at least) an occurrence of the phenomenon under investigation takes place in the HS of interest during the given Lifetime: in turn, the notion of FP can be used both for univariate and bivariate HS's, once these have been well defined (as done in the present work).

Plotted are the following quantities, for each of the four Hazard Scenarios considered: these latter are indicated in the sub-plot titles by showing the pair of critical values (x^*, y^*) used to generate the HS of interest according to the corresponding univariate RP's (e.g., $(X_{5\text{years}}, Y_{5\text{years}})$, etc...).

Top panel. The probability distribution F_{SLR} of the SLR is given in a discrete form by providing, for each of the eight sites of interest, $n_{\text{SLR}} = 7$ increasing quantiles q_i's of orders, respectively,

$$p_i = 0.005, 0.05, 0.17, 0.5, 0.83, 0.95, 0.995$$

with $i = 1, \ldots, n_{\text{SLR}}$. A continuous version of F_{SLR} is constructed via a linear interpolation: this latter procedure corresponds to a (non-parametric) least-informative strategy, since it does not require additional parameters as in Kernel or Spline approximations. Practically, the SLR variates is assumed to be Uniform in any interval (q_i, q_{i+1}), where the density is constant, and the corresponding CDF is simply a continuous sequence of line segments. In order to construct a full distribution, also the lower quantile q_0 (for $p = 0$), and the upper quantile $q_{n_{\text{SLR}}+1}$ (for $p = 1$) must be specified. These are empirically calculated by, first, computing the average μ_q of the differences $q_{i+1} - q_i$, and then by taking $q_0 = q_1 - \mu_q$ and $q_{n_{\text{SLR}}+1} = q_{n_{\text{SLR}}} + \mu_q$. In the Figures, the linear interpolation of F_{SLR} is plotted as a **Black solid line**, while the empirical distribution function of the SLR values (simulated from F_{SLR} via the Probability Integral Transform) are plotted as a **Black marked line**. Note that only positive SLRs are considered, being interested in more "dangerous" conditions.

Bottom panel. Estimated Failure Probabilities, plotted considering a 30-years temporal horizon.

Black line: univariate FP's, both for X and Y (the two are equal, since the univariate X- and Y-HS's have the same probability).

Red line: Bivariate OR FP's.

Purple thick line: Bivariate OR FP's accounting for random SLR's extracted from F_{SLR}.

Purple thin dotted lines: Monte Carlo 95% confidence band for the bivariate OR FP's accounting for random SLR's extracted from F_{SLR}.

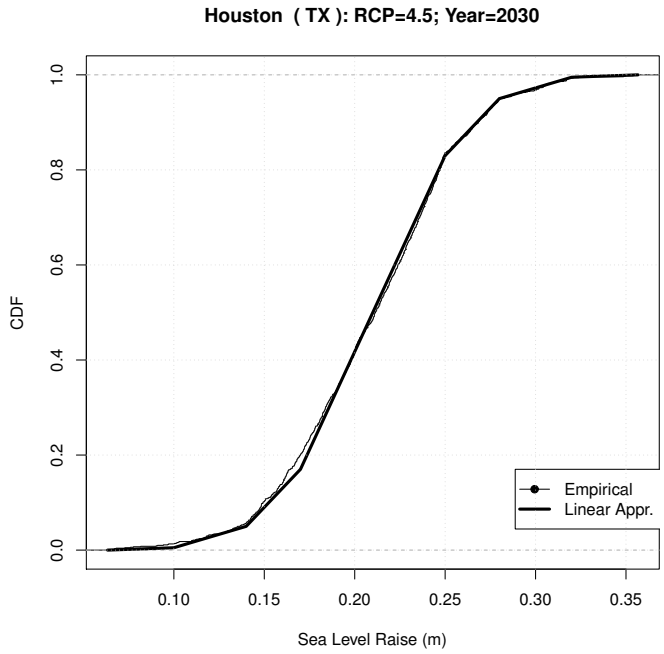

Houston (TX) □ RCP=4.5; Year=2030

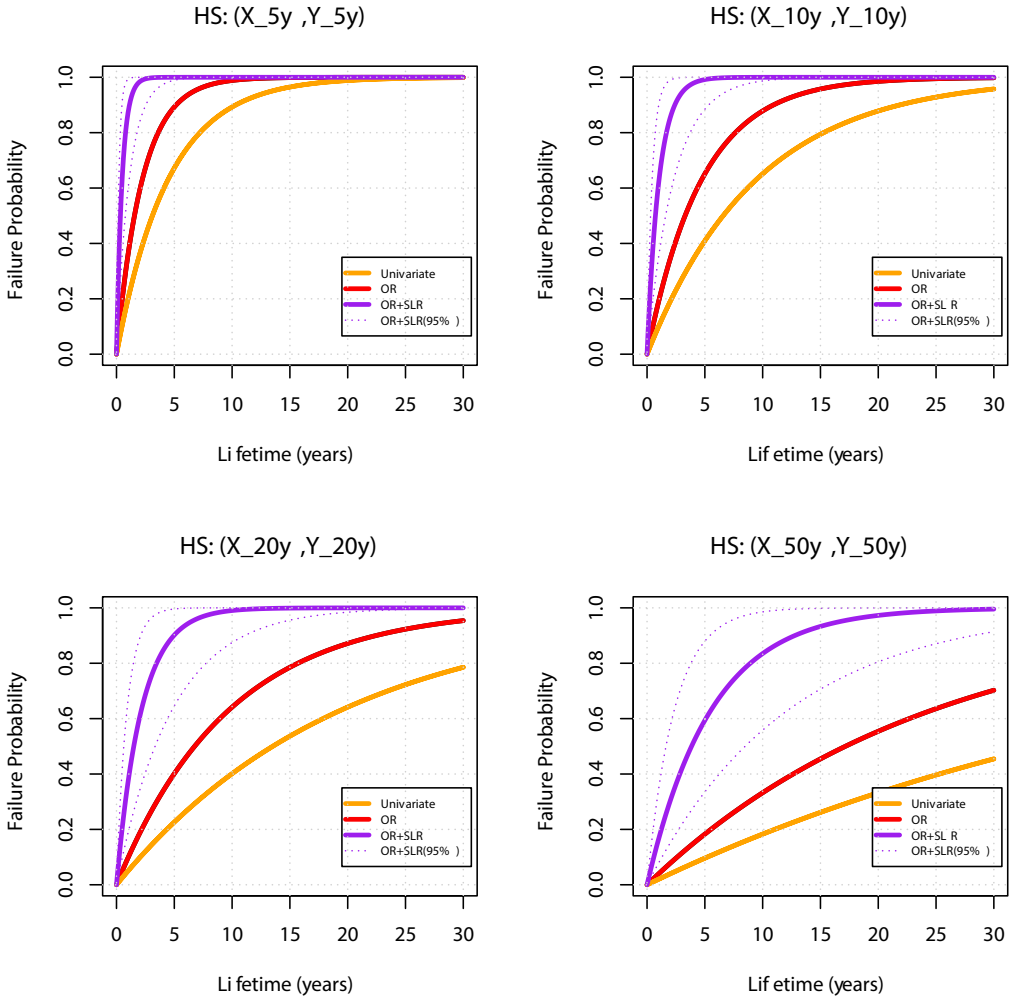

Figure SM.28: see text for explanation.

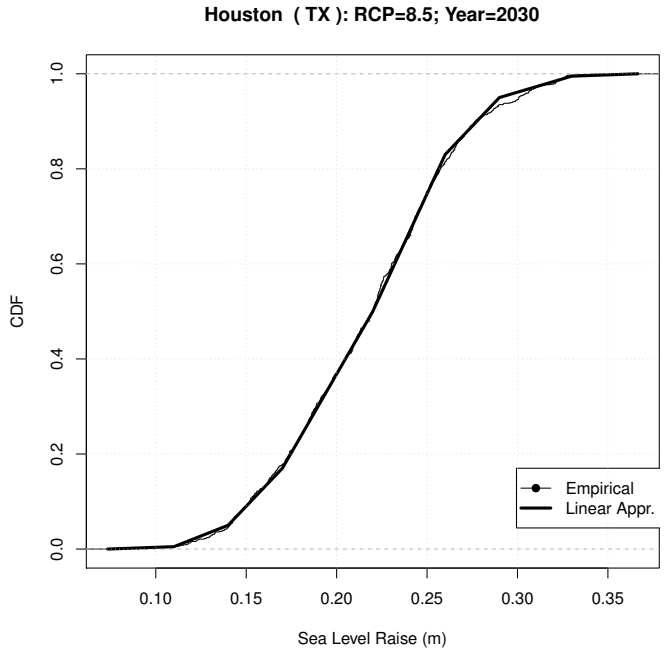

Houston (TX) □ RCP=8.5; Year=2030

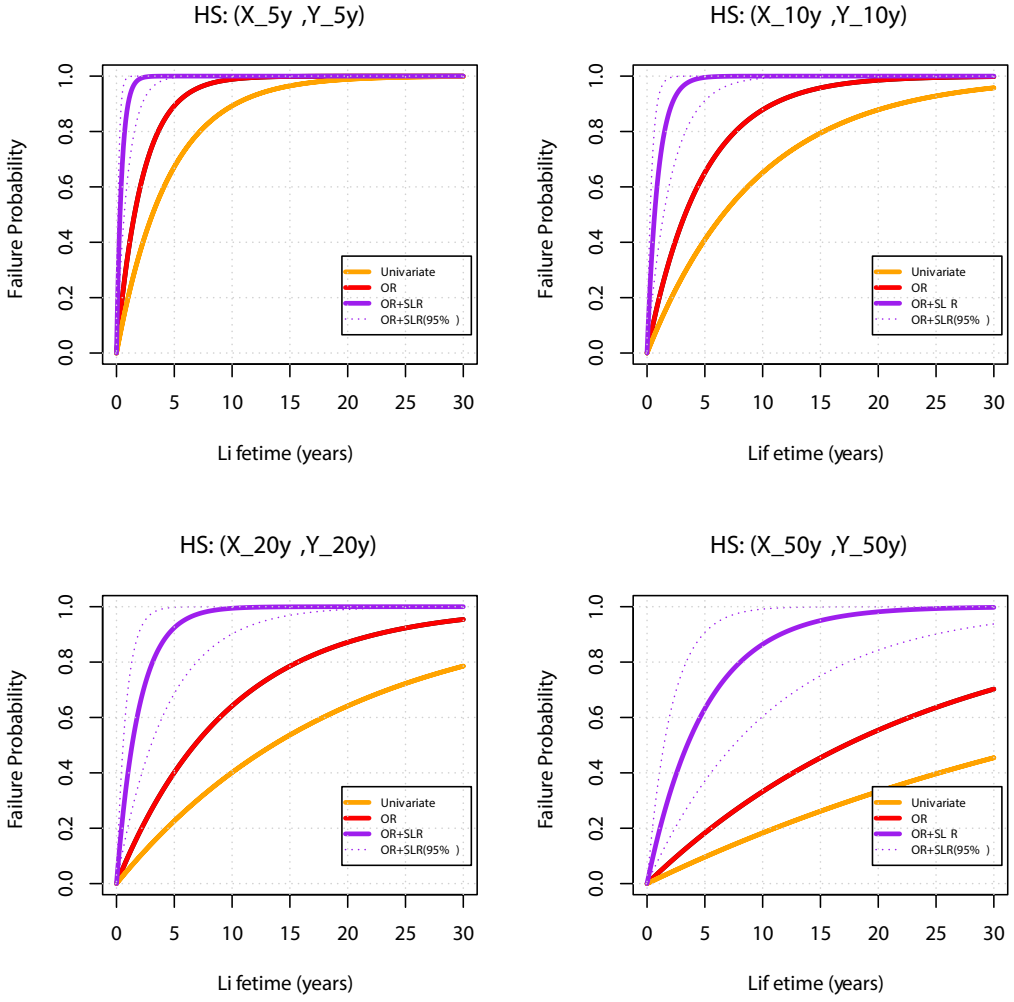

Figure SM.29: see text for explanation.

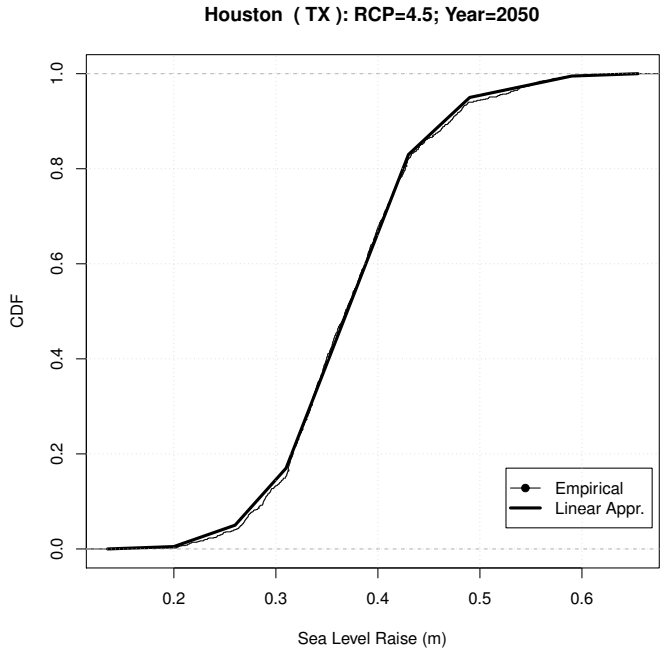

Houston (TX) □ RCP=4.5; Year=2050

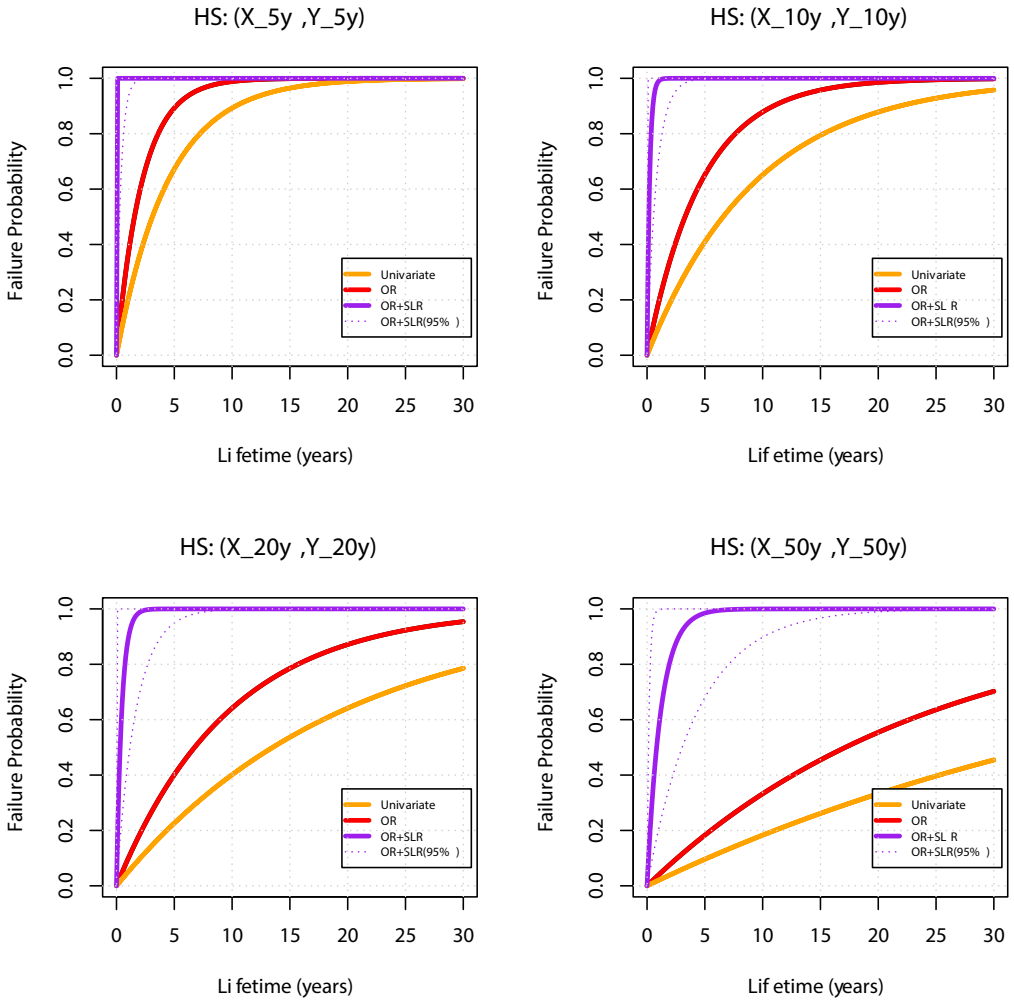

Figure SM.30: see text for explanation.

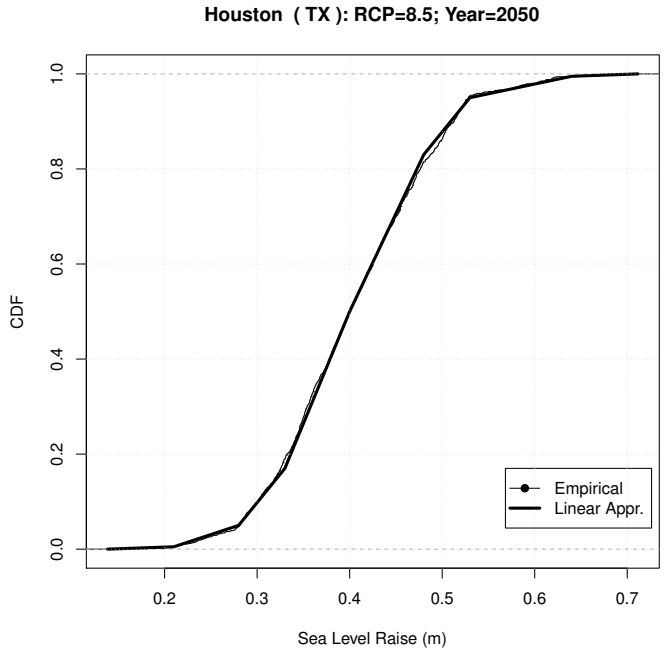

Houston (TX) □ RCP=8.5; Year=2050

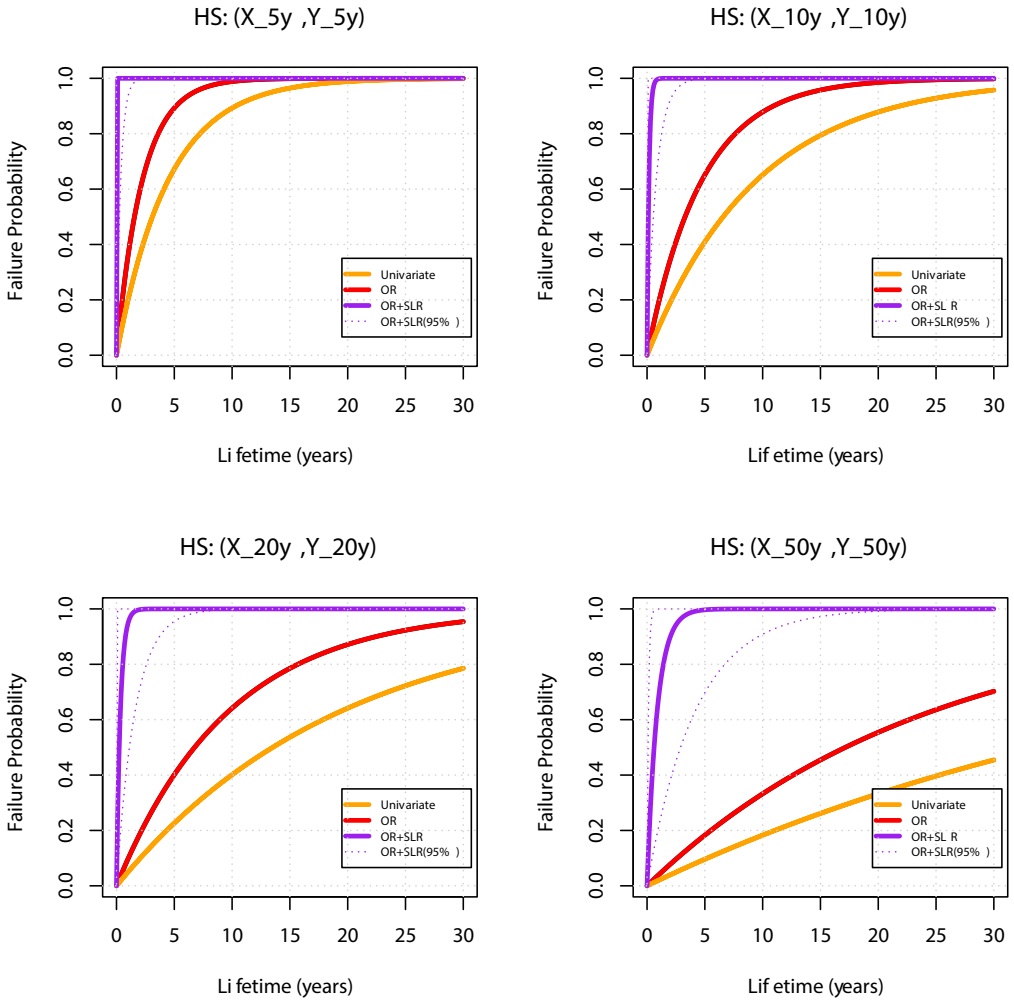

Figure SM.31: see text for explanation.

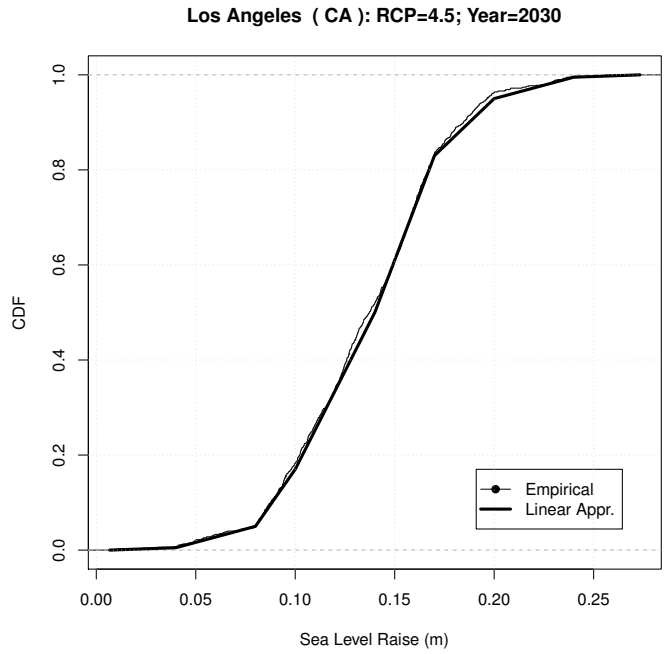

Los Angeles (CA) □ RCP=4.5; Year=2030

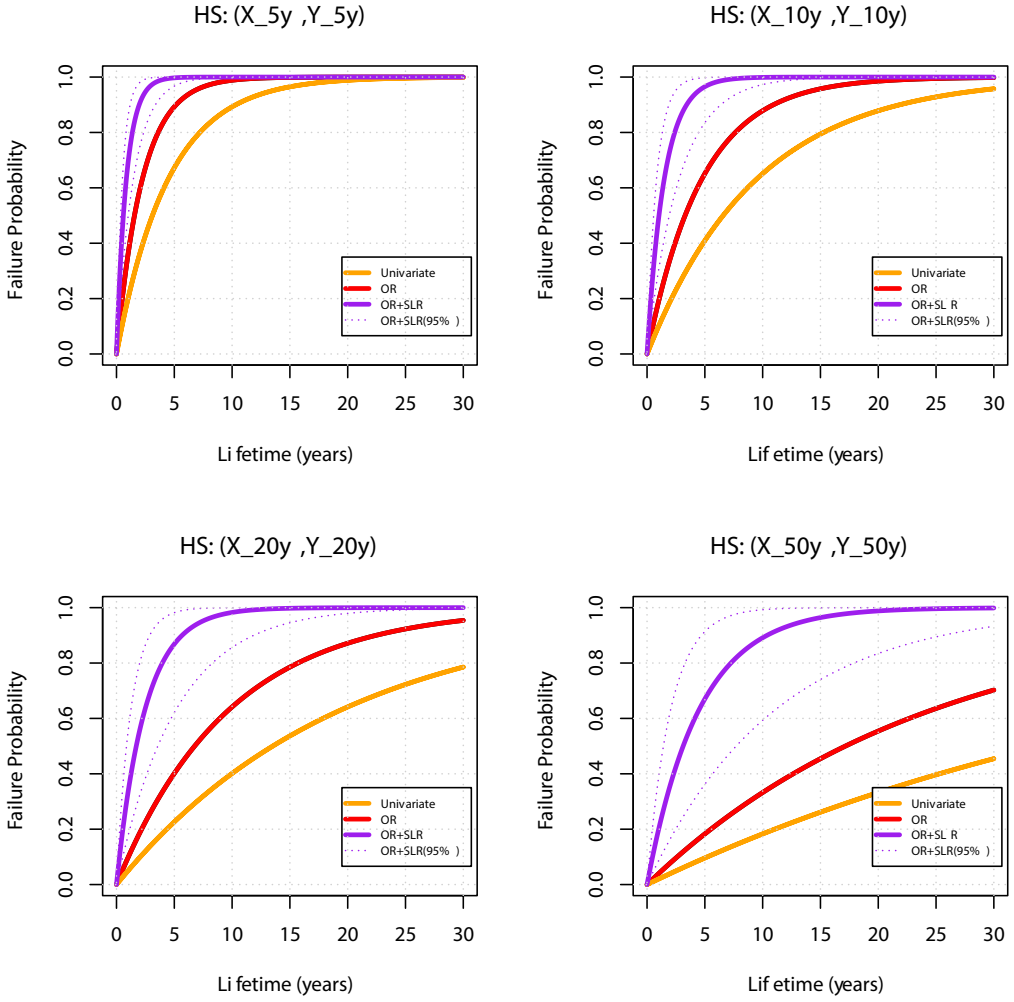

Figure SM.32: see text for explanation.

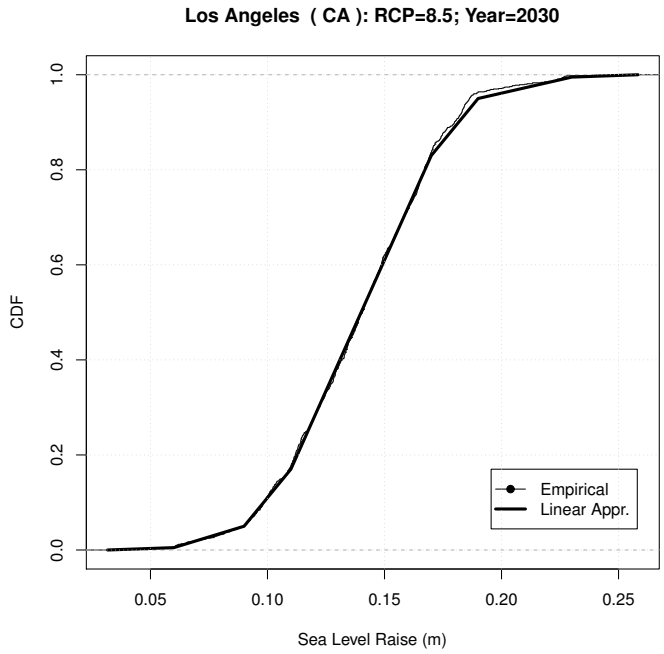

Los Angeles (CA) □ RCP=8.5; Year=2030

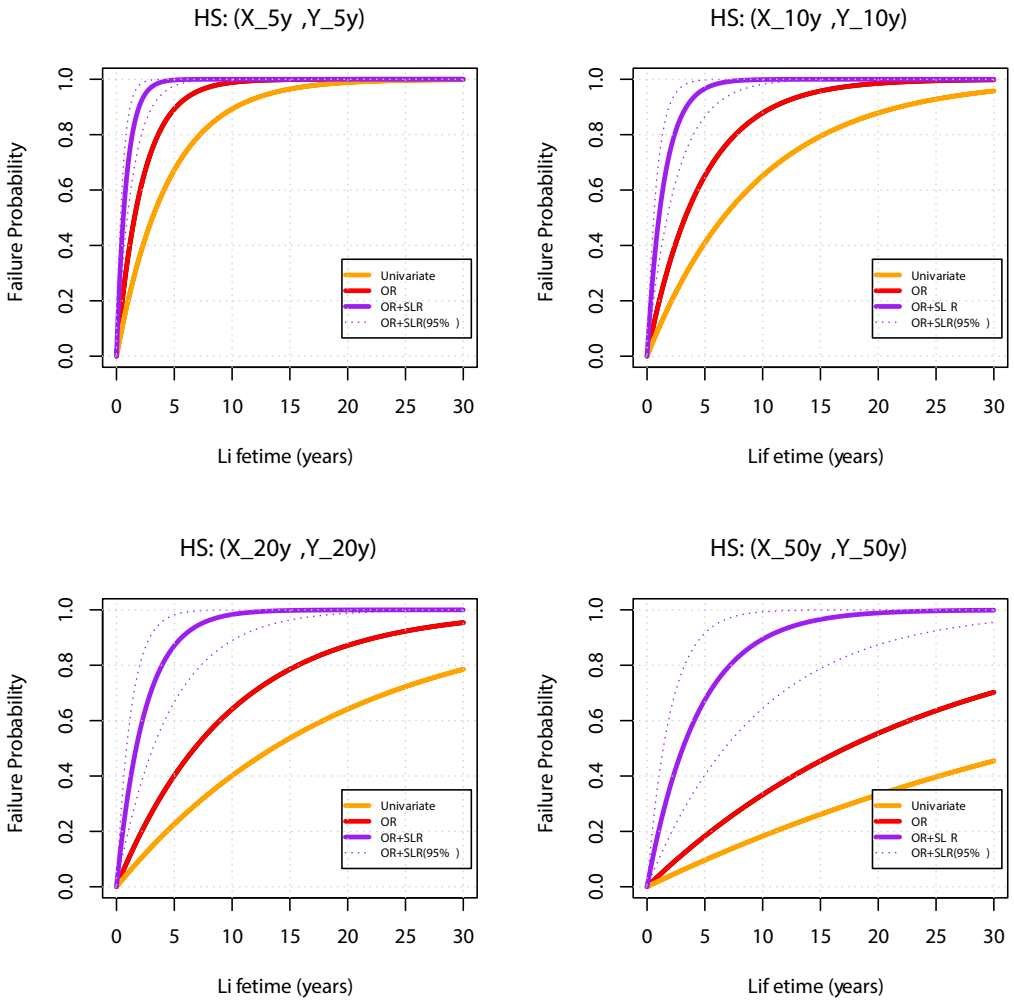

Figure SM.33: see text for explanation.

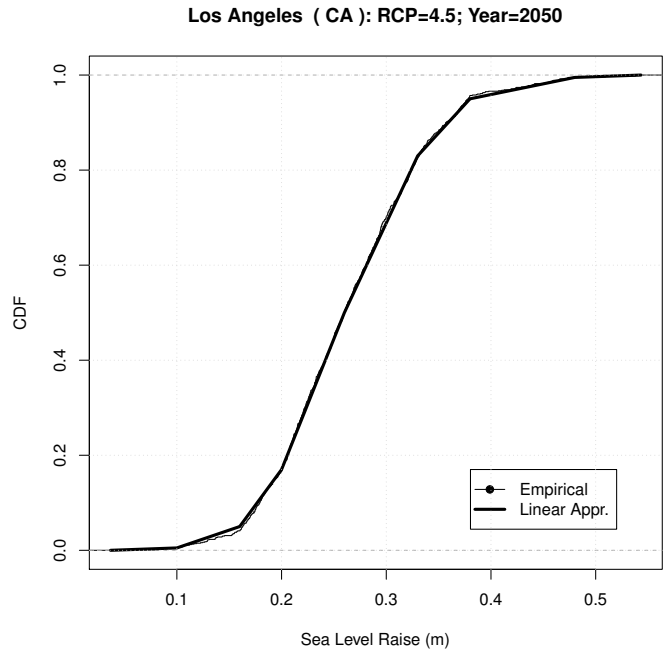

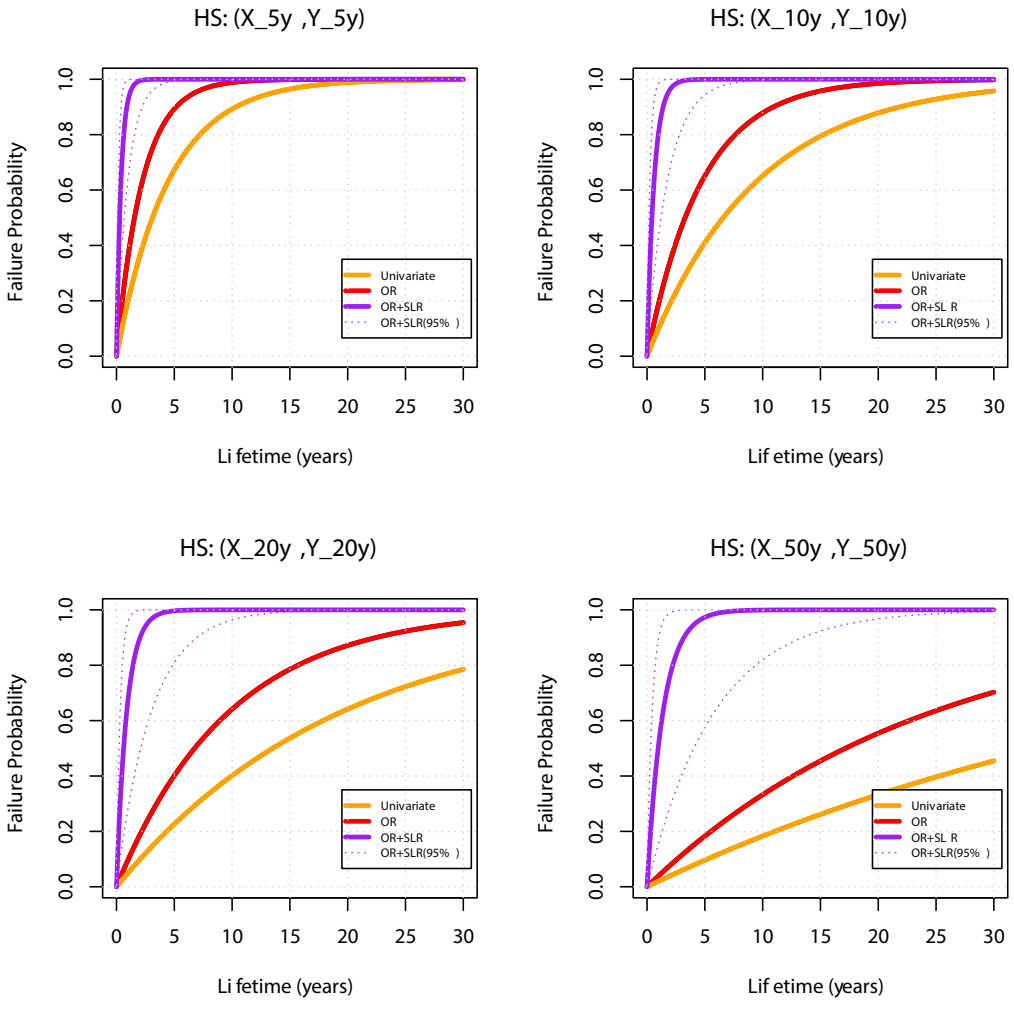

Figure SM.34: see text for explanation.

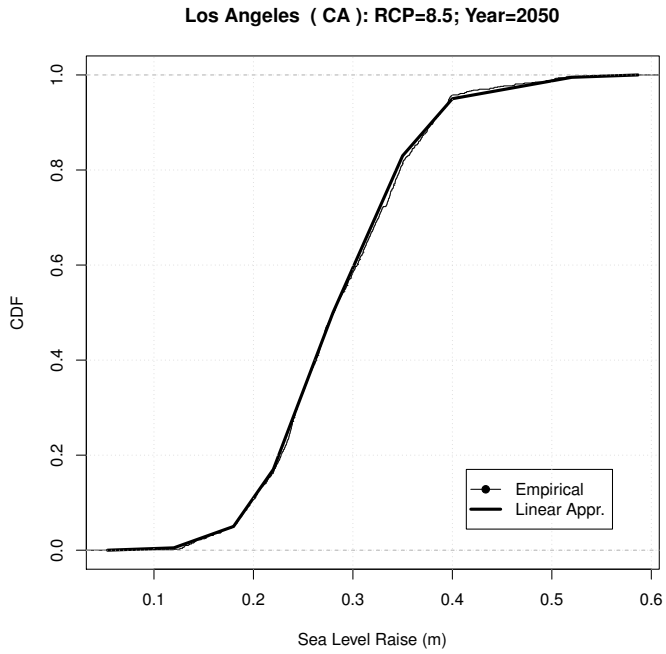

Los Angeles (CA) □ RCP=8.5; Year=2050

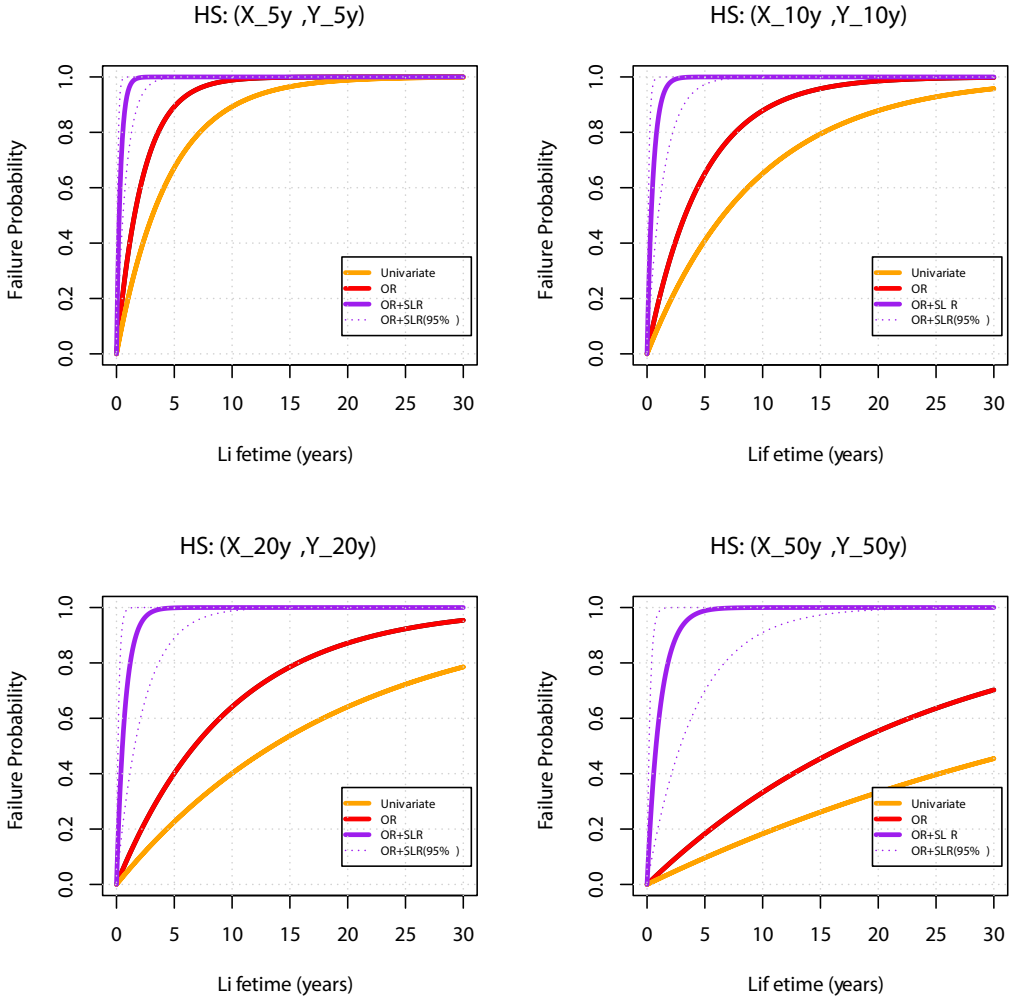

Figure SM.35: see text for explanation.

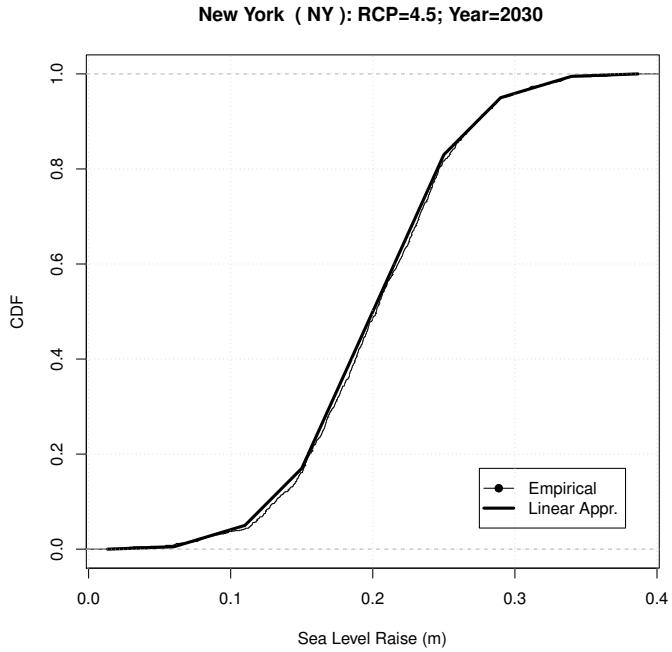

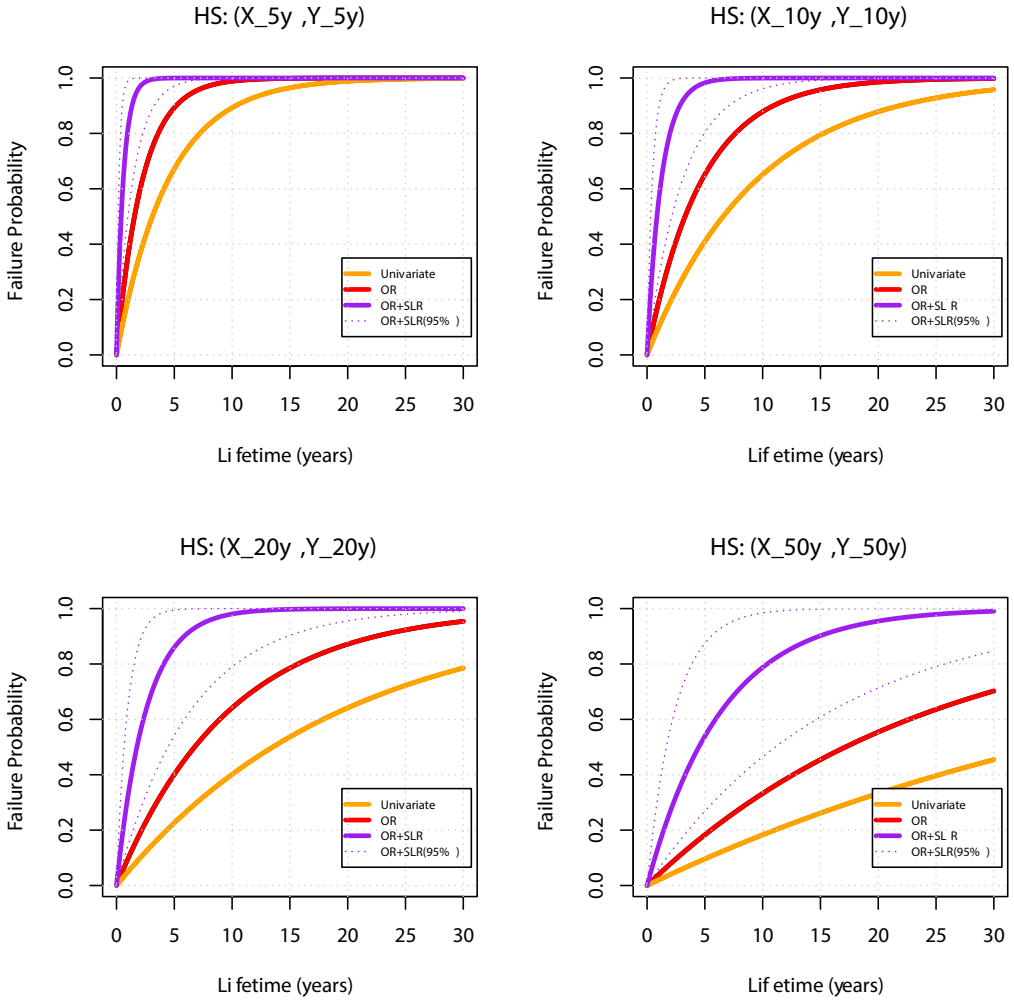

Figure SM.36: see text for explanation.

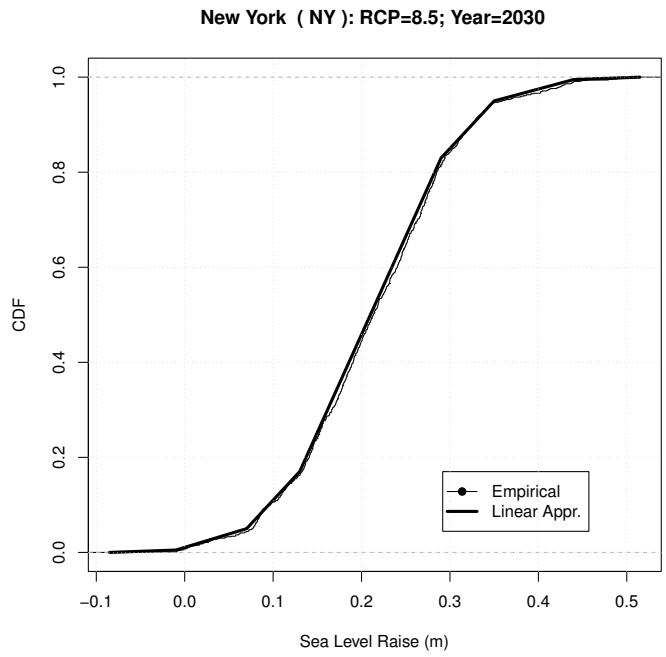

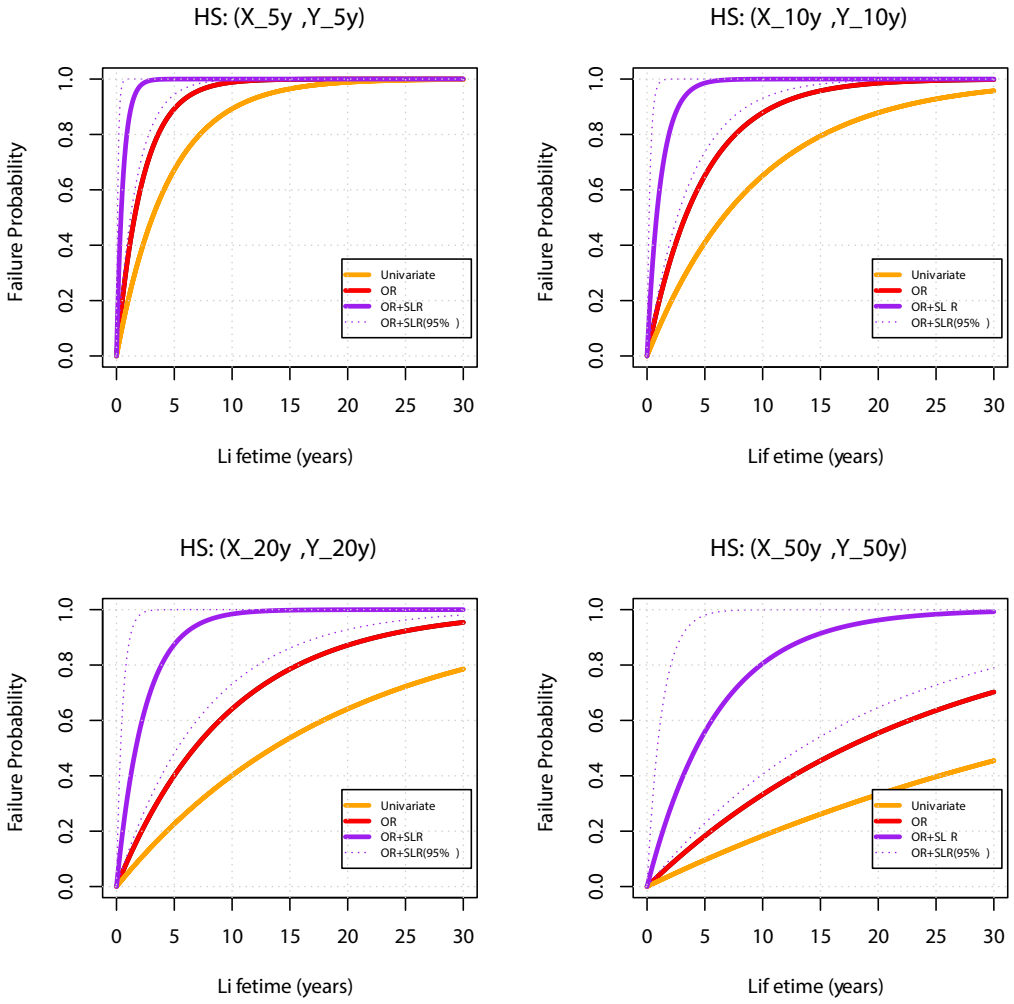

Figure SM.37: see text for explanation.

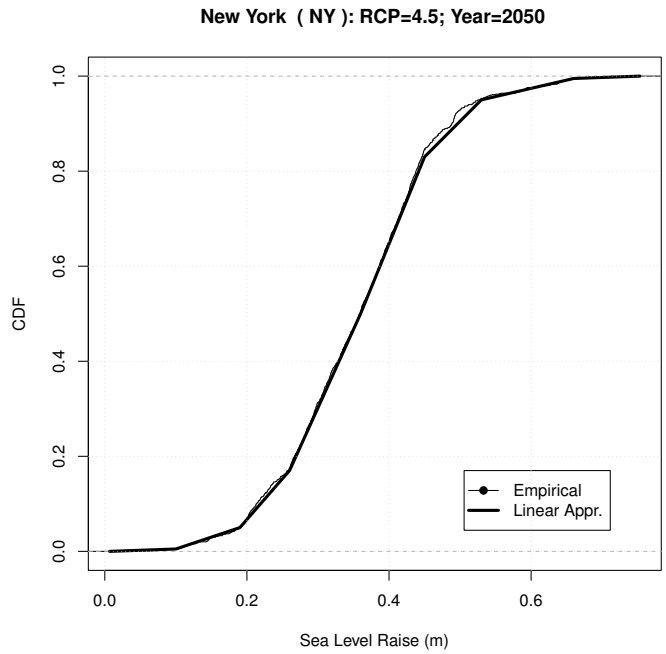

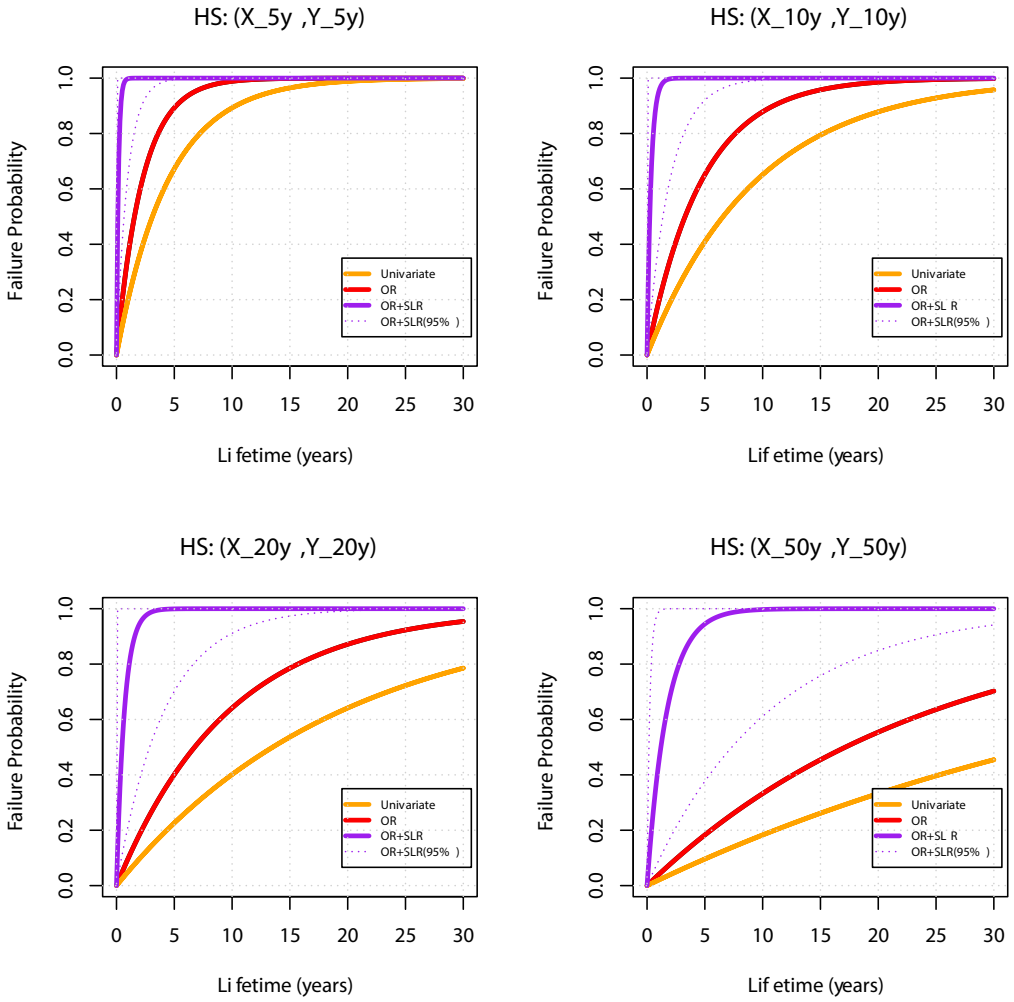

Figure SM.38: see text for explanation.

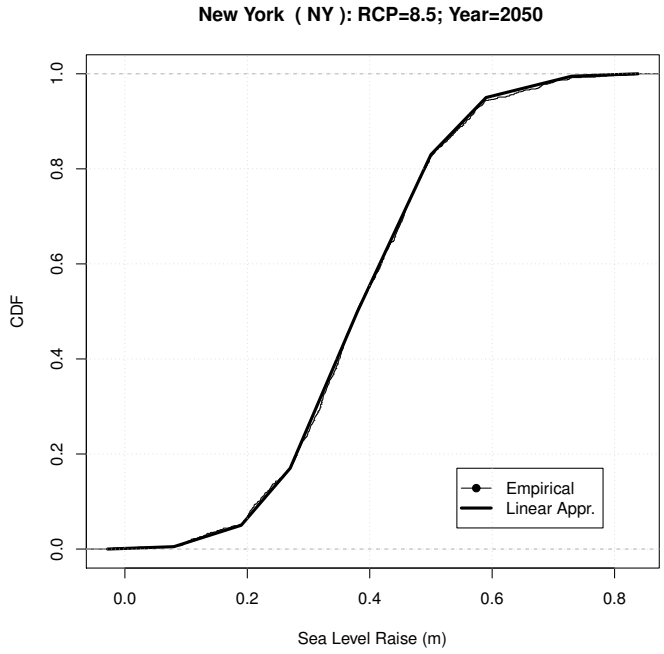

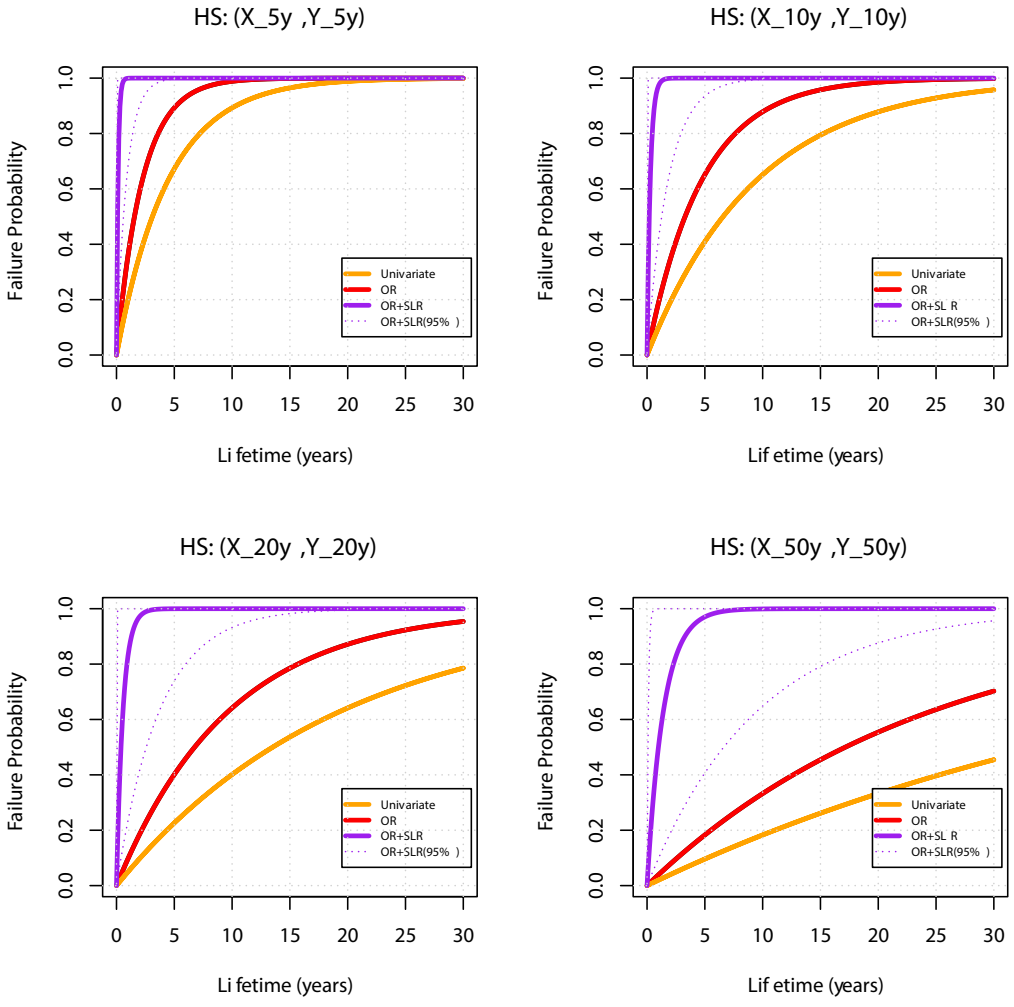

Figure SM.39: see text for explanation.

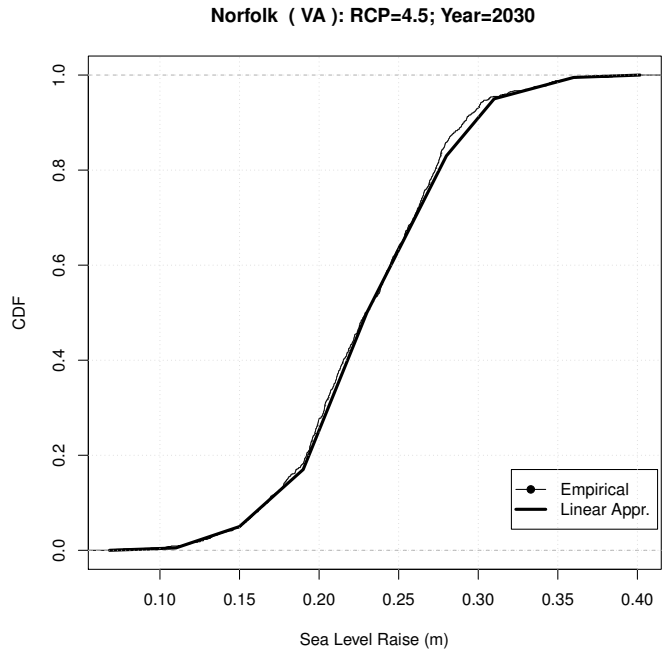

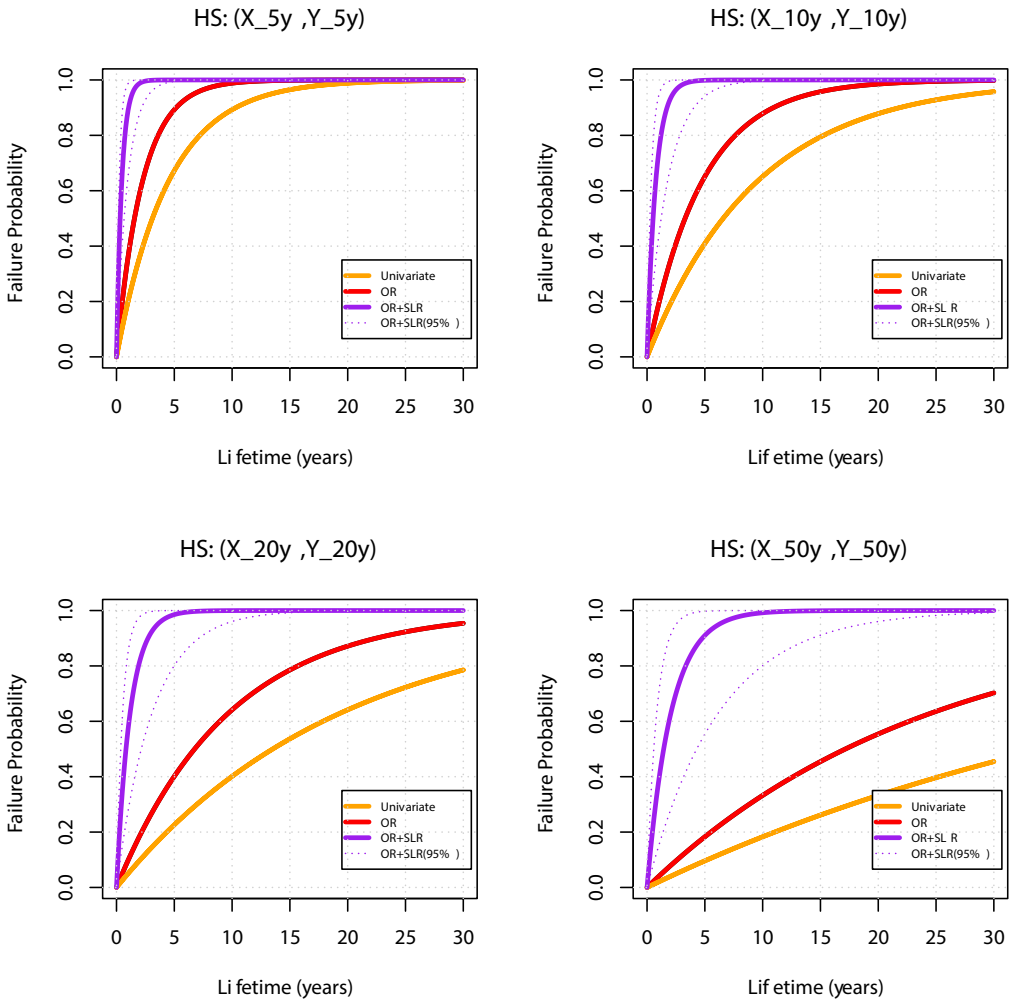

Figure SM.40: see text for explanation.

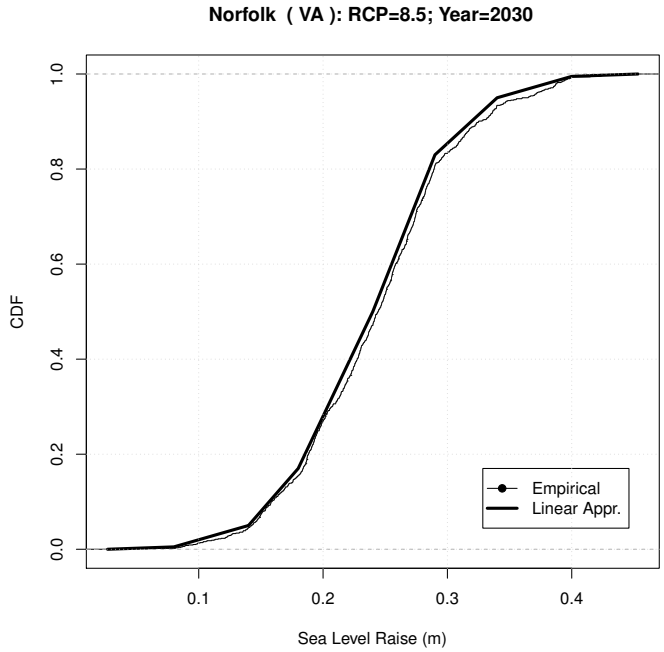

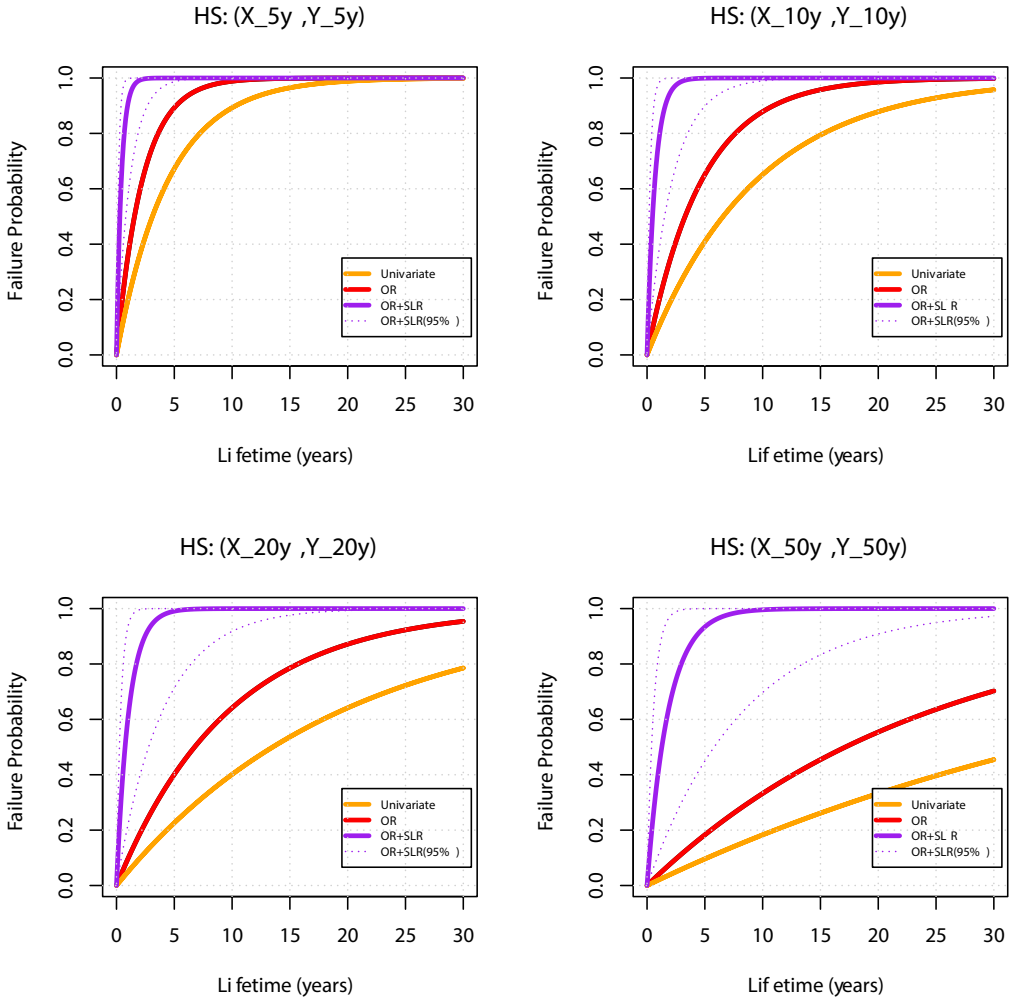

Figure SM.41: see text for explanation.

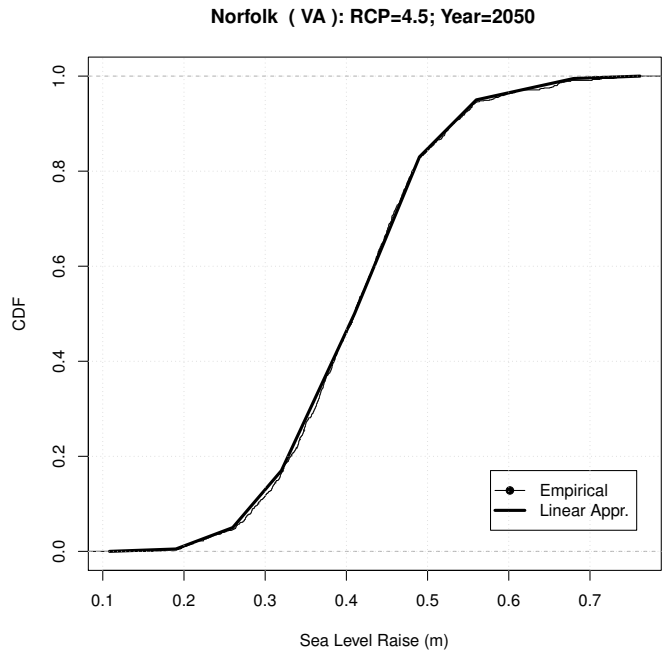

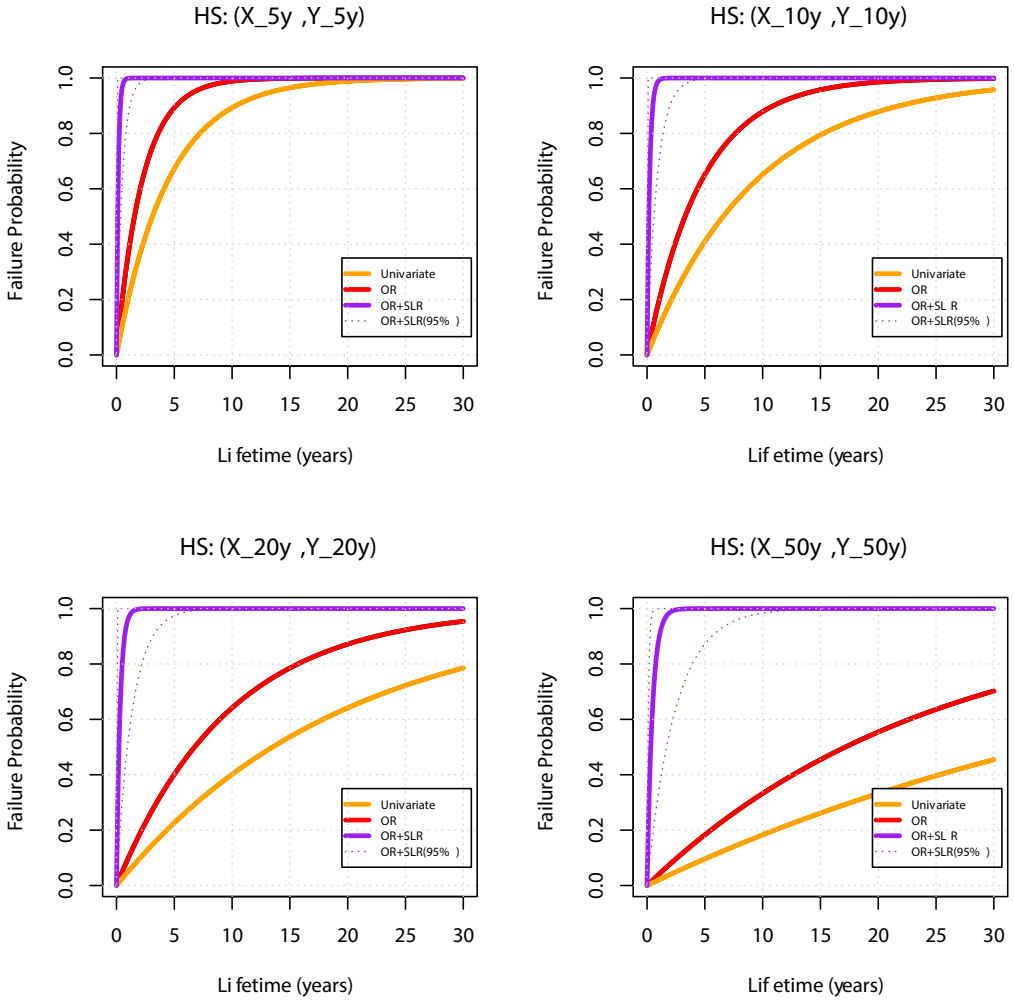

Figure SM.42: see text for explanation.

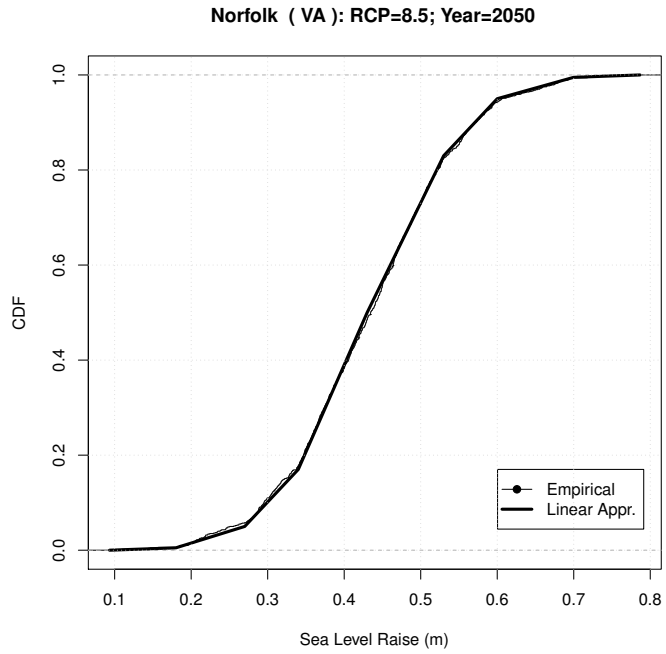

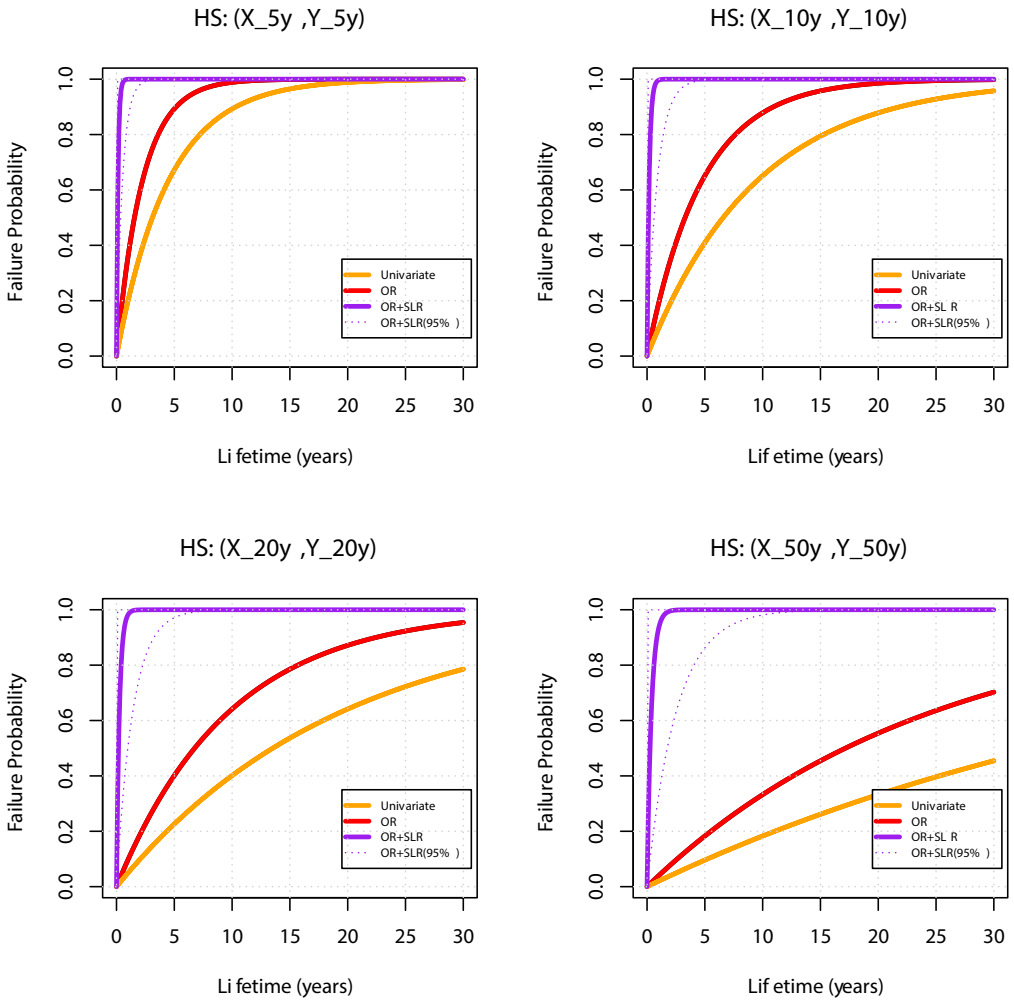

Figure SM.43: see text for explanation.

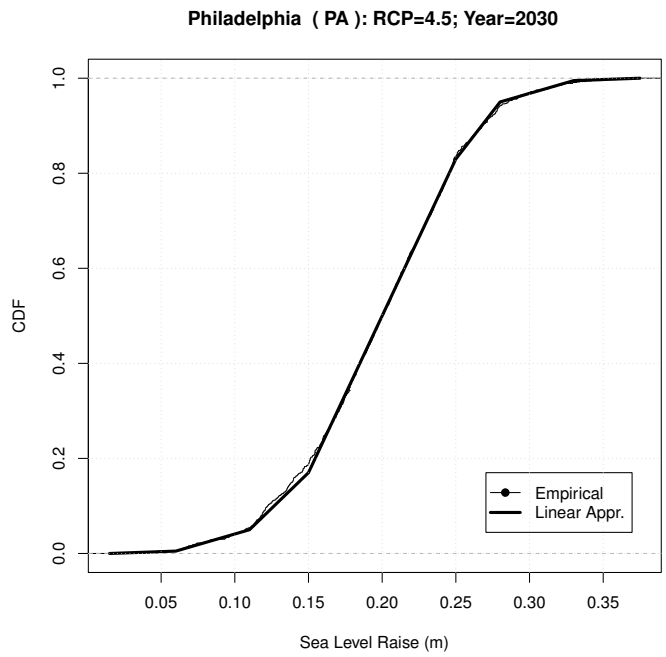

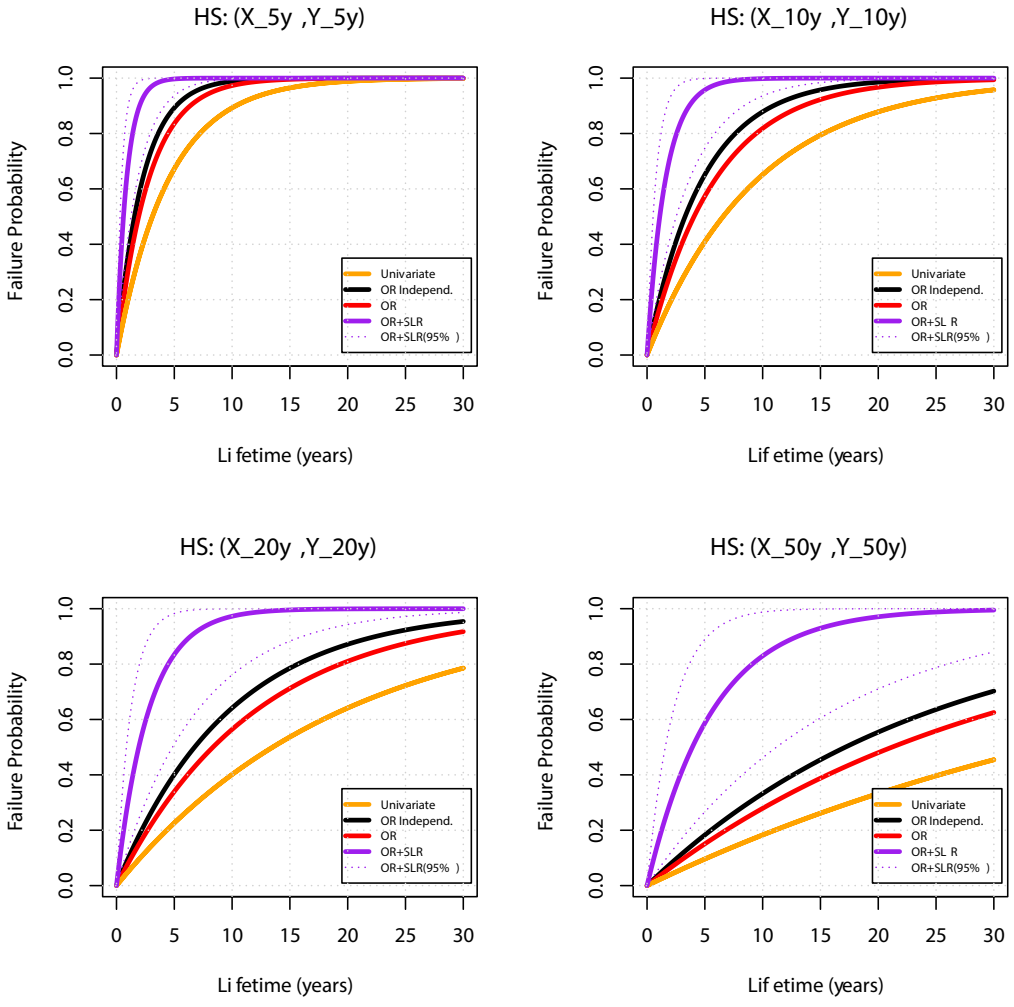

Figure SM.44: see text for explanation.

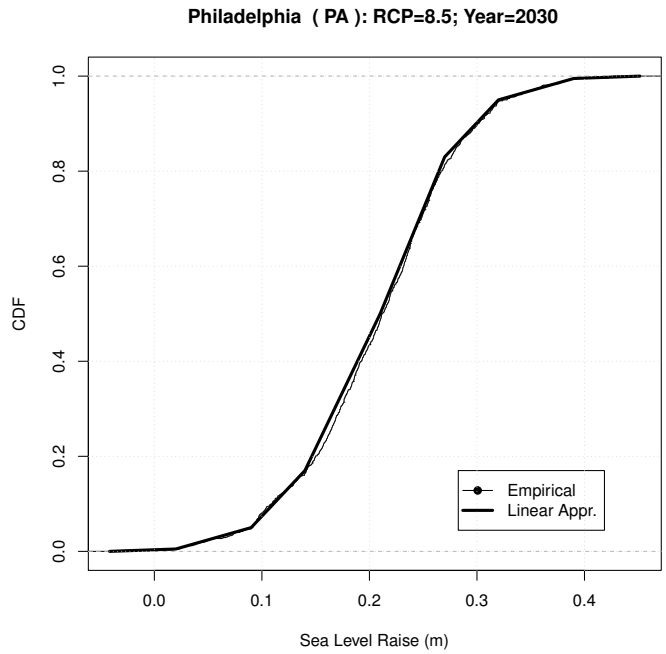

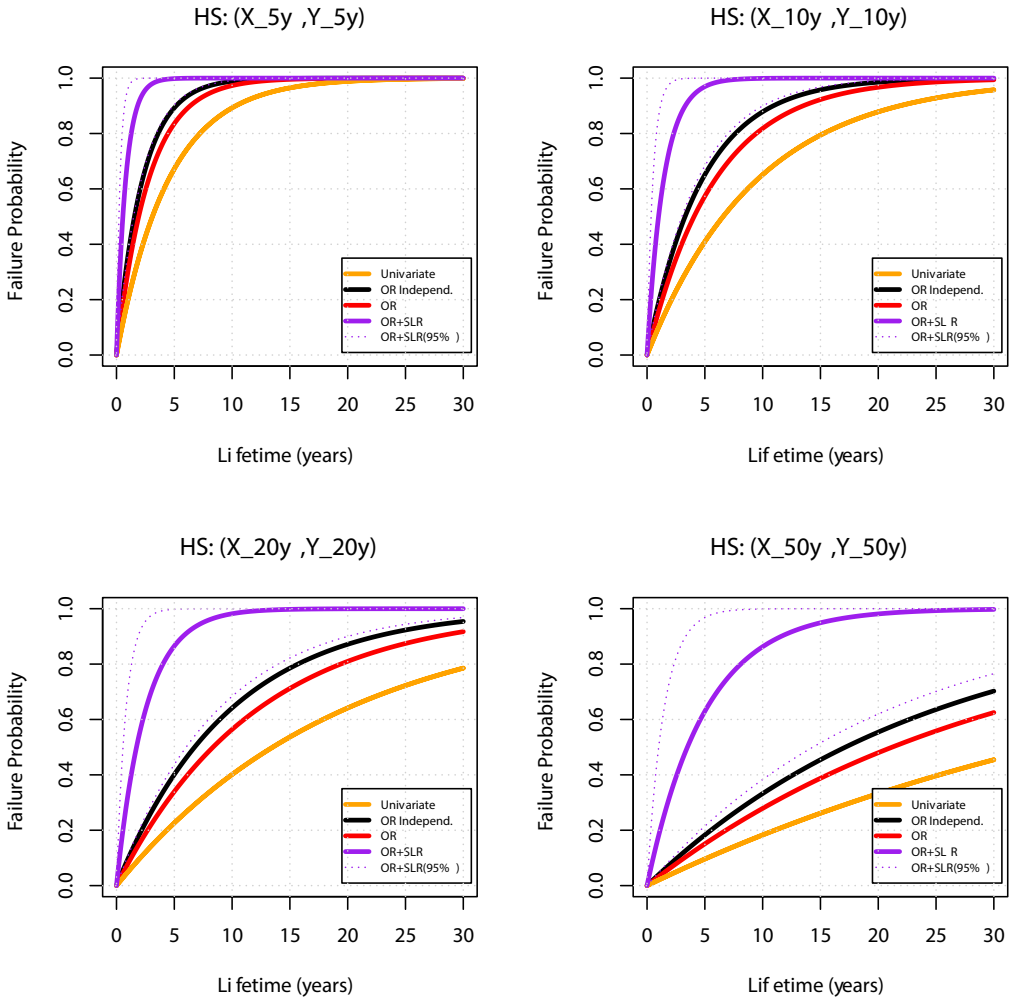

Figure SM.45: see text for explanation.

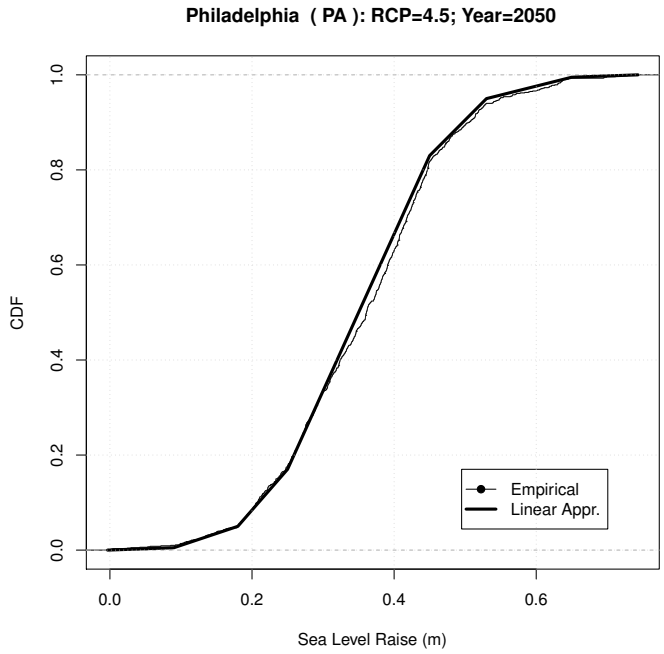

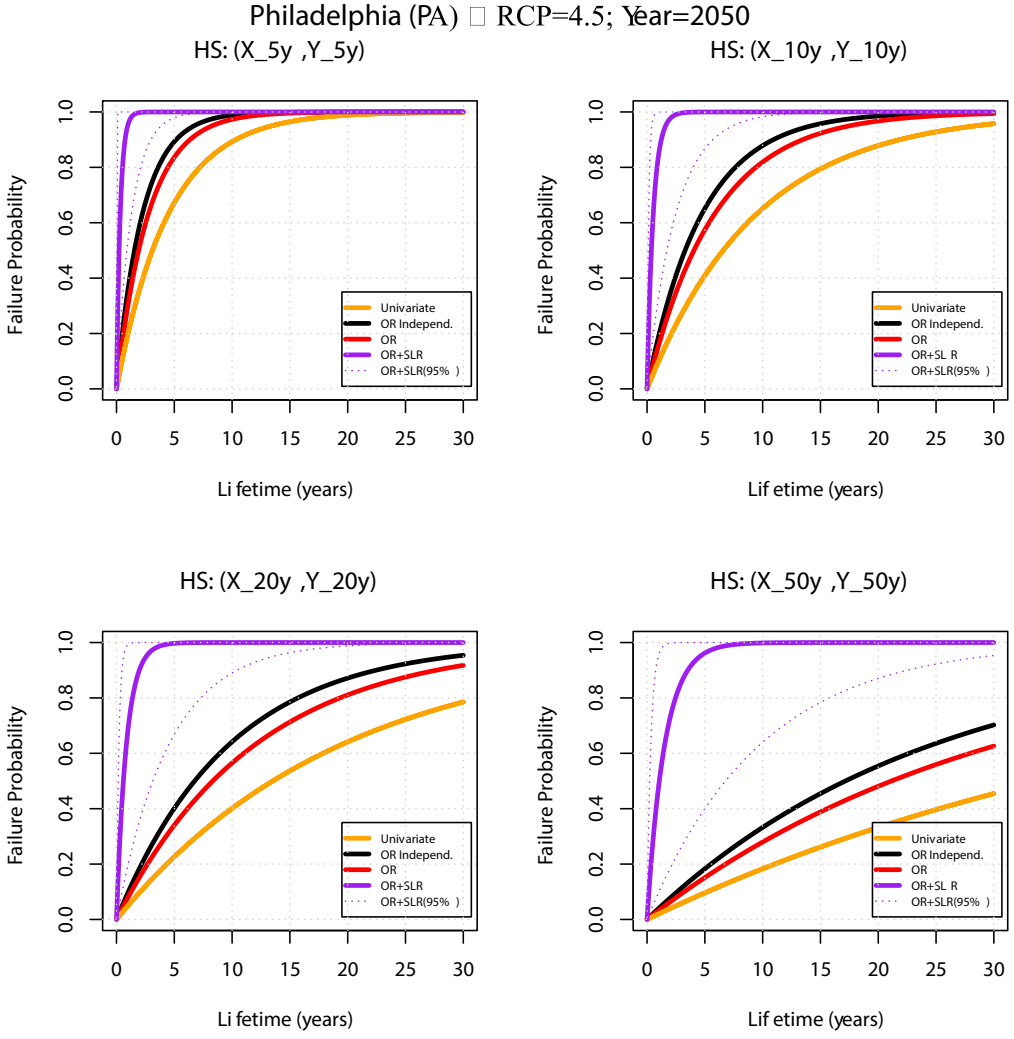

Figure SM.46: see text for explanation.

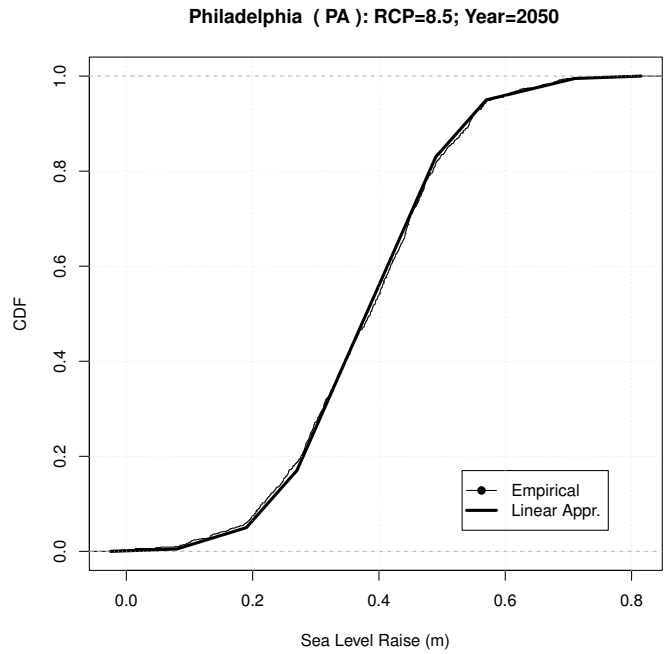

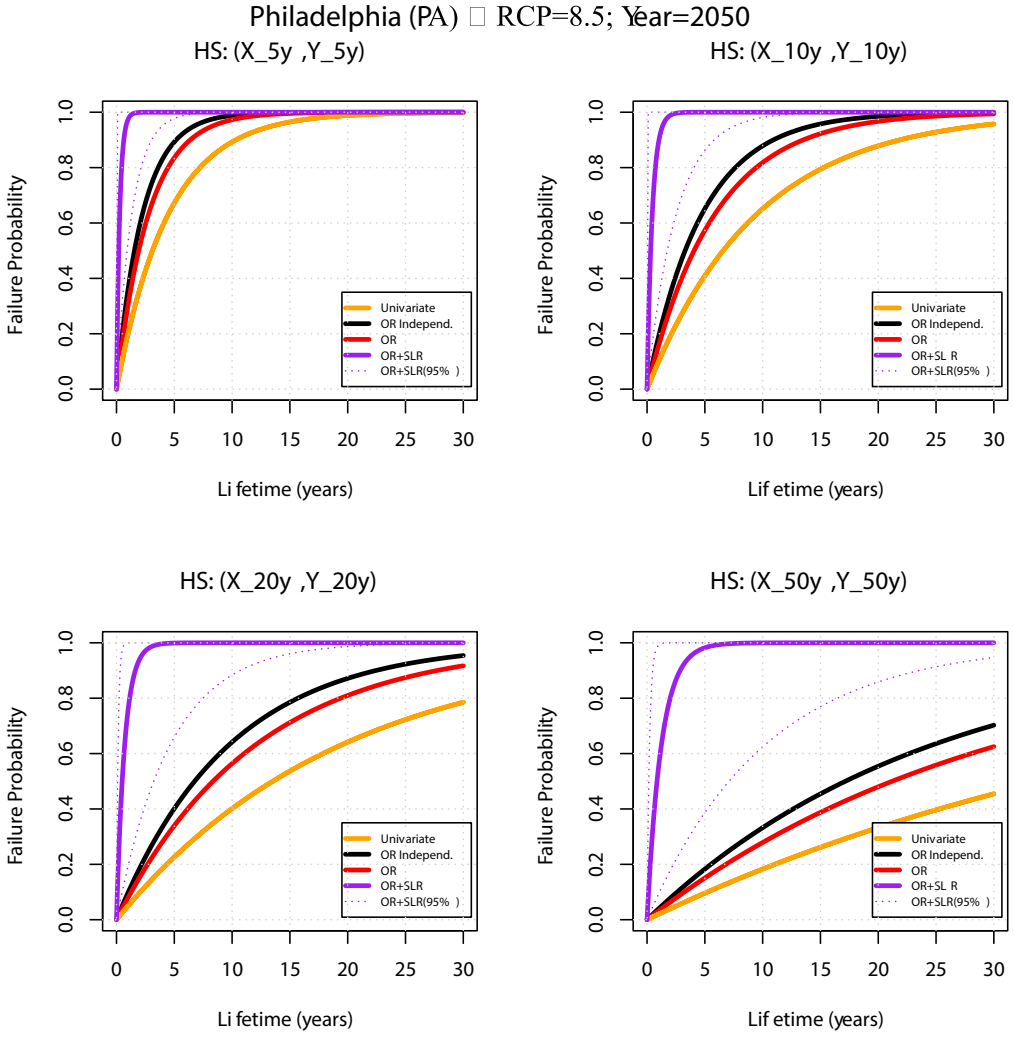

Figure SM.47: see text for explanation.

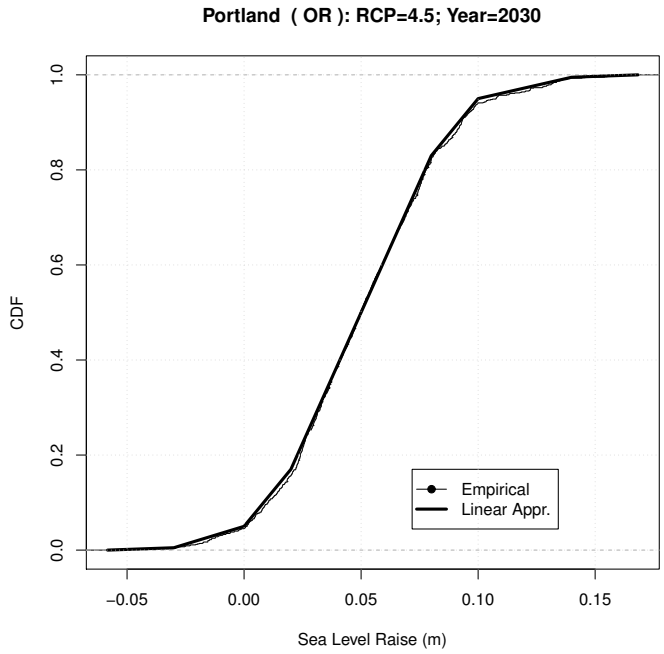

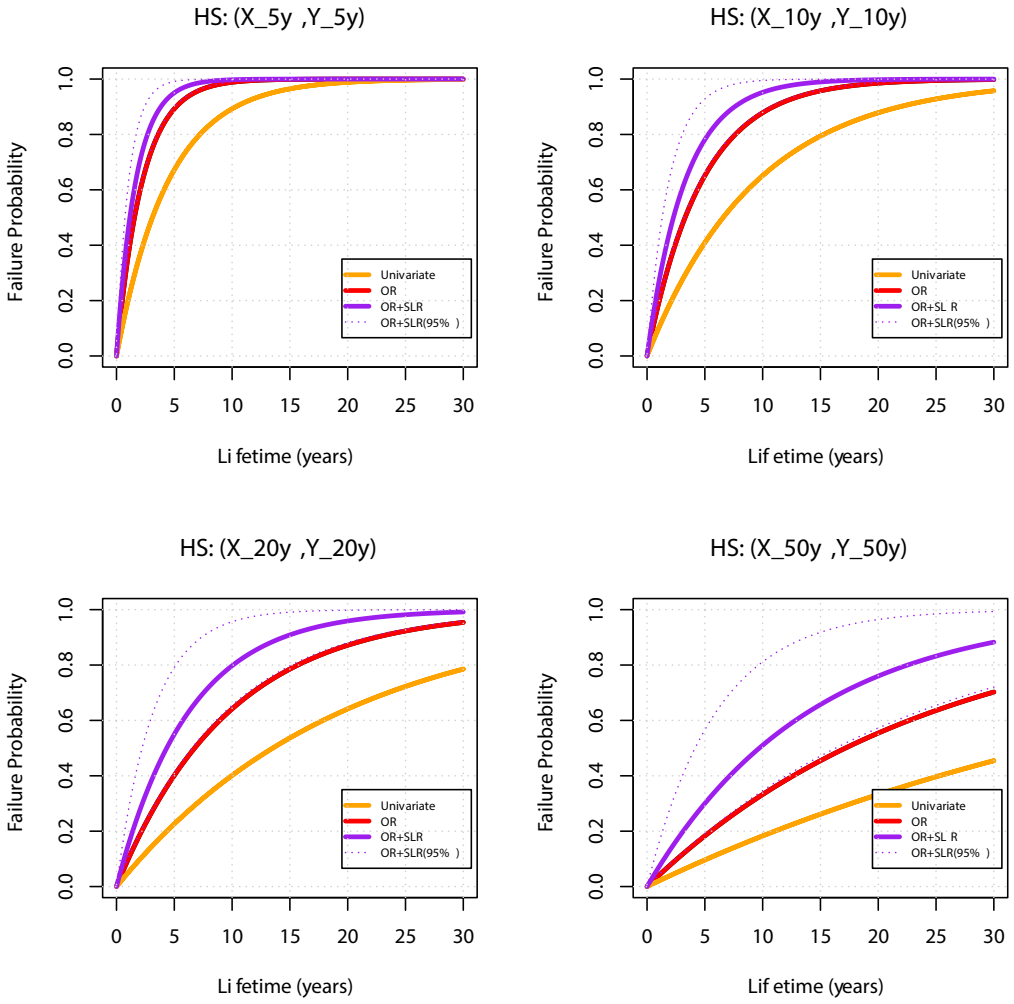

Figure SM.48: see text for explanation.

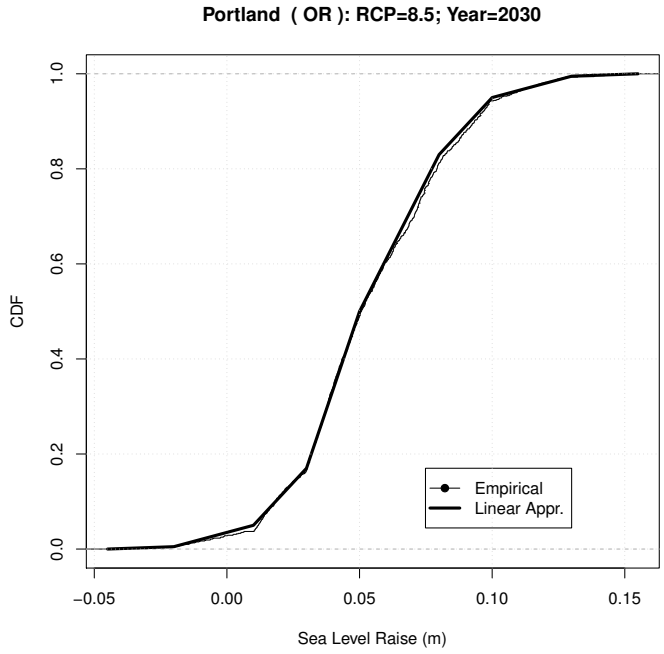

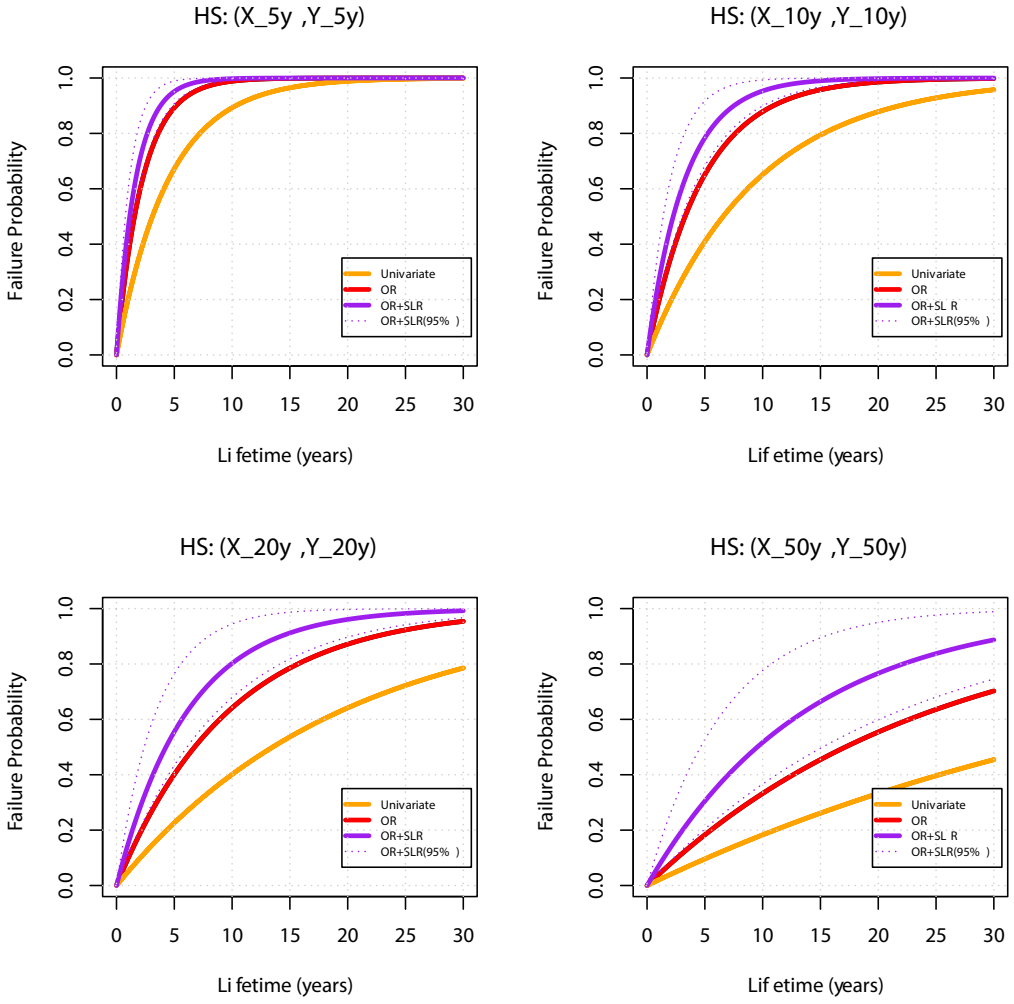

Figure SM.49: see text for explanation.

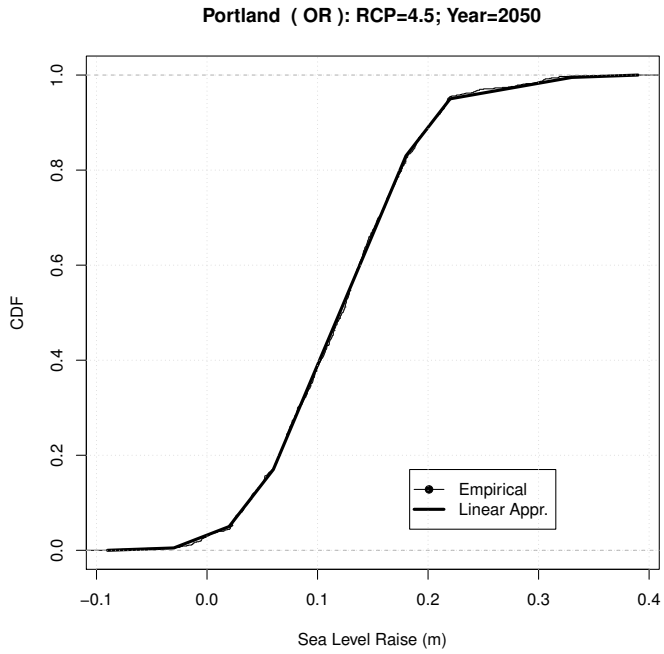

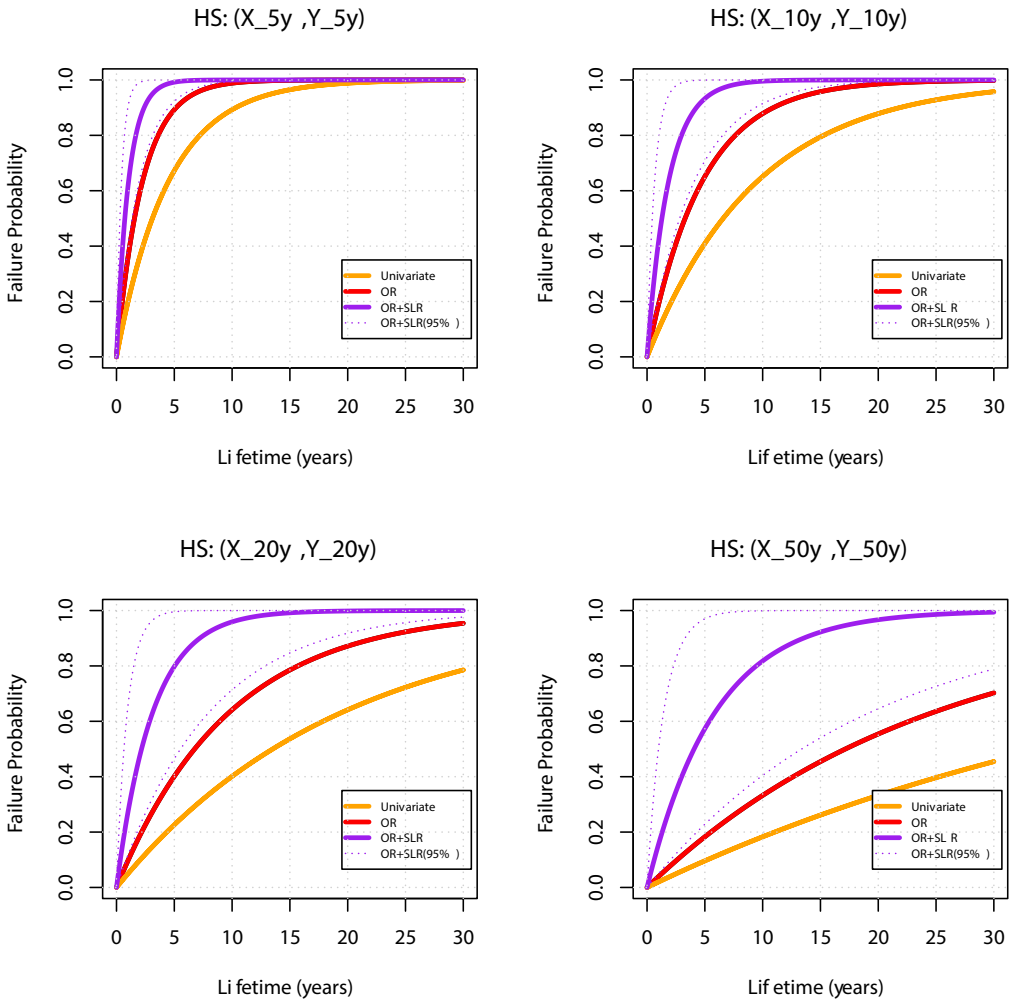

Figure SM.50: see text for explanation.

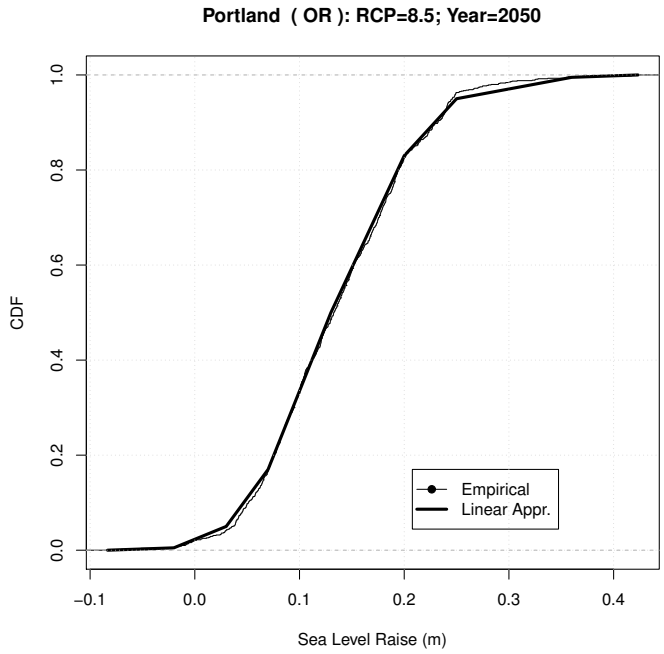

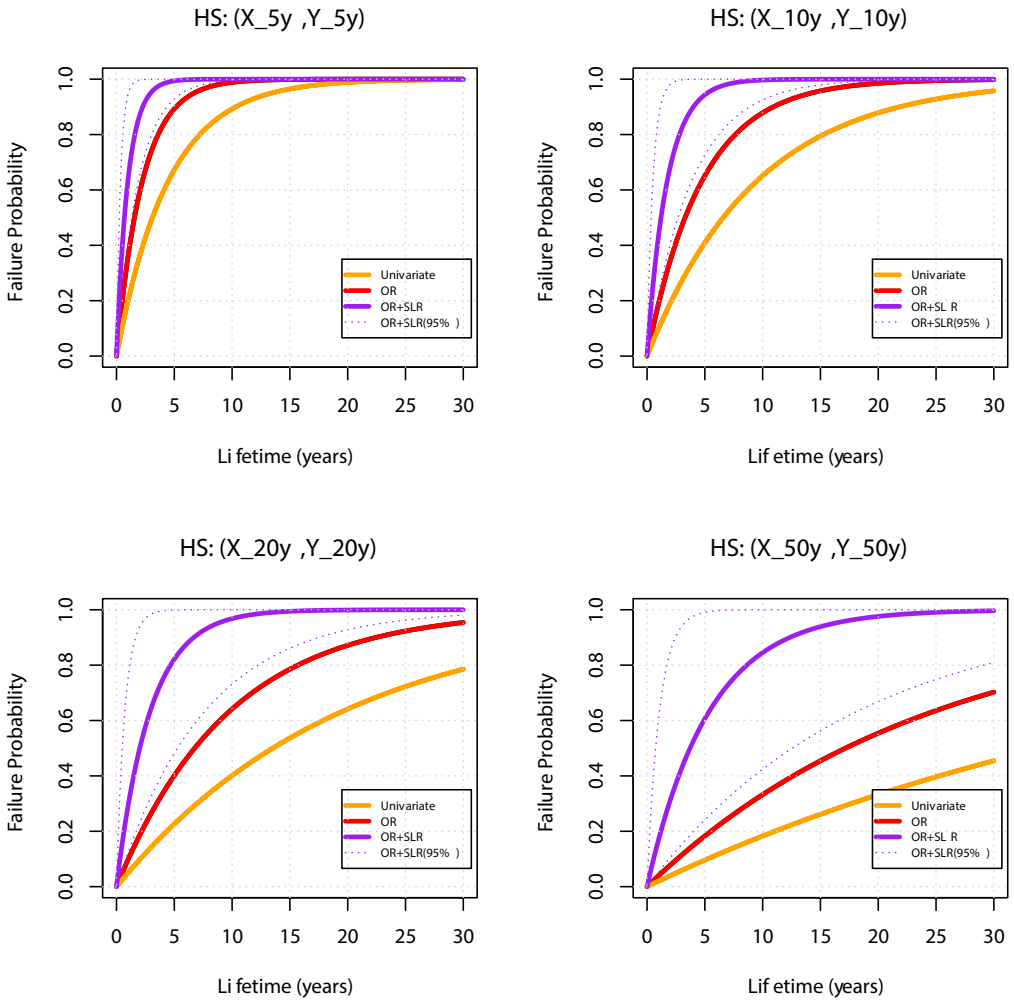

Figure SM.51: see text for explanation.

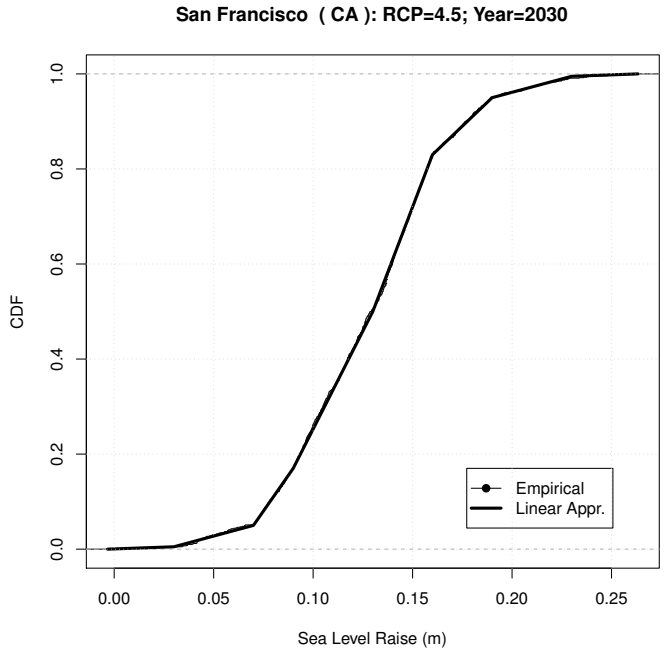

San Francisco (CA) □ RCP=4.5; Year=2030

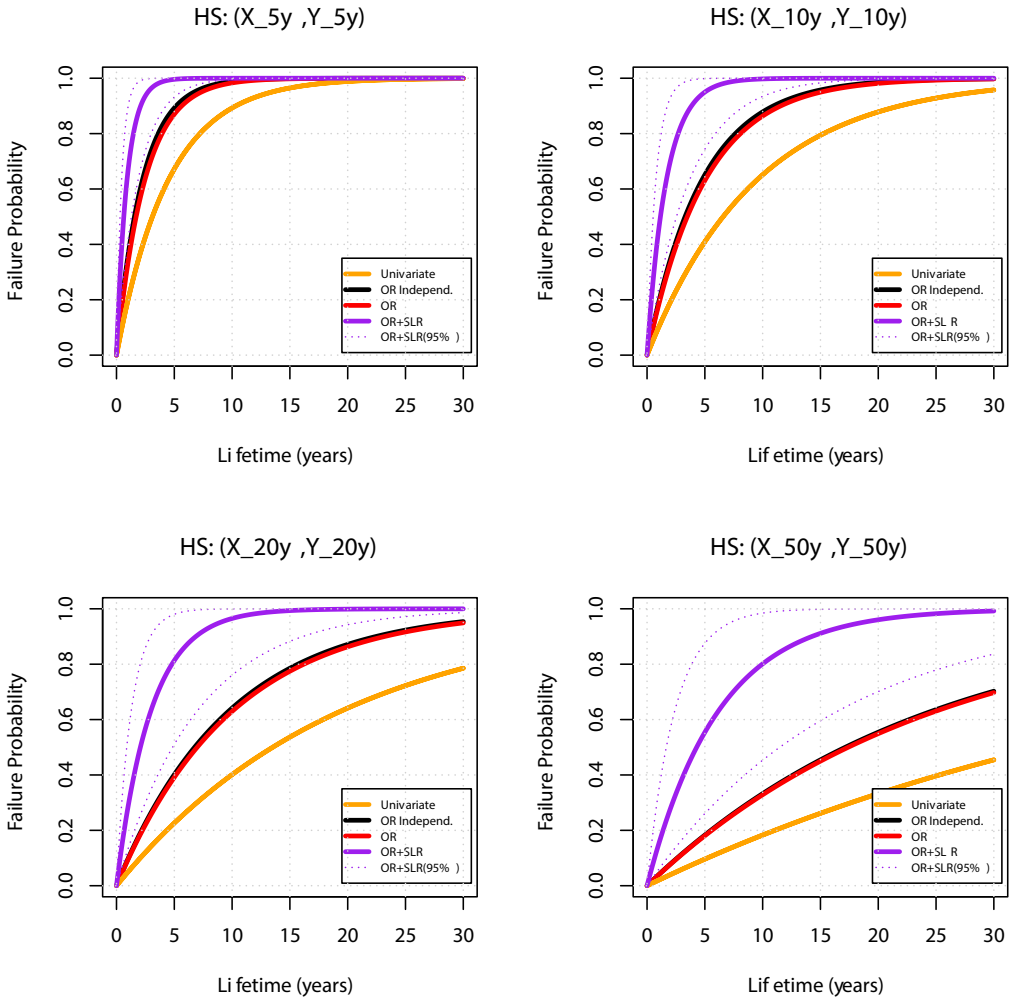

Figure SM.52: see text for explanation.

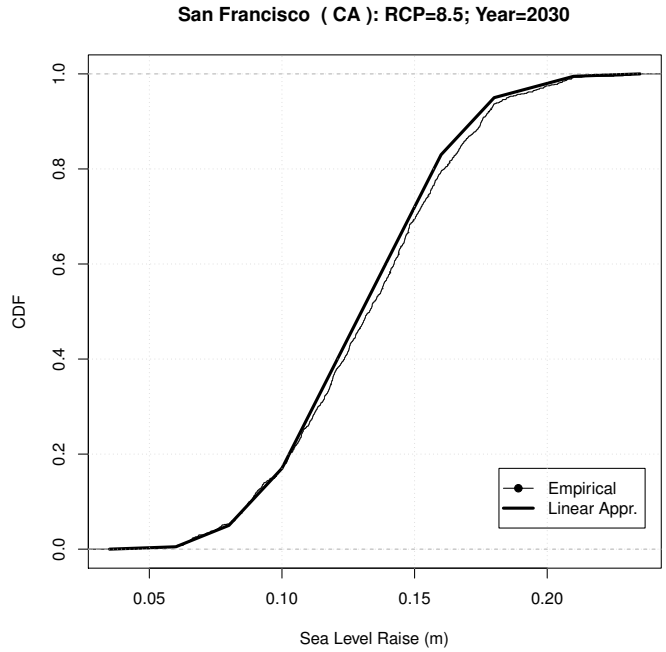

San Francisco (CA) □ RCP=8.5; Year=2030

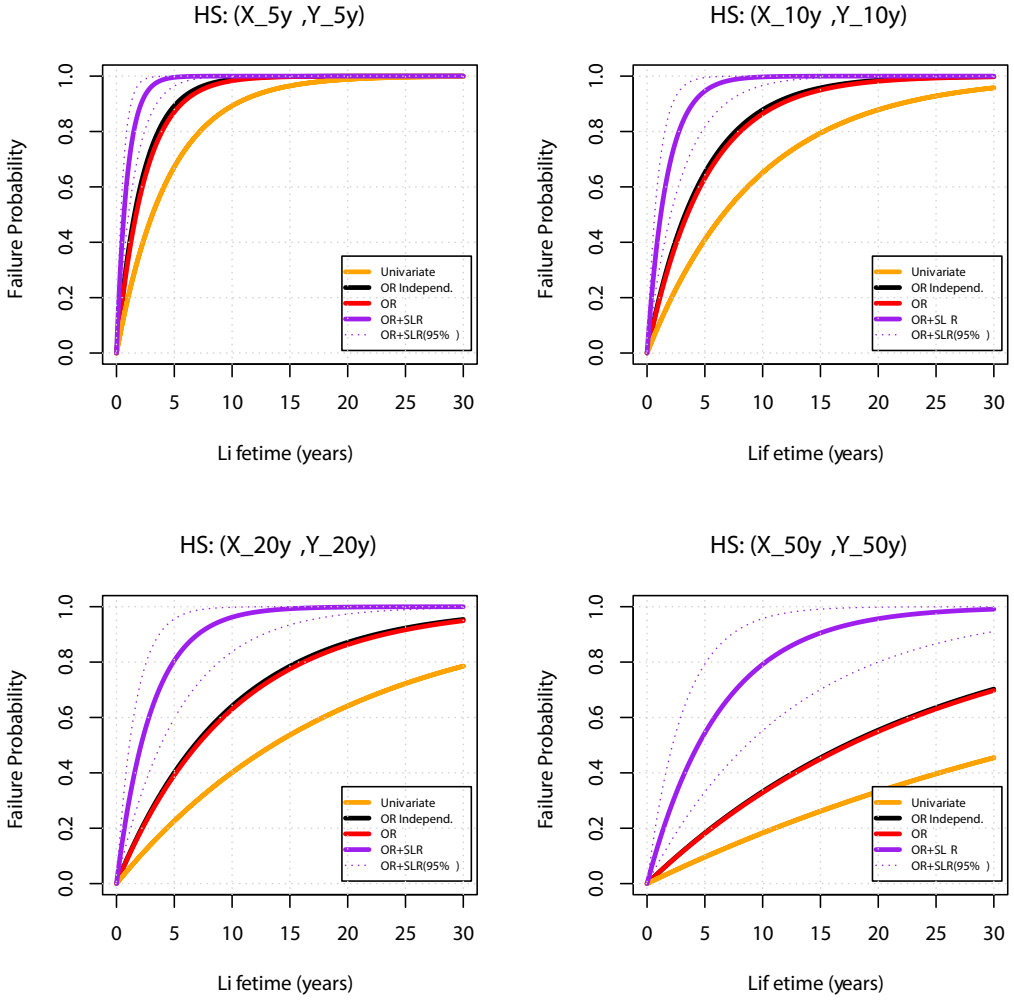

Figure SM.53: see text for explanation.

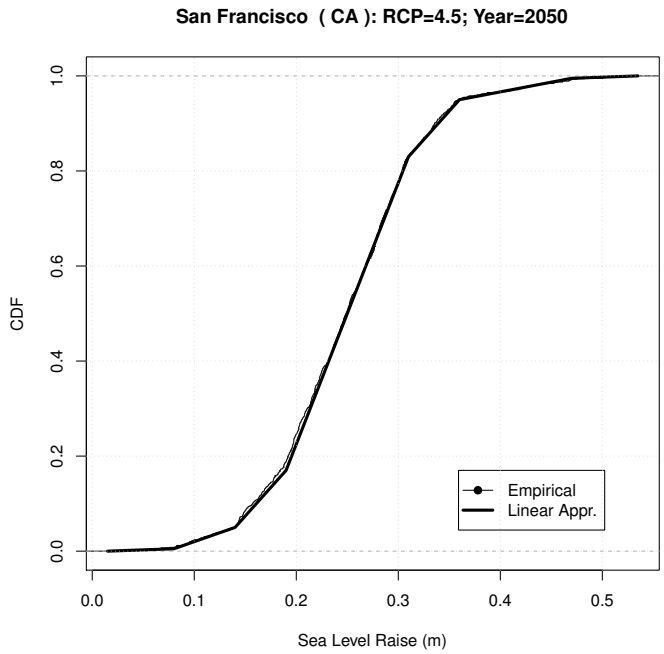

San Francisco (CA) □ RCP=4.5; Year=2050

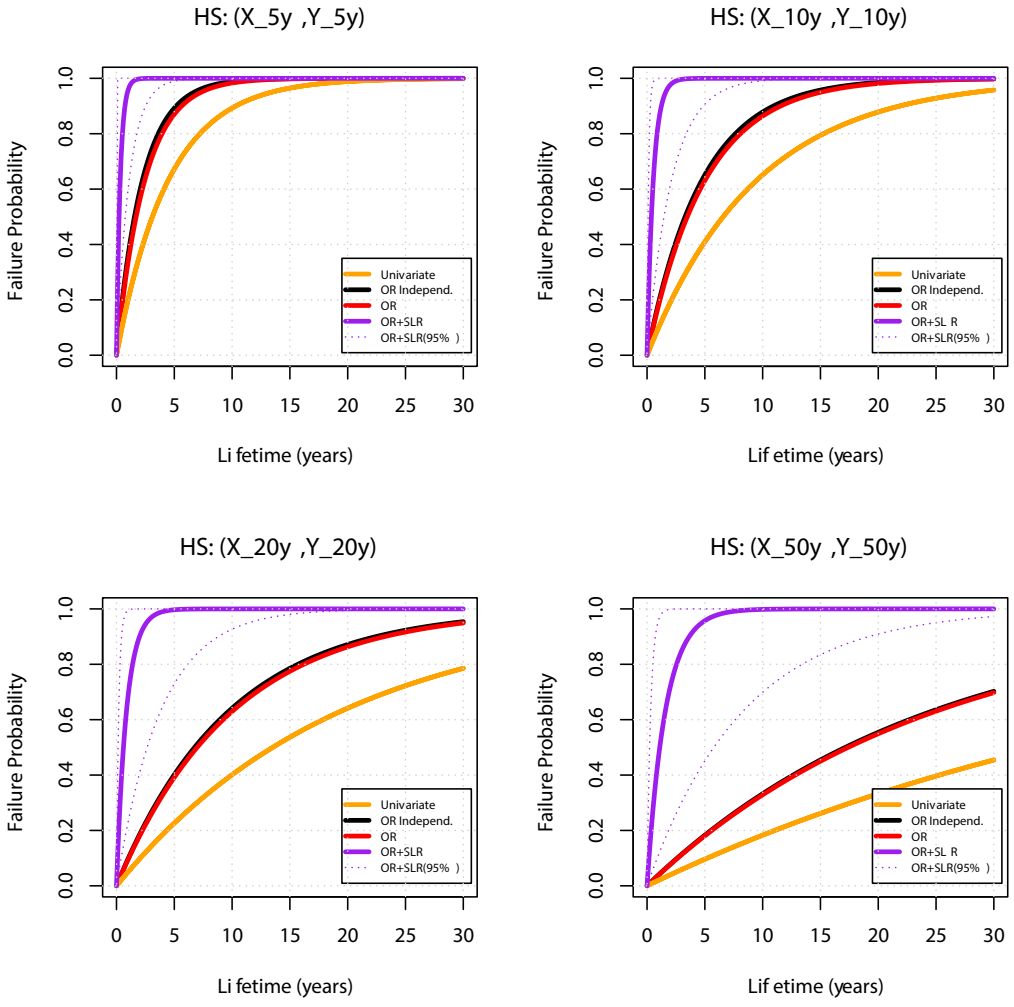

Figure SM.54: see text for explanation.

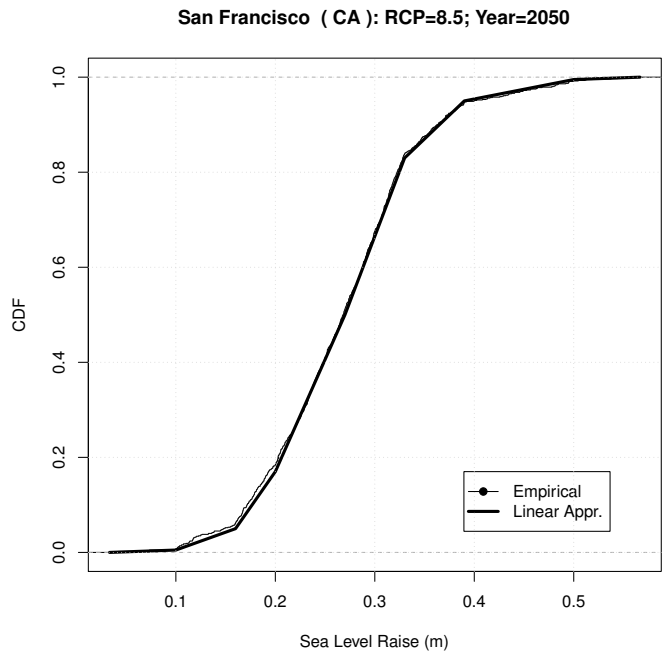

San Francisco (CA) □ RCP=8.5; Year=2050

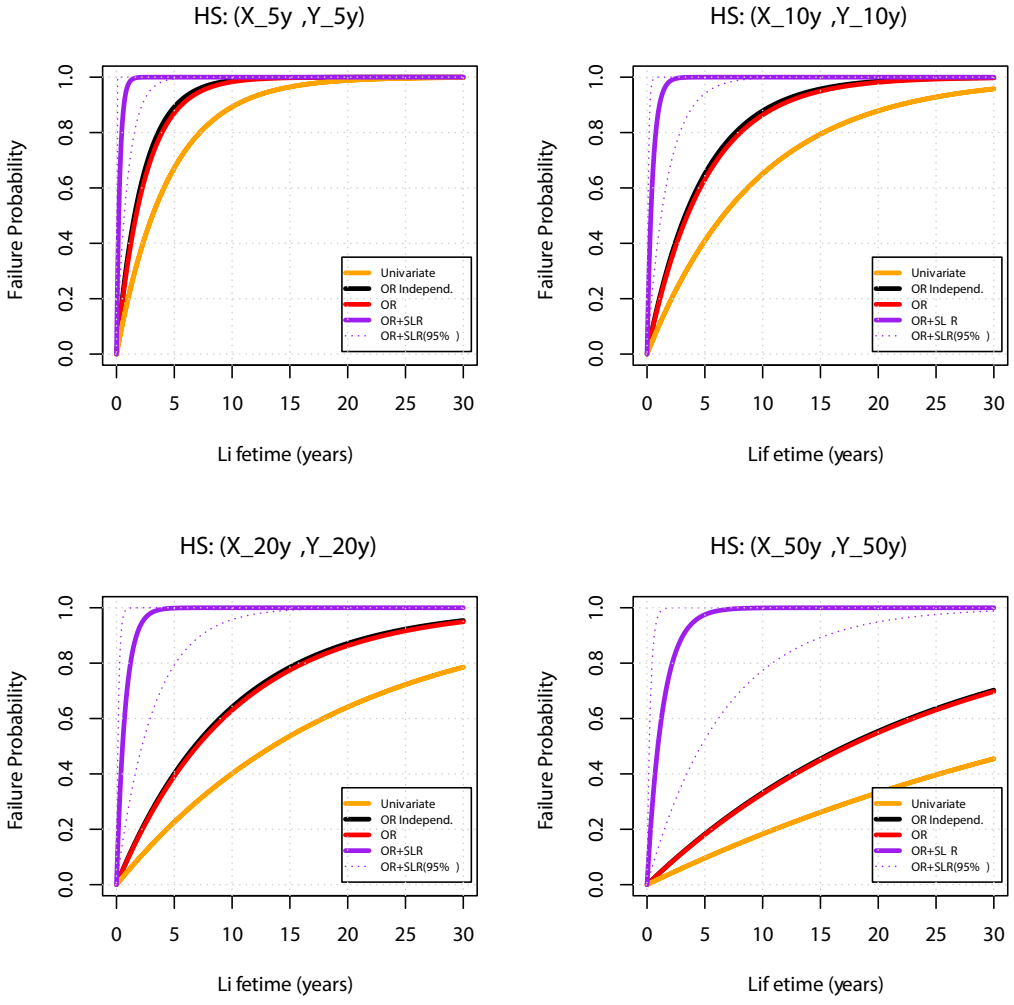

Figure SM.55: see text for explanation.

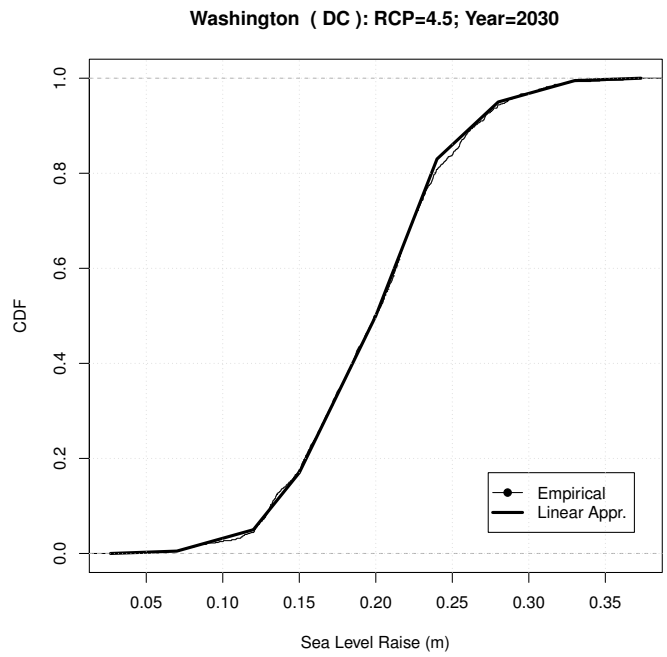

Washington (DC) □ RCP=4.5; Year=2030

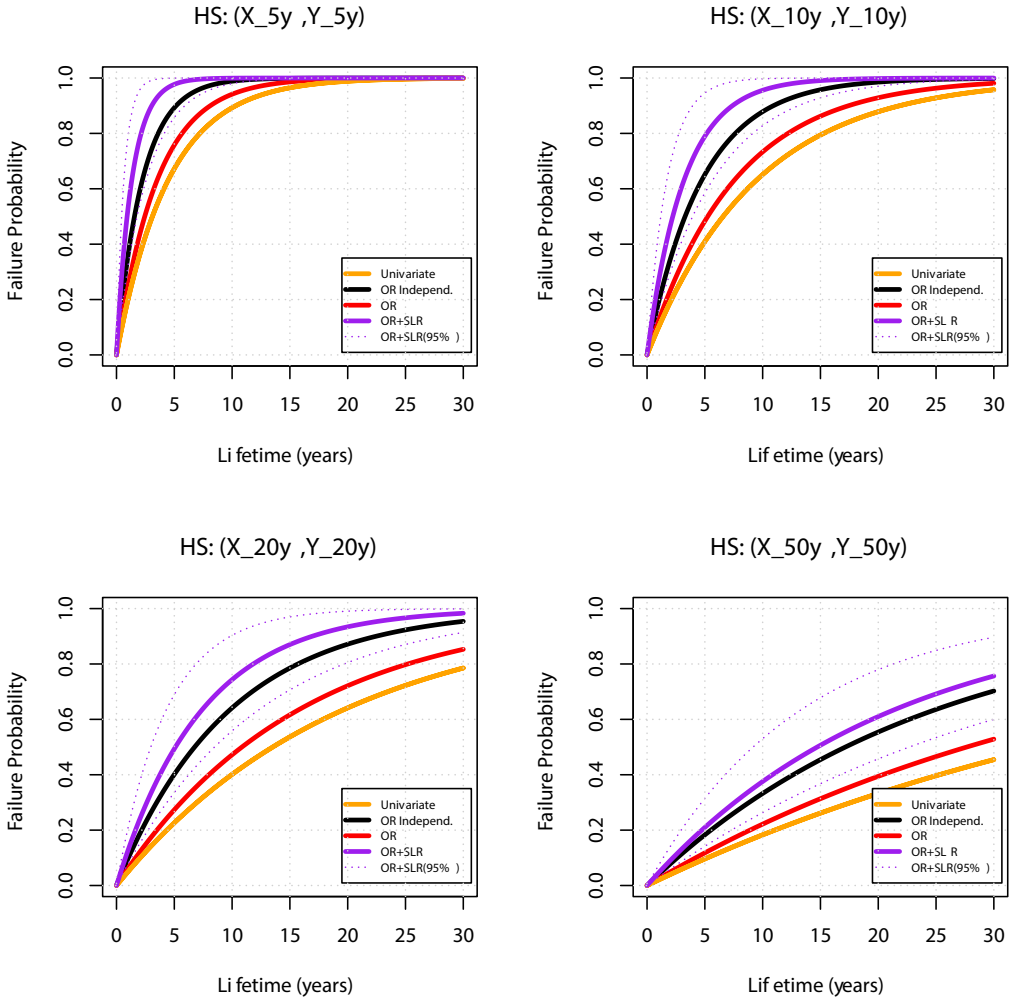

Figure SM.56: see text for explanation.

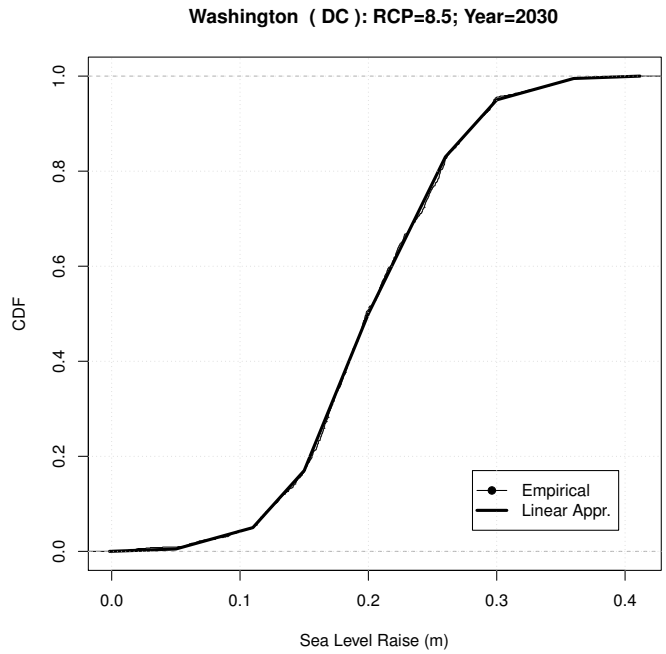

Washington (DC) □ RCP=8.5; Year=2030

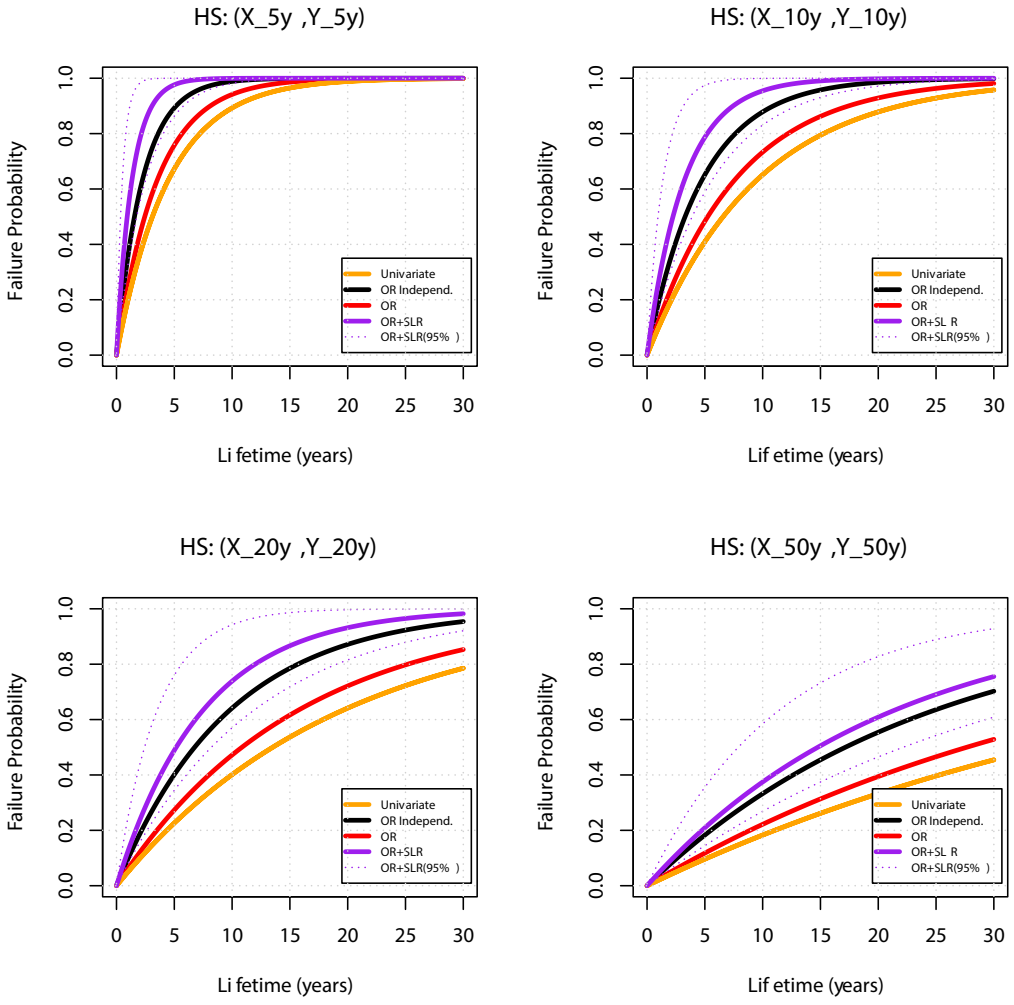

Figure SM.57: see text for explanation.

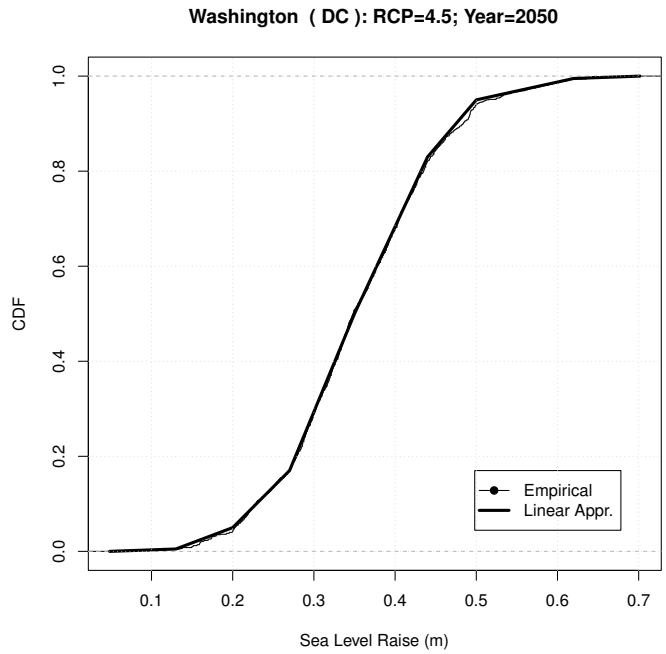

Washington (DC) □ RCP=4.5; Year=2050

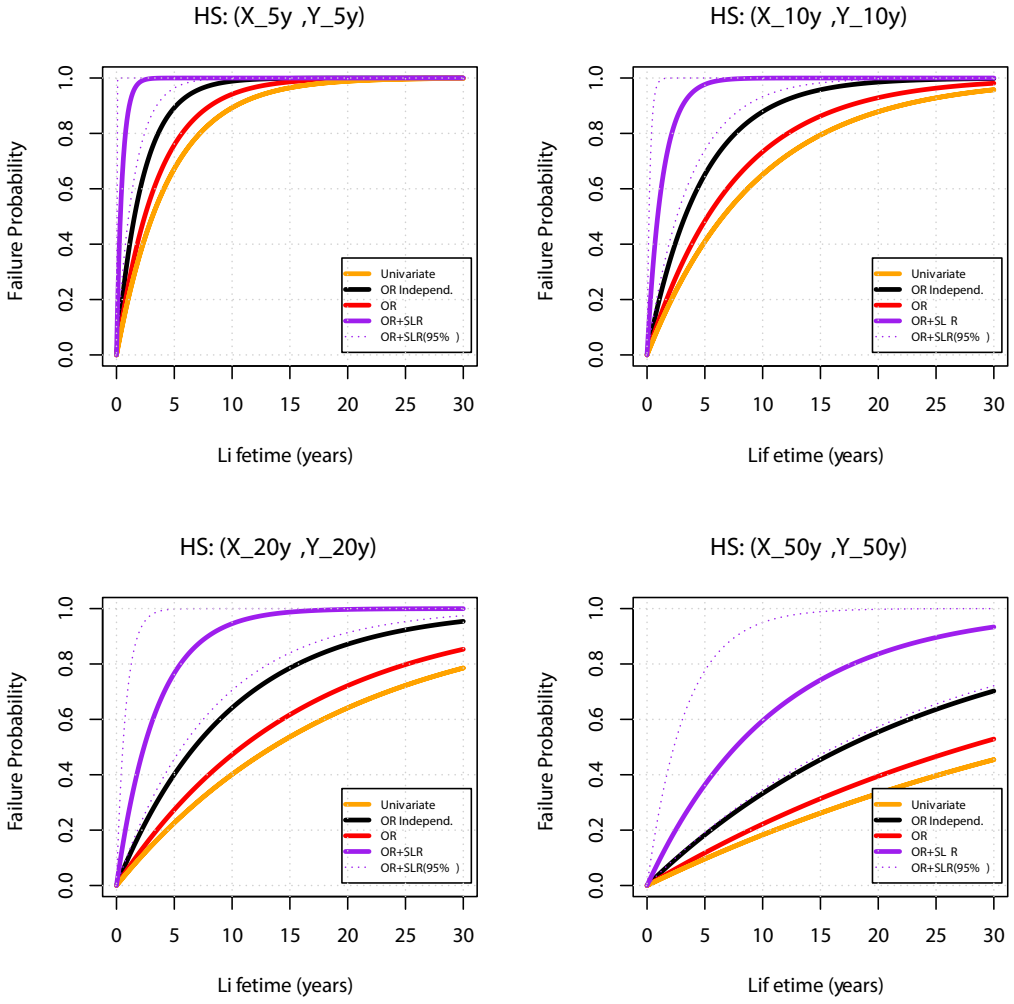

Figure SM.58: see text for explanation.

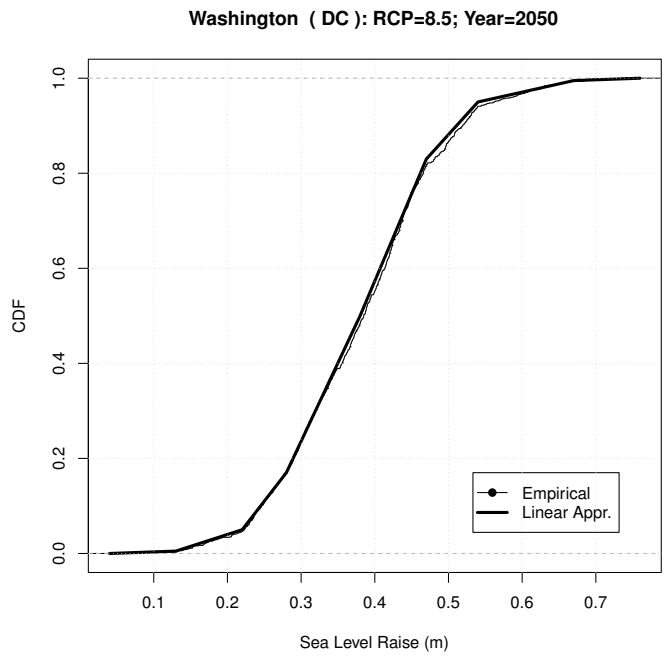

Washington (DC) □ RCP=8.5; Year=2050

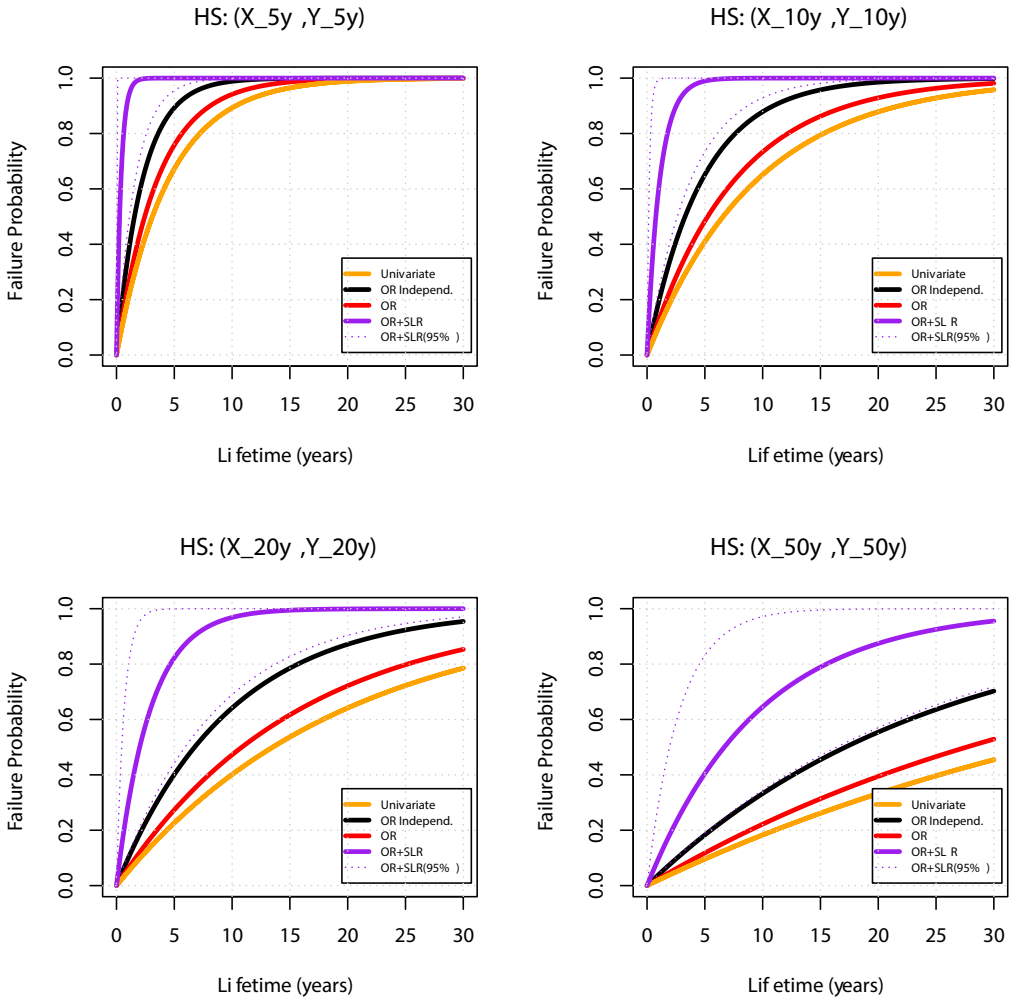

Figure SM.59: see text for explanation.

References

Jens Bender, Thomas Wahl, Alfred Müller, and Jürgen Jensen. A multivariate design framework for river confluences. *Hydrological Sciences Journal*, 61(3):471–482, 2016.

N Chini and PK Stansby. Extreme values of coastal wave overtopping accounting for climate change and sea level rise. *Coastal Engineering*, 65:27–37, 2012.

S Corbella and DD Stretch. Multivariate return periods of sea storms for coastal erosion risk assessment. *Natural Hazards and Earth System Sciences*, 12(8):2699–2708, 2012.

Stefano Corbella and Derek D Stretch. Simulating a multivariate sea storm using archimedean copulas. *Coastal Engineering*, 76:68–78, 2013.

C De Michele, G Salvadori, G Passoni, and R Vezzoli. A multivariate model of sea storms using copulas. *Coastal Engineering*, 54(10):734–751, 2007.

B Gouldby, FJ Méndez, Y Guanche, A Rueda, and R Mínguez. A methodology for deriving extreme nearshore sea conditions for structural design and flood risk analysis. *Coastal Engineering*, 88:15–26, 2014.

Peter J Hawkes, Ben P Gouldby, Jonathan A Tawn, and Michael W Owen. The joint probability of waves and water levels in coastal engineering design. *Journal of hydraulic research*, 40(3):241–251, 2002.

M. Hofert, I. Kojadinovic, M. Maechler, and J. Yan. *copula: Multivariate Dependence with Copulas*, R package version 0.999-15 edition, 2016. URL `http://CRAN.R-project.org/package=copula`.

SF Kew, FM Selten, G Lenderink, and W Hazeleger. The simultaneous occurrence of surge and discharge extremes for the rhine delta. *Natural Hazards and Earth System Sciences*, 13(8):2017–2029, 2013.

Wouter-Jan Klerk, HC Winsemius, WJ van Verseveld, AMR Bakker, and FLM Diermanse. The co-incidence of storm surges and extreme discharges within the rhine–meuse delta. *Environmental Research Letters*, 10 (3):035005, 2015.

Rob Lamb, Caroline Keef, Jonathan Tawn, Stefan Laeger, I Meadowcroft, S Surendran, P Dunning, and C Batstone. A new method to assess the risk of local and widespread flooding on rivers and coasts. *Journal of Flood Risk Management*, 3(4):323–336, 2010.

Ann Lehman, Norm ORourke, Larry Hatcher, and Edward Stepanski. Jmp for basic univariate and multivariate statistics. *SAS Institute Inc., Cary, NC*, page 481, 2005.

F Li, PHAJM Van Gelder, R Ranasinghe, DP Callaghan, and RB Jongejan. Probabilistic modelling of extreme storms along the dutch coast. *Coastal Engineering*, 86:1–13, 2014a.

F Li, PHAJM van Gelder, JK Vrijling, DP Callaghan, RB Jongejan, and R Ranasinghe. Probabilistic estimation of coastal dune erosion and recession by statistical simulation of storm events. *Applied Ocean Research*, 47:53–62, 2014b.

JJ Lian, K Xu, and C Ma. Joint impact of rainfall and tidal level on flood risk in a coastal city with a complex river network: a case study of fuzhou city, china. *Hydrology and Earth System Sciences*, 17(2):679–689, 2013.

A Rueda, P Camus, A Tomás, S Vitousek, and FJ Méndez. A multivariate extreme wave and storm surge climate emulator based on weather patterns. *Ocean Modelling*, 104:242–251, 2016.

G. Salvadori, C. De Michele, and F. Durante. On the return period and design in a multivariate framework. *Hydrol. Earth Syst. Sci.*, 15:3293—3305, 2011. doi: 10.5194/hess-15-3293-2011.

G Salvadori, GR Tomasicchio, and F D'Alessandro. Practical guidelines for multivariate analysis and design in coastal and off-shore engineering. *Coastal Engineering*, 88:1–14, 2014.

G Salvadori, F Durante, GR Tomasicchio, and F D'Alessandro. Practical guidelines for the multivariate assessment of the structural risk in coastal and off-shore engineering. *Coastal Engineering*, 95:77–83, 2015.

G. Salvadori, F. Durante, C. De Michele, M. Bernardi, and L. Petrella. A multivariate Copula-based framework for dealing with Hazard Scenarios and Failure Probabilities. *Water Resources Research*, 53:3701–3721, 2016. doi: 10.1002/2015WR017225. doi: 10.1002/2015WR017225.

Katherine A Serafin and Peter Ruggiero. Simulating extreme total water levels using a time-dependent, extreme value approach. *Journal of Geophysical Research: Oceans*, 119(9):6305–6329, 2014.

Cecilia Svensson and David A Jones. Dependence between extreme sea surge, river flow and precipitation in eastern britain. *International Journal of Climatology*, 22(10):1149–1168, 2002.

Cecilia Svensson and David A Jones. Dependence between sea surge, river flow and precipitation in south and west britain. *Hydrology and Earth System Sciences Discussions*, 8(5):973–992, 2004.

Bart van den Hurk, Erik van Meijgaard, Paul de Valk, Klaas-Jan van Heeringen, and Jan Gooijer. Analysis of a compounding surge and precipitation event in the netherlands. *Environmental Research Letters*, 10(3): 035001, 2015.

T Wahl, C Mudersbach, and J Jensen. Assessing the hydrodynamic boundary conditions for risk analyses in coastal areas: a multivariate statistical approach based on copula functions. *Natural Hazards and Earth System Science*, 12(2):495–510, 2012.

Thomas Wahl, Shaleen Jain, Jens Bender, Steven D Meyers, and Mark E Luther. Increasing risk of compound flooding from storm surge and rainfall for major us cities. *Nature Climate Change*, 5(12):1093–1097, 2015.

Thomas Wahl, Nathaniel G Plant, and Joseph W Long. Probabilistic assessment of erosion and flooding risk in the northern gulf of mexico. *Journal of Geophysical Research: Oceans*, 2016.

Feifei Zheng, Seth Westra, and Scott A Sisson. Quantifying the dependence between extreme rainfall and storm surge in the coastal zone. *Journal of Hydrology*, 505:172–187, 2013.

Feifei Zheng, Seth Westra, Michael Leonard, and Scott A Sisson. Modeling dependence between extreme rainfall and storm surge to estimate coastal flooding risk. *Water Resources Research*, 50(3):2050–2071, 2014.

Feifei Zheng, Michael Leonard, and Seth Westra. Application of the design variable method to estimate coastal flood risk. *Journal of Flood Risk Management*, 2015a.

Feifei Zheng, Michael Leonard, and Seth Westra. Efficient joint probability analysis of flood risk. *Journal of Hydroinformatics*, 17(4):584–597, 2015b.